University of Zurich[UZH]

Swiss Federal Institute for Forest, Snow and Landscape Research WSL

Department of Evolutionary Biology and Environmental Studies
University of Zurich

Research Unit
Biodiversity and Conservation Biology
WSL Birmensdorf

Master Thesis

Modelling the effects of artificial light at night (ALAN) on bat commuting corridor models

Levi Fuchs

16-718-504

10th May 2021

Supervisor: Dr. Eva Knop (IEU | Agroscope)
Supervisor: Dr. Martin K. Obrist (WSL)
Co-Supervisor: Dr. Klaus Ecker (WSL)
Co-Supervisor: Dr. Ruedi Bösch (WSL)

Abstract

In the last century, increased habitat destruction and fragmentation due to urbanization led to alarming bat population declines in Switzerland. Both the Lesser horseshoe bat (*Rhinolophus hipposideros*) and the Greater mouse-eared bat (*Myotis myotis*) therefore appear on the Swiss red list of endangered species. During summer, each species' females unite in maternity roosts, inhabiting attics of old houses, churches or barns. Every night after sunset, they commute from these roosts to nearby forests for foraging. On the paths to their foraging grounds, they are expected to follow along corridors of preferred topographical and ecological characteristics. The reliance on such corridors and generally a life in the immediate vicinity of settlements increases their vulnerability to human induced habitat fragmentation.

Predicting potential flight corridors of the two species may serve greatly in detecting the most vital commuting passages. However, previous approaches to spatially model bat activity and their commuting corridors proved to be insufficient – presumably due to the lack of GIS data representing artificial light at night (ALAN), as both species are known to be highly sensitive to ALAN and prefer flying along dark corridors to escape light-dependent predation.

In this study, I present a method to integrate a light variable into the existing models, with the aim to improve their predictive performances for the two species. After generating nocturnal drone imagery of 20 study sites, I computed lightness raster layers as continuous representations of ALAN. Additionally, single RGB bands were extracted from the drone photography to assess the effects of the three spectral bands on bat commuting activity. I then fitted generalized linear mixed models including the new lightness and RGB predictors to the existing recorded activity data for both species. These newly obtained lightness models were used as inputs to compute new corridor predictions and commuting routes of least cost.

My study shows that the integration of lightness significantly improves the overall fit of both models compared to their respective ones lacking a light parameter. Additionally, it suggests that *M. myotis* are particularly averse towards high proportions of blue – representing shorter wavelengths – in the spectral output of artificial lights.

The newly computed area-wide quantifiable corridor models also show significant improvement compared to models predicted with no lightness parameter. For most sites there are clear visual transformations detectable, which often reveal ALAN to force the bats onto longer and more dangerous routes.

I believe these new findings to be highly valuable in future processes of bat corridor conservation and spatial planning. The improved visualization of such commuting corridors should serve greatly in the communication with local agencies and experts. Generally, the implementation of drone imagery as a representation of ALAN may potentially also be applied to various other nocturnal commuting species in the broader field of light pollution.

Introduction

Human induced pressures on natural environments have contributed to a global habitat loss in the last century. Such losses mainly occur through direct habitat destruction – e.g., conversion of natural habitats to settlements – or the alteration of landscape composition and habitat fragmentation (Tilman et al., 1994). These fragmentations lead to a reduction of patch connectivity, which is common in Switzerland, as urbanization continues to change and dissect natural habitats. Settlement-bound bat species are among the animals most influenced by these pressures as they live in direct human vicinity. In summer, females of many species unite in maternity roosts in human settlements – often inhabiting old attics of big houses, church towers or barns. This life in direct human vicinity leaves them extremely susceptible to anthropogenic change (Hale & Arlettaz, 2019; Voigt & Kingston, 2016), often leading to severe population declines and an appearance on the Swiss red list of endangered species (Bohnenstengel et al., 2014). Among the most influential drivers of these population declines are habitat destruction and deprivation of possible prey. Due to their nocturnality, bats are particularly impacted by effects of light pollution (Azam et al., 2018; Hale & Arlettaz, 2019; Lewanzik & Voigt, 2014; Rowse et al., 2016; Stone et al., 2015). Low reproduction rates and generally high ecological demands – driven by high metabolic rates and the need for several distinct habitats – additionally enhance their vulnerability (Speakman, 2003; Voigt & Kingston, 2016).

In this study I focus on two commuting bat species: The Lesser horseshoe bat (*Rhinolophus hipposideros*) and the Greater mouse-eared bat (*Myotis myotis*). Their habitats typically consist of three main areas: The roosting area, the foraging grounds and the commuting corridors in between. In an effort to protect these species, many conservationists have focused on the conservation and protection of their roosts (Hutson et al., 2015). However, most bat species also hunt while commuting and can thereby cover long distances of up to many kilometers. Whilst many foraging areas – such as forest edges or wetlands – are protected by the Federal Act on Forest or the Ordinance on the Protection of Nature and Cultural Heritage, the commuting corridors have regularly been overlooked by conservationists (Ravessoud, 2017). Processes of fragmentation due to continuous urbanization, however, predominantly affect these corridors. Therefore, it's important for conservational and spatial planning purposes, to know which corridors bats prioritize during their commuting periods and based upon which factors such corridors are chosen.

To fill the gap of knowledge on bat commuting corridors, Ravessoud (2017) aimed to find the best predictors of bat activity to model the main commuting routes for *R. hipposideros* and *M. myotis*. He derived his predictions based on ground-based acoustic measurements of activity around the roosts. Integrating various possible factors (90 for *R. hipposideros* and 96 for *M. myotis*), he fitted a generalized linear mixed model (GLMM) to identify the most significant predictors of bat commuting activity. Working with a Least Absolute Shrinkage and Selection Operator (LASSO) (Tibshirani, 1996), he could deal with the great number of predictors by only retaining the most significant ones (Ravessoud, 2017). He concluded that the most important predictors for the activity of both species were artificial light at night (ALAN) along with various structure and terrain variables. These models were validated by Meier (2019) through the collection of more count data at other locations. Based on the model coefficients of the spatial variables, Meier (2019) afterwards computed landscape resistance maps to calculate least cost paths and current flow models to identify the best suitable corridor areas.

However, the spatial corridor models needed improving. As there were no available GIS layers representing intensities of ALAN, Meier (2019) was forced to omit the light predictor from her spatial models. Nater (2019) has afterwards exposed the model's predictions to still fall short when compared to local expert's experiences and concluded this to potentially be a consequence of the missing light predictor in the model. The two chosen species are indeed known to be especially sensitive to ALAN, as increased illuminance leads to higher predation risk (Rydell et al., 1996). Both species are therefore expected to avoid light and highly depend on dark corridors to commute to their foraging areas.

Meier (2019) initially tried to integrate an artificial light variable from images taken by astronauts on the international space station (ISS). Pauwels et al. (2019) have validated the utilization of such imagery for extracting night light intensity for environmental study and modelling its impacts on bats. As their study was conducted in very heavily light-polluted cities (up to 40 times higher than under natural conditions), light gradients were distinctly recognizable on these images. However, the roosts of *M. myotis* and especially *R. hipposideros* are located in more rural and less light polluted vicinities. As less light radiation is detected by the camera sensor, illumination visibility decreases in these regions. Furthermore, many of the study areas are embedded into hilly landscapes, promoting small-scale variations in illumination. These variations are hard to account for with the ISS images, which reach spatial resolutions of around 75 to 110 meters depending on the covered region (Obrist, 2019). As Meier's (2019) results could not confirm the potential of remote sensing data to account for the

impact of artificial light on bat commuting in rural areas, she specifically suggested the usage of drone imagery.

In this study, I generated nocturnal raster images of the regions around the roosts, using a *DJI Mavic Pro 2* drone (DJI Entertainment Technology, 2021). From such imagery I extracted representative lightness and RGB values, which were integrated into the model as fixed predictors. The study aimed to answer the following questions:

1. *Are models including ALAN better predictors for commuting activities of R. hipposideros and M. myotis than conventional models neglecting light?*
2. *What influences do the red, green and blue spectral ranges have on these activities based on RGB-values of optical imagery?*

The null hypothesis would accordingly state that ALAN has no significant effect on the commuting counts of the study species. I hypothesized a variable for ALAN to significantly improve model fit and the resulting corridor maps. Additionally, I expected that RGB values can serve in the representation of spectral characteristics of nocturnal light. Some studies have already highlighted the bat's especially high aversion to light-emitting diodes (LEDs) in consequence of the large proportions of short wavelength blue light in their spectral outputs (Hale & Arlettaz, 2019; Stone et al., 2012, 2015). I therefore anticipated the blue channel to have the most negative effect on the commuting of *R. hipposideros* and *M. myotis*.

This study is not supposed to create a general model for commuting bat species in Switzerland. It specifically includes these two endangered species, and it aims to help in the effort of conserving their commuting pathways. Nevertheless, it may be used for bats with similar adaptations and serve as an example for related conservation efforts on other bat species, and possibly trigger the instalment of ecological infrastructures along these corridors in general.

Materials and Methods

Study species

Ravessoud's (2017) species selection was based on the following characteristics: a) It had to be a commuting species, b) its distribution range and foraging habitats had to be well known and c) there had to be available knowledge by local experts and monitoring data for the roost's population. Along these criteria he chose *R. hipposideros* and *M. myotis.*

R. hipposideros is a small species with a very high frequency echolocation (≈ 110 kHz). This leads to a short detection range of around five meters, due to heavier attenuation of high frequencies in air. Factors such as moisture and temperature also negatively influence transmission of the bats' sound waves. Due to these limitations, *R. hipposideros* needs vertical elements in close vicinity as guidelines to commute between the roost and its foraging area (Motte & Libois, 2002; Zahn et al., 2008). *M. myotis* is larger and has an extended foraging range with longer commuting paths and it also uses vertical structures for orientation. However, it emits signals of lower frequency (≈ 25-30 kHz), allowing for an increased detection range. This makes it less dependent on close vertical objects, enabling it to commute through and forage in less structured habitat like open, deciduous forests, orchards or freshly mown meadows (Arlettaz, 1996; Audet, 1990; Drescher, 2004).

While few abundant and light tolerant species may exploit insects attracted by streetlights (Azam *et al.*, 2018; Hale and Arlettaz, 2019), *R. hipposideros* and *M. myotis* are both known to be highly sensitive to ALAN. Even at low light intensity levels, their activity numbers tend to decrease significantly (Stone et al., 2012).

Study sites

The selection of study sites was mainly determined by the availability of count data from previous research or monitoring. As this study is built upon an existing model, which is fitted to manually acquired count measurements, I had to choose among sites for which such data already existed. Because Meier (2019) and Ravessoud (2017) used comparable data collection schemes, I combined both data sets for the evaluation of locations. Veltheim – a site surveyed by Nater (2019) – was also included. As in Amsoldingen, Sachseln, Beggingen and Giswil data had been collected by both Meier (2019) and Ravessoud (2017), I initially had data of 27 sites to choose from (15 for *M. myotis* and 12 for *R. hipposideros*).

Sites were chosen by respecting all regulations of the Swiss *Federal Office of Civil Aviation (FOCA)*, which is part of the Federal *Department of the Environment, Transport, Energy and Communications (DETEC)* (FOCA, 2020). I furthermore evaluated the respective importance of each site on an implementation viewpoint. Hence, municipalities already cooperative to lighting regime implementations were favored and roosts with bigger population sizes were considered more relevant from a conservational perspective.

To safeguard model robustness and plausibly demonstrate a potential improvement in the models, I had to make sure that activity measurement sample sizes were large enough for the model fits of both species. Therefore, I split the study sites roughly among the two species, ensuring enough data for both models. My goal was to obtain aerial imagery from 10 to 20 study sites, depending on work progress and external factors such as weather conditions or flying authorization delays. As the data collection proceeded at a satisfactory pace, I managed to gather data from all 20 municipalities (Table 1), which contained twelve roosts of *M. myotis* and nine of *R. hipposideros*.[1] Veltheim was later omitted in the model fitting process due to a different study design by Nater (2019).

Ravessoud (2017) recorded species activity on three circles around the roosts, with six recordings at a radius of 60 meters, nine at 190 meters and 15 at 350 meters (Figure 1). Meier (2019) collected data at four locations on the inner (60-meter radius), eight on the middle (200-meter radius) and four on the outer circle (400-meter radius). Corresponding to the extent of these measurements and due to drone battery constraints, I chose to acquire images with an extent of 0.64 km^2 (800x800 m) and the roost at their center. These patches ensured the generation of data for all available activity measurements around the roost.

[1] Sachseln hosts both species. Commuting activity data for modelling was only available for *R. hipposideros,* however.

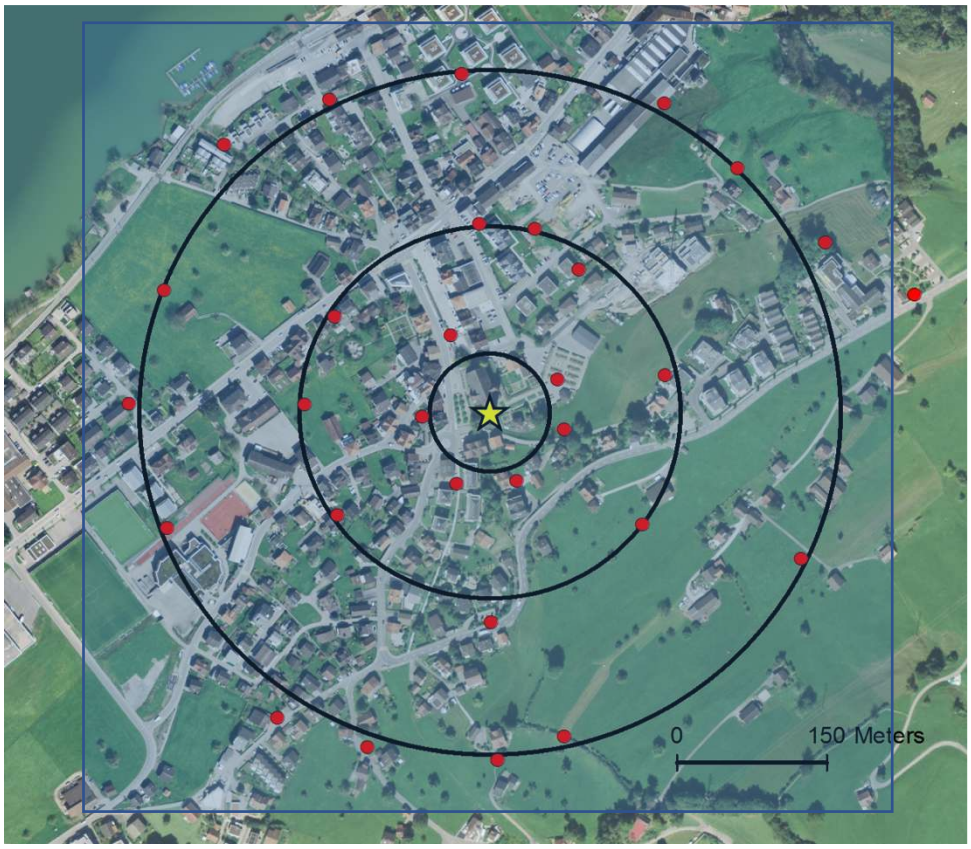

Figure 1: Example from the sampling locations (red dots) of Ravessoud (2017) in Sachseln with the three radii (60m, 190m, 350m), the roost (star) and the blue square representing the extent of my drone imagery (Source base map: Swisstopo)

Table 1: Table of selected study sites, the hosted species, census year and additional information on the population and photography time

Municipality	**Roost coordinates** (CH1903)	**Species**	**Year of census**	**Population size**	**Population trends**	**Time and date of imagery**
Veltheim (AG)	653450/254400	*M. myotis*	Nater 2018	770	Slow decline since 2012	*00:30-01:05* 20.06.20
Beggingen (SH)	682350/291275	*M. myotis*	Ravessoud 2016	488	Sharp increase until 2012, slow decline since then	*23:38-00:14* 12.-13.06.20
Altendorf (SZ)	705500/227700	*M. myotis*	Ravessoud 2016	200		*23:02-23:37* 08.07.20
Steinen (SZ)	689239/211663	*M. myotis*	Ravessoud 2016	293		*23:49-00:45* 25.-26.06.20
Kallnach (BE)	584592/207473	*M. myotis*	Meier 2019	411		*23:13-23:53* 14.07.20
Buttisholz (LU)	650150/216950	*M. myotis*	Meier 2019	569	Relatively constant	*23:24-00:12* 26.-27.06.20

Municipality	**Roost coordinates** (CH1903)	**Species**	**Year of census**	**Population size**	**Population trends**	**Time and date of imagery**
Eysins (VD)	505170/137598	*M. myotis*	Ravessoud 2016	915		*23:15-23:52* 13.07.20
Mühlau (AG)	672050/231450	*M. myotis*	Meier 2019	476	Continuous increase until 2012, stagnation since then	*22:57-23:33* 22.07.20
Courtételle (JU)	590550/243400	*M. myotis*	Ravessoud 2016	804		*23.11-23:46* 18.08.20
Burgdorf (BE)	613655/212316	*M. myotis*	Ravessoud 2016	250		*23:03-23:38* 17.07.20
Lipperswil (TG)	721375/275275	*M. myotis*	Meier 2019	186	Once more than 300 individuals, continuous decline since 2005	*23:13-23:48* 18.07.20
Sachseln (OW)	661100/191000	*M. myotis* + *R. hipposideros*	Ravessoud 2016	120		*23:12-00:19* 30.06.-01.07.20
Lumnezia Surcasti (GR)	732925/173200	*R. hipposideros*	Meier 2019	202		*20:56-22:15* 20.07.20
Lumnezia Uors (GR)	733425/173625	*R. hipposideros*	Meier 2019	234		*20:56-22:15* 20.07.20
Metzerlen-Mariastein (SO)	601965/257264	*R. hipposideros*	Ravessoud 2016	31		*23:08-23:55* 01.07.20
Amsoldingen (BE)	610680/175140	*R. hipposideros*	Meier 2019	60		*23:13-23:52* 09.07.20
Waltensburg Vuorz (GR)	728250/182000	*R. hipposideros*	Meier 2019	105		*23:14-00:53* 19.-20.07.20
Giswil (OW)	654700/187050	*R. hipposideros*	Ravessoud 2016	400		*22:48-23:30* 25.08.20
Sarnen Wilen (OW)	659820/192360	*R. hipposideros*	Ravessoud 2016	41		*23:11-23:56* 23.07.20
Castiel (GR)	765000/189750	*R. hipposideros*	Meier 2019	67		*23:02-23:55* 27.08.20

Drone imagery

To guarantee legal transparency towards municipalities I got in touch with the respective agencies for UAV operation and photography permission. Also, I contacted airports in close vicinity for authorization of my project. I used a DJI Mavic 2 Pro drone and the corresponding iPad software (*DJI GS PRO* and *DJI GO 4*) provided by DJI to control it. Images were taken at night and mostly around villages with low light contamination. Under these circumstances, the greatest challenge was to get enough light intensity onto the sensor. Maintaining high image resolution also proved to be important, as for georeferencing purposes I depended on the detection of distinct geographic locations. There were various camera and drone parameters to be tested and adjusted: Sensor sensitivity (ISO), aperture, exposure time, focus, flight height and flight speed. After assessment of a series of different test flights, the following settings were chosen, giving an optimal compromise of drone battery life, image sharpness, image noise and brightness (Table 2):

Table 2: Drone and camera settings chosen for nocturnal photography

Parameter	Specified setting
ISO sensitivity	12'800
Aperture	f/2.8
Focus	Automatic
Shutter speed	1/30 seconds
Flight height	~120 meters (80 – 160m, terrain dependent)
Flight speed	5 meters per second

By keeping sensor sensitivity, the aperture and shutter speed stable, I was able to get comparable pixel values for all sites.

Based on the inverse-square law, I expected a signal intensity drop by a quarter of the initial intensity with double the distance from a light source. However, the chosen flight height revealed that the expected light intensity drop had an influence of only 15% on the pixel cell values. As intensity declines logarithmically, most of it is already lost after a few meters from the emitting source. At heights above 60 meters, other factors – such as humidity or aerosol density – are assumed to be more influential on the absolute intensity received at the sensor. On that account I refrained from aerial height calibration of the light data. I chose a maximum difference in flight height of 60 meters for moderately steep landscapes and 80 meters for areas with very large altitude gradients. For the four alpine sites in Castiel, Surcasti, Uors and

Waltensburg-Vuorz, I neglected deep and dark valleys by simply flying over them without downwards adjustment of flight height.

Drone flying plans were constructed on an iPad, using the DJI GS PRO application, where I chose flight paths with North- and South orientation (Figure 2b). For optimal georeferencing, reproduction and battery life purposes, I set the side and front overlap of pictures at a compromise of 50%. With the chosen settings, the whole area could be covered with 10 flight lines and 20 waypoints (Figure 2b) – with an output of at least 170 images per area. For sites with larger altitude gradients, I had to split the area into segments of similar altitude not to exceed the maximum height difference of 60 or 80 meters respectively. Images were only taken during clear nights as optical sensors are susceptible to high humidity, due to the deflection and reflection of light waves through water vapor. As I wanted to visualize artificial light at night, I started recording after nautical sun dusk. Many municipalities have implemented lighting regimes which dictate streetlamps to turn off or dim late at night (often around 00:00 to 01:00). However, as bats departure earlier, I wanted to capture the actual lighting conditions present at commuting times. Therefore, I tried to retrieve all imagery before 00:00 o'clock – but technical issues led to delays for few sites (Table 1).

GIS

For image processing and analyzing I used ArcGIS Pro 2.4.3 (Esri Inc., 2019) and ArcGIS Desktop 10.6.1 (Esri Inc., 2018). Automatic georeferencing and mosaicking of the nocturnal imagery could not be applied as the images didn't provide enough tie points for the typical photogrammetric workflows used in these processes. Therefore, ground control points had to be found and assigned manually in each of the approximately 3400 pictures. After the single images were georeferenced, I made use of the *Mosaic to New Raster Tool*, which stitches the mosaic of small images together to one large raster, where overlapping pixel cell values were averaged. (see overlaps in Figure 2c).

As I retrieved a multi-band output, band calculation was necessary in order to get a valuable representation of luminance. RGB (red, green, blue) values were hereby transformed to HSL (hue, saturation, lightness). This lightness term may then be treated as a suitable representation for light intensity (Nishad & Chezian, 2013). The calculation of lightness from RGB looked as follows:

$$Cmax = \max(R, G, B)$$
$$Cmin = \min(R, G, B)$$

$$\text{Lightness} = \frac{Cmax + Cmin}{2}$$

To obtain values for lightness, one must subtract the smallest of the three RGB values from the biggest one ($C_{max} - C_{min}$) (Nishad & Chezian, 2013). This is done for every raster cell. In addition, I extracted single RGB band values from the images for spectral analysis. Usually, lightness and RGB values are transformed to a proportion scale (0-1) through a division by 255 (pixel value range for each color). For the model fit, I renounced from this step, as it was not essential. Model predictions and other plots of lightness and band parameters, however, are presented on the percentage scale (0-100).

The lightness and RGB layers were now attributed to the existing sampling points, where acoustic activity measurements of the bats had been performed. Using the *focal statistics tool* in ArcGIS, I created buffers with three different radii around these points: 2.5m, 5m and 10m. Buffer values were calculated using the mean of the pixels enclosed. Testing the best buffer size seemed important in order to get a clearer picture on how bat's sensitivity to light changes with distance to the light source. As I was dealing with large data (~2.5 Gigabytes per image), pixel resolution was initially decreased from approximately 2 centimeters to one meter. This resampling was performed using the *aggregate tool* in ArcGIS. Each output raster cell value is hereby calculated using the mean of the input cells encompassed within the one-meter extent of that cell. Measurement points on the margins of the imagery extent led to unreliably small values due to the averaging inside the buffers. Such sampling points were omitted later in the modelling process.

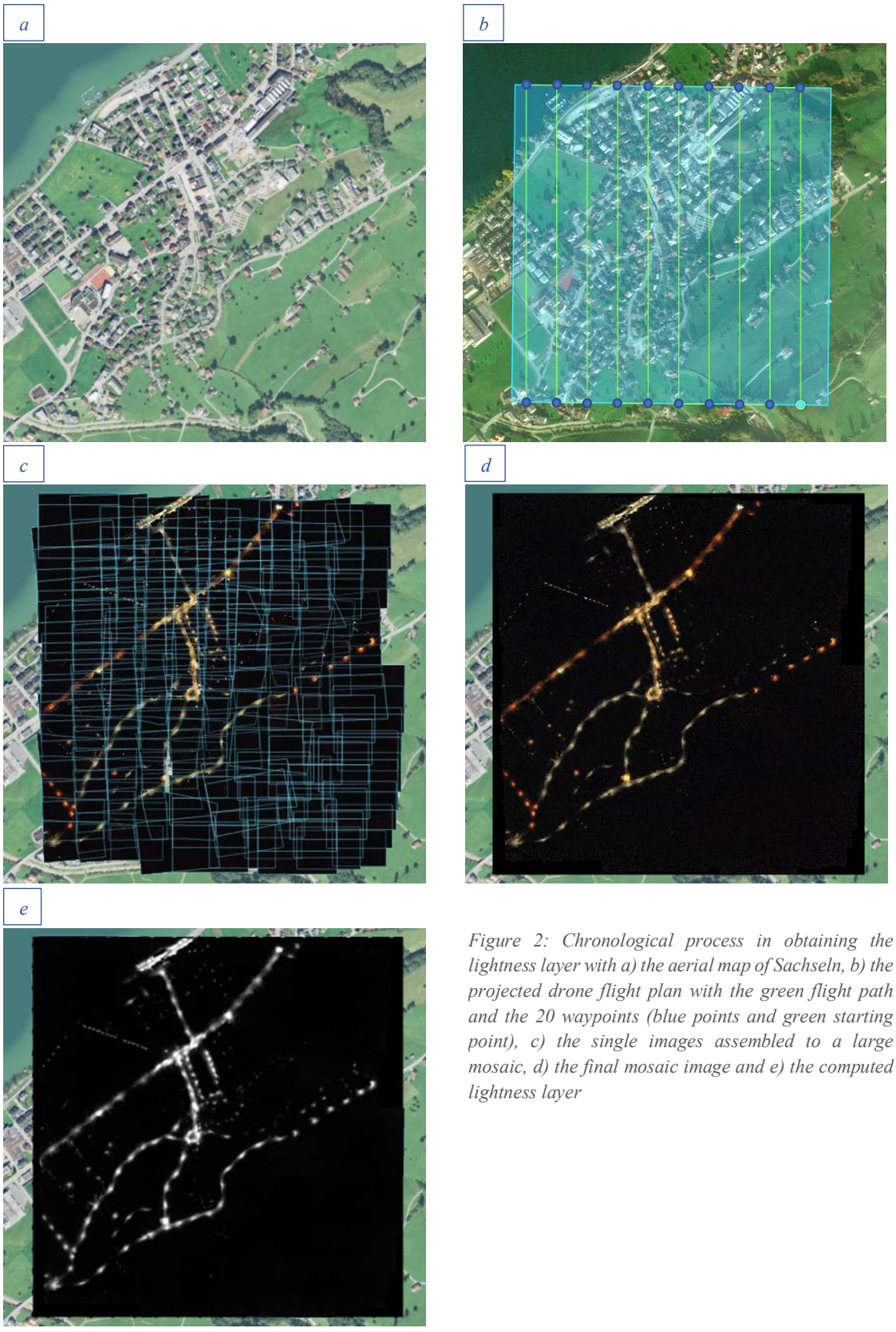

Figure 2: Chronological process in obtaining the lightness layer with a) the aerial map of Sachseln, b) the projected drone flight plan with the green flight path and the 20 waypoints (blue points and green starting point), c) the single images assembled to a large mosaic, d) the final mosaic image and e) the computed lightness layer

Collection of ground truth data and preparations for the model

As I used older commuting activity recordings (Meier, 2019; Ravessoud, 2017) as the dependent variable in my model, I had to ensure, that lighting regimes hadn't changed significantly over the study years. Therefore, I partially replicated the manual Luxmeter measurements for 49 random data points. All hand measured Lux data was sourced during the same time as drone imagery was retrieved (around 23:00-00:00). I used the same measurement scheme as Ravessoud (2017) and Meier (2019), recording five lux measurements for each sampling point – one in the middle and four with a distance of two meters in each cardinal direction. The old and new measurements correlate with $R^2 = 0.59$ and $p < 0.001$ (Figure 3).

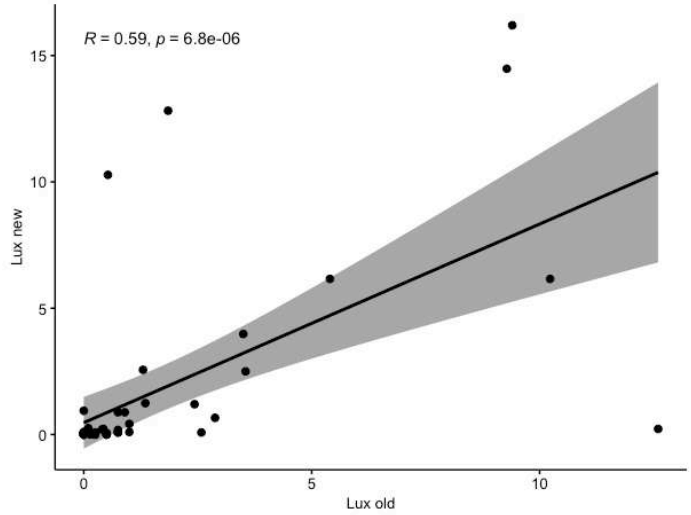

Figure 3: Correlation between old and new upward Lux measurements (n = 49)

I also tested the correlation of hand lux measurements and the lightness variable extracted from the UAV imagery[2]. This ground truth lux data was also conducted with five measurements per data point at two meters above ground, but by turning the Luxmeter upside down the aerial perspective of the camera sensor was simulated.

Furthermore, spectral ground truth data was collected to connect the RGB data to actual spectral indices in the field. I used the MavoSpec Base spectrometer from Gossen to measure spectral irradiance at various site locations. Data sourcing proved to be challenging, however, as the spectrometer sensor was not as sensitive as the one from the luxmeter. Therefore, the spectrometer requires an increased minimal irradiance to generate data. Hence, I couldn't record spectral data at random points on the sites and holding the device facing downwards was

[2] For all the lightness correlations I chose the 5-meter buffer as it best represented the five manual measurements.

also unfeasible. I measured direct irradiance of streetlamps, however, and obtained data from 19 LED lamps and 18 others (mostly high-pressure sodium-vapor lamps). To test the correlation between RGB measures and my ground truth measurements, I first visually analyzed the spectral outputs of the spectrometer for the two streetlamp categories (Figure 4). Based upon these, I chose long (595 nm) and short (445 nm) wavelength peaks to correlate with the red and blue band respectively. [3]

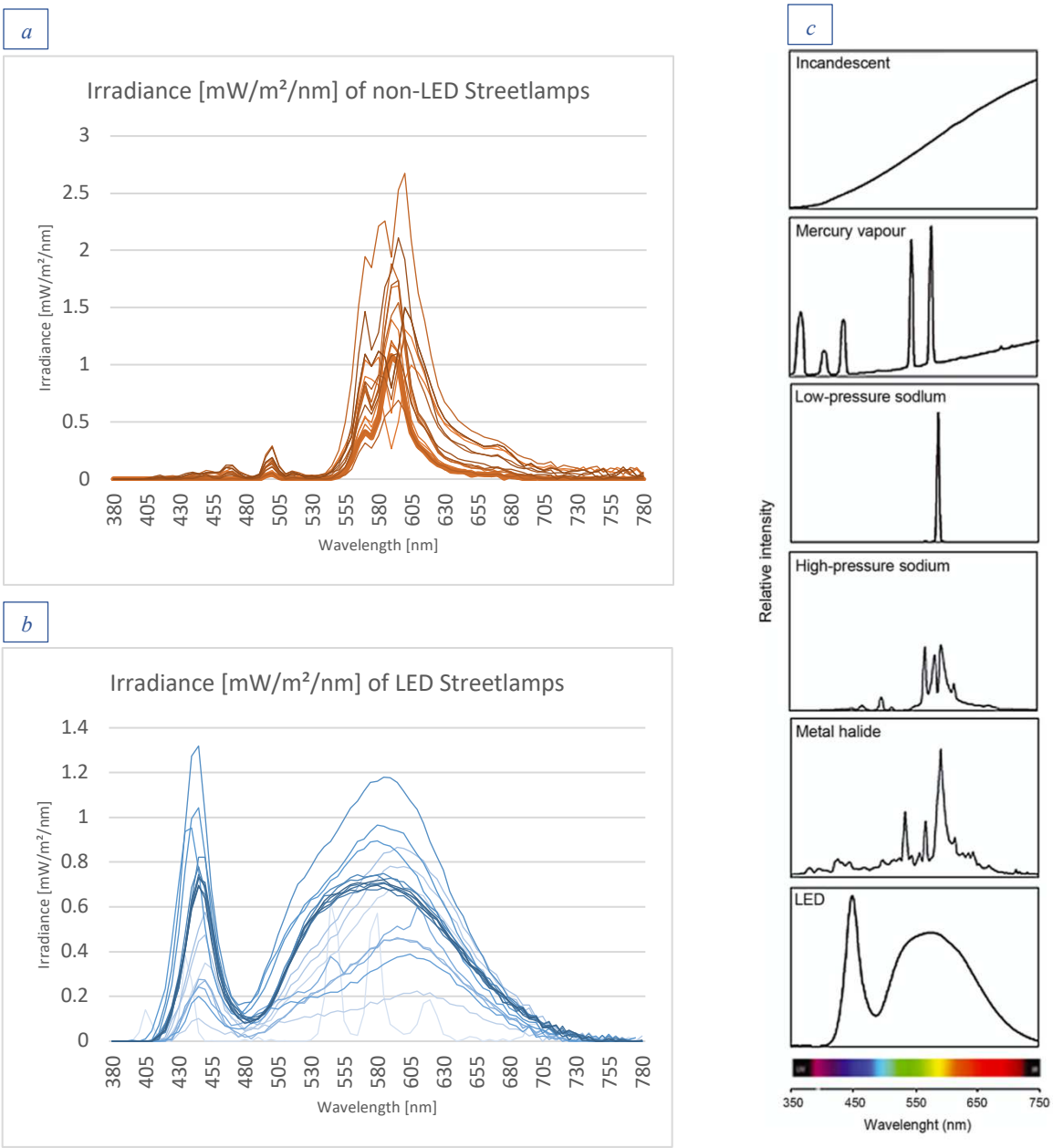

Figure 4: Measured irradiance of a) non-LED streetlamps and b) LED streetlamps; c) Representation of spectral signatures from various streetlamp types (Gaston et al., 2013); LED streetlamps radiate over a broader spectrum, but have a lower peak irradiance compared to traditional lamps

[3] For all the band correlations I chose the 2.5-meter buffer as it best represents the single measurements.

Generalized linear mixed effects model

Using the centered and scaled predictors chosen by Ravessoud (2017) and including my new lightness variable, I fitted a generalized linear mixed effects model (GLMM) to the data. After the omission of rows with missing values, there were a total of 393 observations (n) for *R. hipposideros* and 422 for *M. myotis*. The model fit was obtained with a *glmmTMB* model from the *glmmTMB* package (Brooks et al., 2017) in R Studio 1.3.1 (RStudio Team, 2019) using R statistical software 4.0.3 (R Core Team, 2020). As commuting count data was collected at different days and varying sites, I expected it to be hierarchically structured. Therefore, I included the factor variables *Community* (roosting site), *Location* (measurement locations within the sites) and *Day* (recording day) as random effects. For some communities there were commuting counts at different days due to the merging of count data from Ravessoud (2017) and Meier (2019). The random effects as structured should account for correlation structures within *Community* and *Day.* The three levels of *Radius* were integrated into the model as a fixed effect.

Meier (2019) recorded roost departure activity per night for a duration of 1:15 hours for *R. hipposideros* and 1:25 hours for *M. myotis,* while Ravessoud (2017) recorded for 1:30 hours and 2 hours respectively. These different recording lengths had to be accounted for by using an offset in the model. The offset can be applied to transform an integer response to rates. Therefore, I included the logarithm (see link function on the following page) of duration in hours as an offset, leading to rates of activity per hour.

In GLMMs, there are various techniques for parameter estimation. I used the Laplace approximation as the parameter estimation method, as it is more accurate than the widely implemented Penalized quasilikelihood technique (Table 3). I refrained from choosing even more accurate methods as they were not feasible for the model selection in later stages. Hence, I followed Benjamin Bolker, one of the authors of the *glmmTMB*-Package, proposing to choose "the most accurate method that's available and feasible" (Bolker, 2019).

Table 3: GLMM parameter approximations, their advantages and disadvantages and software packages that implement them (Bolker et al., 2009)

Technique	Advantages	Disadvantages	Software
Penalized quasilikelihood	Flexible, widely implemented	Likelihood inference inappropriate; biased for large variance or small means	PROC GLIMMIX (SAS), GLMM (Genstat), glmmPQL (R), glmer (R)
Laplace approximation	More accurate than PQL	Slower and less flexible than PQL	PROC GLIMMIX [56], glmer (R), glmm.admb (R), AD Model Builder, HLM
Gauss-Hermite quadrature	More accurate than Laplace	Slower than Laplace; limited to 2–3 random effects	PROC GLIMMIX [56], PROC NLMIXED (SAS), glmer (R), glmmML (R)
Markov chain Monte Carlo	Highly flexible, arbitrary number of random effects; accurate	Very slow, technically challenging, Bayesian framework	WinBUGS, JAGS, MCMCpack, (R), AD Model Builder

Dealing with count data, I expected the activity measurements to follow a Poisson distribution, where mean and variance of the response are assumed to be equal. However, I chose a negative binomial distribution model with a log link function to account for overdispersion and avoid potential pseudoreplication. The negative binomial distribution has one parameter more than the Poisson regression, making it more suitable for the data (Figure 5), as the variance is assessed independently from the mean (Bliss & Fisher, 1953).

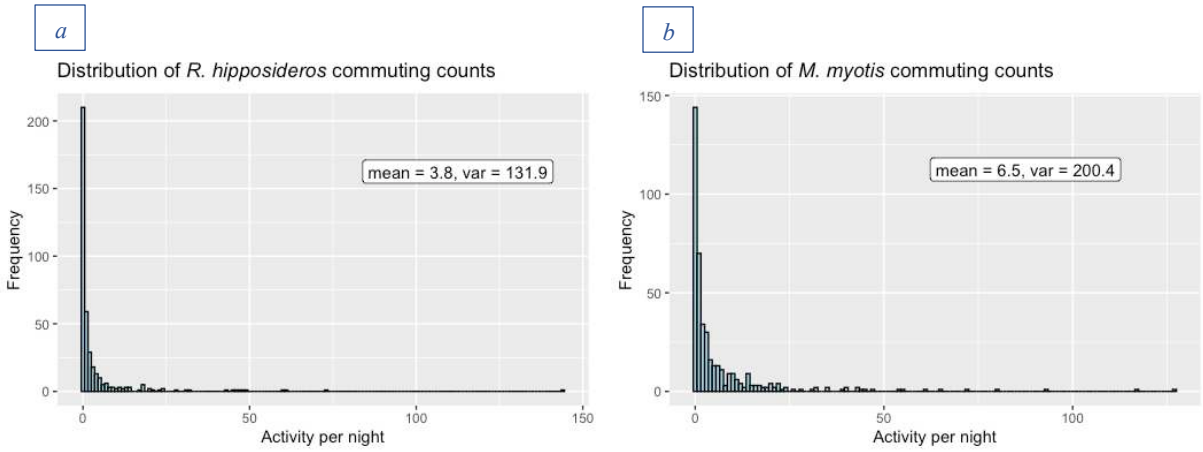

Figure 5: Commuting count distributions for a) R. hipposideros and b) M. myotis

Additionally, I tested the models of both species on zero-inflation. Residual diagnostics on dispersion and zero-inflation were performed with the simulated residuals approach provided by the *DHARMa* package (Hartig, 2020). Both models were able to account for zero-inflation and overdispersion, showing no significant deviations from the observed simulated residual distribution to the expected distribution under the fitted model. As a zero-inflation parameter wasn't necessary, I kept the negative binomial models without the additional parameter.

Variable selection

The *glmmLasso* (Groll, 2017) model fit (Ravessoud, 2017) led to the selection of some quadratic variables without the respective linear one and some collinearity issues. As the LASSO model served for predictive purposes only, there was no need to account for such phenomena (Graham, 2003). However, I was interested in how and to what degree my various predictor variables impact the response variable and therefore in the interpretation of effect sizes and significances of the predictors in the model. Hence, the selected predictors by Ravessoud (2017) needed some adjustments.

Following Peixoto (1990) I included linear terms where only the quadratic ones were retained by the LASSO model. Peixoto defines such a model structure to be “hierarchically well formulated” (Peixoto, 1990:28). To justify the retention of the higher term, I tested individual models with the first and the second order variables – creating also a higher degree variable for lightness. Only in case of a significant improvement of fit based on a likelihood ratio test (LRT; see *tests and assessment of model fit*), I kept the bigger model with the second order variable. Otherwise, only the linear predictor was retained.

Multicollinearity had to be avoided. Therefore, I centered linear terms before computing the second order term and removed correlations with Pearson’s R^2 of 0.7 or higher. Choosing between intercorrelated variables was conducted along the following procedure: 1. Which variable is ecologically more meaningful? 2. Which variable contributes more to the overall goodness of fit based on AIC (see *tests and assessment of model fit*). Comparisons of AIC were performed by fitting smaller models including only the respective fixed effects. The remaining predictors were chosen for the model (Table 4 | Table 5).

Table 4: Selected variables for R. hipposideros, their scales and metrics and additional implementations

Variable	**Scale** [m]	**Model abbreviation**	**Computation and metric**	**Additional implementations** (computational and ecological)	**Source**
Lightness	2.5	Lightness_a1_b2_5	Mean Lightness value calculated from RGB bands	Light barrier	Mavic Pro 2 multiband RGB imagery
Structure $ruggedness_v$ Structure $ruggedness_v^2$	5	SAVav0 SAVav0_qd	Mean ruggedness value of structure surface with height >3m: calculated with vector method	Vegetation and buildings	nDSM-ADS
Open ground Open $ground^2$	10	OGcv0 OGcv0_qd	Cover percentage of all surfaces which are not in: Water, Buildings, Forest, Isolated trees, Tree lines, Artificial Tree Groups, Lidar elements	Barrier due to absence of vertical structures for orientation	$SwissTLM^{3d}$ v 1.4
Terrain $ruggedness_v$	5	TEVav0	Mean Ruggedness value of terrain surface (at ground level) calculated with vector method	Potential guidelines at ground level	DTM-Lidar
Terrain $ruggedness_v$	25	TEVav2	Mean Ruggedness value of terrain surface (at ground level) calculated with vector method	Potential guidelines at ground level	DTM-Lidar
Terrain $ruggedness_t$	5	TETav0	Mean Ruggedness value of terrain surface (at ground level) calculated with terrain method	Potential guidelines at ground level	DTM-Lidar
Radius		Radius	a = 60m from roost b = 190/200m from roost c = 350/400m from roost	Measurement points on radius	

ADS hereby is a color intensity-based method for the extraction of structures heights and the computation of various height models. Other height models are calculated from Lidar data. $SwissTLM^{3d}$ is the Swiss Federal vector-based topographic landscape model. Ruggedness measures are generally calculated with either of the three methods: Vector (Sappington, Longshore and Thompson, 2007), terrain (Riley et al., 1999) or curvature[4].

[4] https://pro.arcgis.com/en/pro-app/latest/help/analysis/raster-functions/curvature-function.htm

Table 5: Selected variables for M. myotis, their scales and metrics and additional implementations

Variable	**Scale** [m]	**Model abbreviation**	**Computation and metric**	**Additional implementations** (computational and ecological)	**Source**
Lightness	10	Lightness_a1_b10	Mean Lightness value calculated from RGB bands	Light barrier	Mavic Pro 2 imagery
Structure height	5	SLHav0	Mean height of structures	Vegetation and buildings	nDSM-Lidar
Structure height Structure height^2	25	SLHav2 SLHav2_qd	Mean height of structures	Vegetation and buildings	nDSM-Lidar
Structure Edge density Structure Edge density^2	25	SAed2 SAed2_qd	Edge density of vertical structures with height >3m	Vegetation and buildings	SHM (VHM+Buildings)
Terrain ruggedness$_c$	10	TECav1	Mean Ruggedness value of terrain surface (at ground level) calculated with curvature method	Potential guidelines at ground level	DTM Lidar
Structure ruggedness$_c$	25	SLCav2	Mean ruggedness value of structure surface with height >3m: calculated with curvature method	Vegetation and buildings	nDSM-Lidar
Canopy ruggedness$_c$	5	CACav0	Mean ruggedness value of canopy surface of vegetation with height >3m: calculated with curvature method	Vegetation only	nDSM-ADS
Tree Cover	25	CAcv2	Cover percentage of vegetation with height >3m	Vegetation only	VHM-ADS
Distance to road	distance to street polygons	R2di	Shortest distance to street polygon	Roads from 1m wide to highways; railways Barrier: Traffic, light, noise	SwissTLM^{3d} v 1.4
Radius		Radius	a = 60m from roost b = 190/200m from roost c = 350/400m from roost	Measurement points on radius	

Finalizing the model

With the remaining predictors I fitted negative binomial *glmmTMB* models with the following structures:

```
glmmTMB_RHI_fuchs_final <- glmmTMB(Activity_per_night ~ Lightness_a1_b2_5+OGcv0+SAVav0+TETav0+TEVav0+
          TEVav2+OGcv0_qd+SAVav0_qd+Radius+
          (1|Gemeinde)+(1|Site_ID_Projekt)+(1|Day),
        data = RHI, family = "nbinom2", offset = log(Duration_in_hours))
```

```
glmmTMB_MYM_fuchs_final <- glmmTMB(Activity_per_night ~ Lightness_a1_b10+R2di+SAed2+CACav0+CAcv2+SLCav2+SATav1+
                                     SLHav0+SLHav2+TECav1+SLHav2_qd+CAcv2_qd+SATav1_qd+Radius+
                                     (1|Gemeinde)+(1|Site_ID_Projekt)+(1|Day),
                                   data = MYM, family = "nbinom2", offset = log(Duration_in_hours))
```

Figure 6: Model structures in R: RHI (R. hipposideros) and MYM (M. myotis) are respective species abbreviations. Gemeinde (Community), Site_ID_Projekt (Location) and Day are crossed random effects. Activity_per_night is the dependent variable and the offset is set to Duration_in_hours. The link function is set to log by default

These final *glmmTMB* models were checked for linearity on the model's log scale by once again making use of the rescaled *DHARMa* residuals. No suspicious occurrences concerning non-linearity, zero-inflation, overdispersion or general misfit (Kolmogorov-Smirnov Test) were detected.

Using the *dredge* function from the *MuMin* package (Bartoń, 2020), I ran an automated model selection with AICc (see *tests and assessment of model fit*) as the sorting criterion. All models within an AICc difference of ≤ 2 from the best model were weighted and averaged using the model averaging function in *MuMin*. To assess the factor lightness in the model, I also computed an averaged model without a light variable and one with the old manually retrieved lux variable. Coefficients of such model averagings are either computed fully or conditionally. Conditional techniques only average over models, where a certain parameter appears, while in the full average the parameter is set to zero if it's not in the model. Therefore, full averages are less vulnerable to biasing the estimate away from zero. For my study, I preferred the less biased full coefficients.

The best models including the extracted spectral variables from the three single band (RGB) values were also averaged. As the RGB parameters and lightness were all intercorrelated, I fitted four separate models for each species with either of the four variables R-, G-, or B-Band and Lightness. Model fit was then analyzed with AICc.

Tests and assessment of model fit

Variable and model selection was mostly based on model goodness of fit determined by the Akaike Information Criterion (AIC) (Akaike, 2011). AIC hereby has the ability to consider both model fit (like conventional R^2 measures) and complexity. It specifically allows the simultaneous comparison of multiple models with nested and non-nested structures as it approximates the information lost – the Kullback-Leibler divergence (Kullback & Leibler, 1951) – by estimating reality with the fitted model (Burnham & Anderson, 2004; Johnson & Omland, 2004). It is used in various fields of ecology (Burnham, Anderson, & Huyvaert, 2011) or psychology (Wagenmakers & Farrell, 2004) and widely believed to be the most convincing measure for mixed model comparison due to it's high flexibility and generality. For models including all predictors I depended on the corrected AIC (AICc), as it is more suitable for complex models with relatively small sample sizes (Hurvich & Tsai, 1989; Burnham & Anderson, 2004).

I also compared the best pre-averaged models on the basis of Nakagawa and Schielzeth's (2013) R^2 term for GLMMs. It is comprised of two outputs: The marginal R^2 and the conditional R^2. The former provides the variance explained only by fixed effects and the latter provides the variance explained by the entire model – including random effect variance. It can be a useful addition to AIC measures for model fit assessment. Nakagawa and Schielzeth (2013) themeselves state, that it "should only be used on models that have been checked for quality by other means" and despite a few limitations it "will be a useful summary statistic of mixed-effects models for both biologists and other scientists alike".

Displayed p-values of the averaged model predictors are based on the Wald Z-statistics. These test the null hypothesis by scaling parameter estimates by their approximated standard errors and comparing the resulting test statistic to zero (Bolker et al., 2009). To determine the contribution of single predictors, however, the likelihood ratio test (LRT) supplies a more sophisticated alternative (Bolker, 2021). It assesses the goodness of fit of two nested models by comparing their likelihood function. One model is hereby bigger – including all parameters – and the other is stripped from a parameter. I therefore tested the effect of my lightness parameter by fitting a model without lightness and performing an LRT with the *anova* function and χ^2 as the test statistic. As *anova* can't be performed on averaged models, I chose the best pre-averaged models with and without the lightness predictor. LR tests can also prove valuable in analyzing the significance of random effects (Bolker, 2021). By fitting three models with either one random variable removed, I additionally assessed the random variables. However, as the

random effects are a representation of the experimental design structure, it is advised to retain the random effects even if they are not significantly contributing to a better fit. Otherwise, one performs what Hurlbert (1984) defined as *sacrificial pseudoreplication*.

Displaying individual effects

Prediction plots of the individual effects of the final averaged model with confidence intervals proved to be unfeasible, as there were technical issues with the extraction of the random effects uncertainty. I therefore decided to compute predictions from the best pre-averaged models containing the respective predictor. Intervals were calculated with the *ggpredict* function from the *ggeffects* package (Lüdecke, 2018) and the plots were produced for the three radius levels.

Predictive spatial modelling

To visualize the enhanced predictive performance of my new model, the coefficients of the chosen variables were integrated into a GIS to compute habitat suitability maps (HSM). Following the same steps as Meier (2019), the inverses of the HSMs were used to generate resistance maps. These resistance maps served as input in Linkage Mapper 2.0 for ArcGIS (Gallo & Greene, 2018) to calculate corridors of least cost from the roost to potential foraging grounds. Additionally, corridor connectivity was predicted according to circuit-theory, which allows to obtain multiple corridors of small cost based on the principles of current flow, where landscapes are depicted as conductive surfaces. Low resistances hereby represent areas of increased movement and high resistances are assigned to low movement or even impermeable barriers (B. McRae & Shah, 2009). Meier (2019) describes circuit-theory to be widely applicable in connectivity science and conservation, as it can characterize relative frequency of movements along various possible paths through heterogeneous landscapes (Braaker et al., 2014; Malakoutikhah et al., 2014; Yoon et al., 2019). Circuitscape 4.0 for ArcGIS (B. H. McRae et al., 2013) was applied to model current density as probability of bat commuting by choosing the roosts as the electric source and forest polygons in the vicinity as the respective grounds. The various outputs were computed on the basis of my averaged model including light as well as the one without light.

To compare the spatial corridor model improvement, I additionally subtracted the current flow map without lightness from the one with lightness. Positive pixel values of these difference maps may then be interpreted as an increase in modelled current flow density when the lightness

variable is included and negative values indicate a decrease in expected commuting with the inclusion of a lightness predictor. For better visualization and comparability, I reclassified the difference maps into eleven classes with intervals of 0.002. The uppermost class includes pixel values above 0.01 while the lowest class contains all values of -0.01 and below. Cells with values from -0.002 to 0.002 were excluded and classified as *no difference*.

Results

As the aim of this study was to test the capabilities of a UAV-obtained lightness variable in modelling of bat commuting corridors, I focus results and their subsequent discussion especially on the lightness parameter. Concerning other variables, only the most significant ones are discussed in this paper.

Ground truth data

My lightness measure correlates strongly with the downwards measured lux data (Figure 7a: $R^2 = 0.84$ | $p < 0.001$ | $n = 41$). Similarly, there is a high correlation between all available upwards measured lux data (Figure 7b: $R^2 = 0.71$ | $p < 0.001$ | $n = 914$) and lightness. Measuring lux downwards, proves to be a better technique in retrieving ground truth data for the lightness variable from drone imagery.

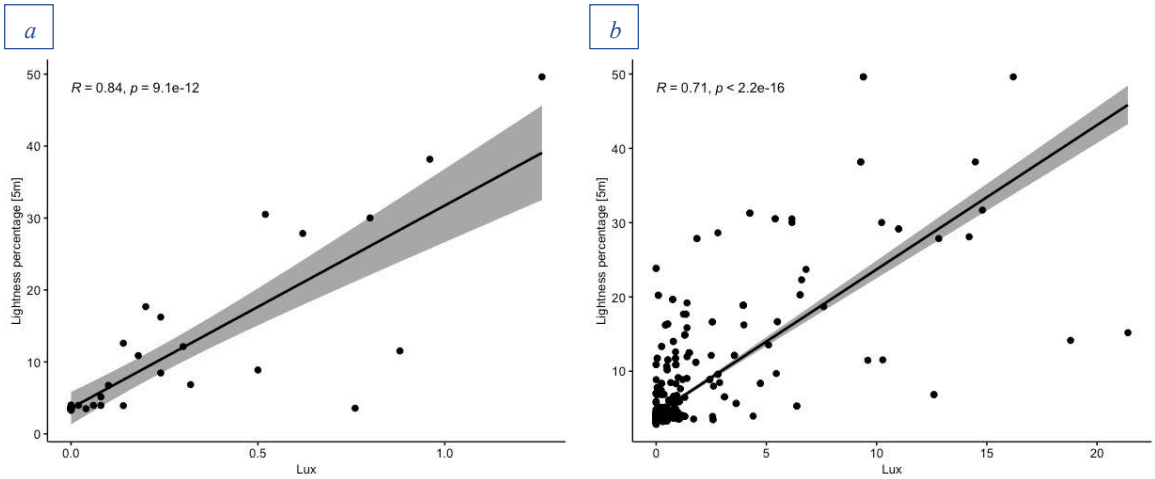

Figure 7: Correlation between Lightness and a) downward Lux measurements (n = 41) b) upward Lux measurements (n = 914)

Additionally, the peak irradiance values from the streetlamps were found to be correlated to the red and blue bands (Figure 8). The long wavelength red peak and the red channel correlate with R^2 of 0.61 ($p < 0.001$ | $n = 37$) and the short wavelength blue peak relates to the blue band with an R^2 of 0.45 ($p < 0.01$ | $n = 37$).

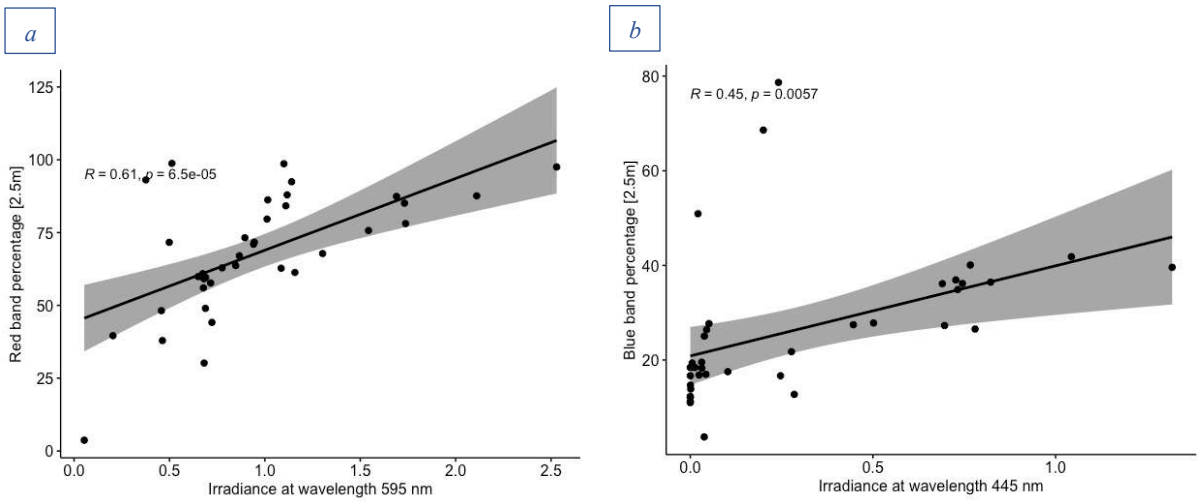

Figure 8: Correlations between a) red band percentage and measured peak irradiance at wavelength 595 nm and b) blue band percentage and measured peak irradiance at wavelength 445 nm (n = 37)

Linear mixed modelling

Lesser horseshoe bat (*Rhinolophus hipposideros*), RHI

Model selection and averaging of the *R. hipposideros* model led to the following predictors, effect sizes and Wald p-values:

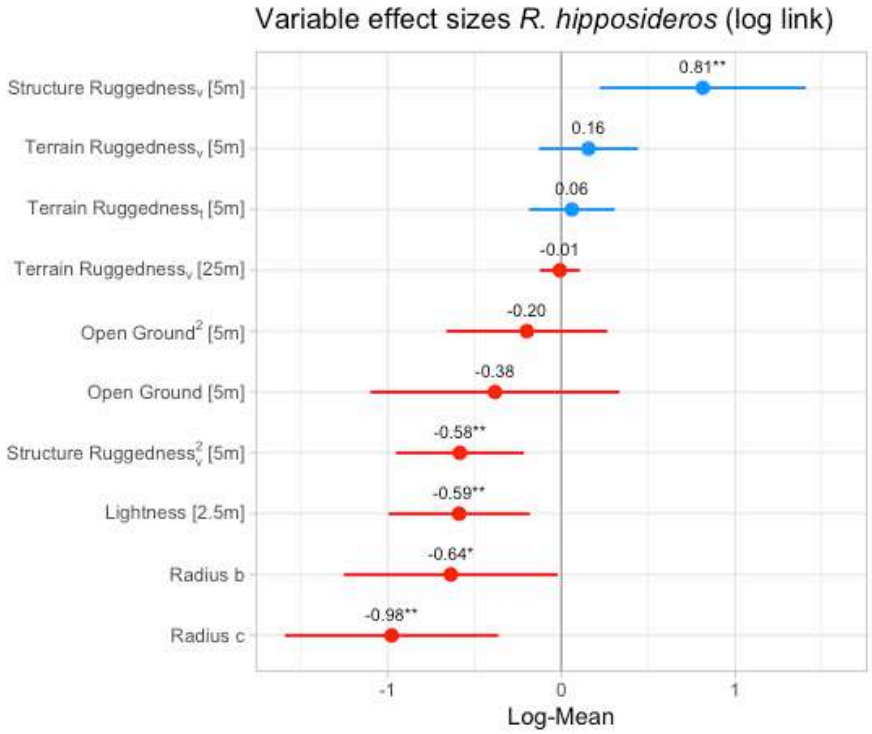

*Figure 9: Modelled variable effect sizes for R. hipposideros presented on the log link scale. Significance codes: $\alpha < 0.001$***, $\alpha < 0.01$**, $\alpha < 0.05$**

Table 6: RHI model summary table including coefficients, standard errors and p-values

Predictor	Estimate	Std. Error	Adjusted SE	z value	Pr(>|z|)
Intercept	-0.56727	0.39291	0.39415	1.43925	0.15008
Lightness [2.5m]	-0.58868	0.20717	0.20782	2.83264	0.00462 **
Open ground [5m]	-0.38241	0.36570	0.36611	1.04453	0.29624
Open ground^2 [5m]	-0.19841	0.23637	0.23668	0.83830	0.40186
Radius b (190/200m distance to roost)	-0.63618	0.31314	0.31412	2.02529	0.04284 *
Radius c (350/400m distance to roost)	-0.97716	0.31278	0.31375	3.11440	0.00184 **
Structure ruggedness$_v$ [5m]	0.81407	0.30225	0.30277	2.68876	0.00717 **
Structure ruggedness$_v^2$ [5m]	-0.58407	0.18740	0.18786	3.10903	0.00188 **
Terrain ruggedness$_v$ [5m]	0.15627	0.14539	0.14561	1.07316	0.28320
Terrain ruggedness$_t$ [5m]	0.06019	0.12560	0.12578	0.47858	0.63224
Terrain ruggedness$_v$ [25m]	-0.00893	0.05893	0.05908	0.15122	0.87981
*Significance codes: $\alpha < 0.001$***, $\alpha < 0.01$**, $\alpha < 0.05$**					

LIGHTNESS

Based on the Wald Z-statistic, the newly obtained lightness variable is clearly significant ($p < 0.01$) within the averaged model and the coefficient ($\beta = -0.59$) indicates a strong negative effect on bat activity. With a standard error of 0.21, 95% Confidence intervals for the lightness coefficient are estimated at -1.00 and -0.18 respectively.

Comparing the full averaged model to the one without a lightness parameter, I detected a significant improvement in model fit. The model including the lightness variable incorporates models with AICc values ranging from 1399.08 to 1401.07, while AICcs of the one with no lightness term lie between 1407.53 and 1409.46.

Tested with LRT, I additionally observed that the bigger model (including lightness) accounts for significantly more of the variability in the activity data than the smaller one (no lightness) ($p < 0.01$).

Table 7: ANOVA table comparing the best models with and without lightness

```
                          Df    AIC    BIC  logLik deviance  Chisq Chi Df Pr(>Chisq)
RHI_bestmodel_noLightness 12 1408.5 1456.2 -692.24   1384.5
RHI_bestmodel_Lightness   13 1399.9 1451.5 -686.94   1373.9 10.593      1   0.001135 **
---
Signif. codes:  0 ‘***’ 0.001 ‘**’ 0.01 ‘*’ 0.05 ‘.’ 0.1 ‘ ’ 1
```

R^2 measures also show an increase in variance explanation for the lightness model (Table 8). Especially, when only the fixed effects are assessed (marginal R^2), an increase in model fit (no light: 0.206 | light: 0.267) can be detected. The conditional R^2 on the other hand doesn't increase much when including lightness into the model. However, the estimates of random effect variances are expected to be imprecise when the predicted distribution mean of the response is as small as in my model. According to Lüdecke et al. (2020) this can lead to explicitly unreliable conditional R^2 calculations.

Table 8: Nakagawa and Schielzeth's marginal and conditional R^2 measures for RHI

Best pre-average models	**Marginal R^2**	**Conditional R^2**
No lightness	0.206	0.763
Lightness	0.267	0.766

The best pre-averaged model predicts an exponential decrease in commuting activity of *R. hipposideros* with increase of luminance (Figure 10a). There is hardly any activity expected at 20 percent lightness with the highest prediction of 0.13 counts per night on the innermost radius a. At 30 percent, the model already predicts less than 0.02 counts per night on the inner radius.

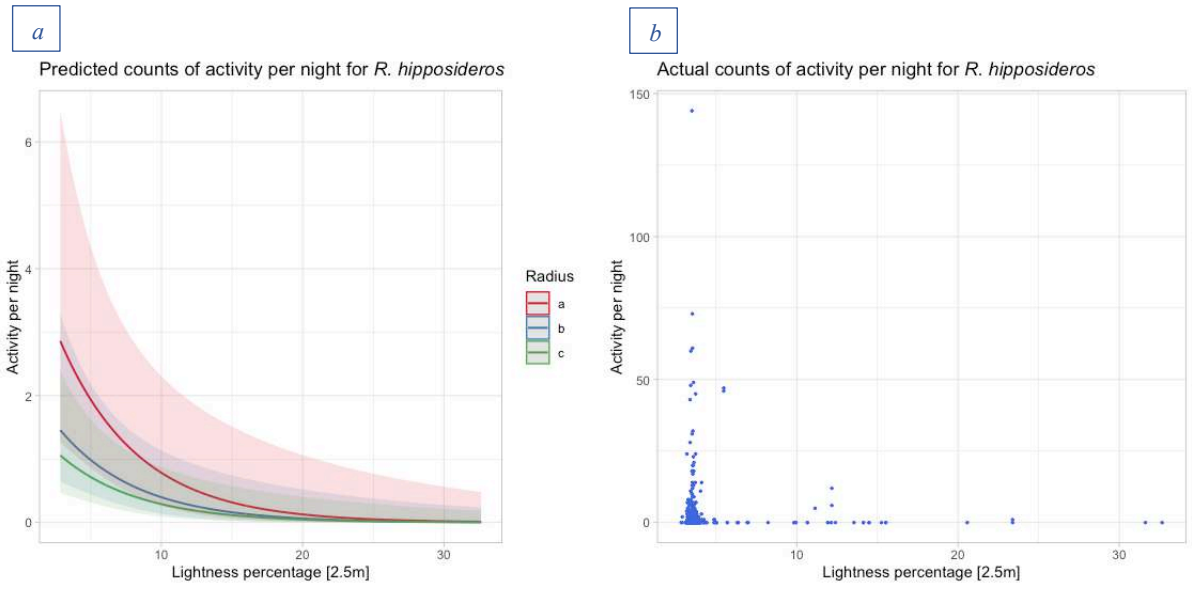

Figure 10: a) Model predicted relationship between commuting activity and lightness [2.5m] compared to b) actual counts of commuting activity

STRUCTURE RUGGEDNESS

This measure represents the mean ruggedness of all buildings and vegetation above three meters at a 5-meter resolution. Both the linear and the quadratic variable were kept in the model. The model fitted coefficients of 0.81 and -0.58 for the linear and the quadratic term respectively and both variables have a highly significant effect on activity based on the Wald test ($p < 0.01$). The opposite directions of the first and second order parameters propose a parabolic relationship between structure ruggedness and commuting activity of *R. hipposideros*. Prediction plots emphasize such observations (Figure 11a). The model predicts that the Lesser horseshoe bat highly favors rugged structures compared to smooth structure surfaces. However, if structures are too coarse, they are apparently avoided by this species.

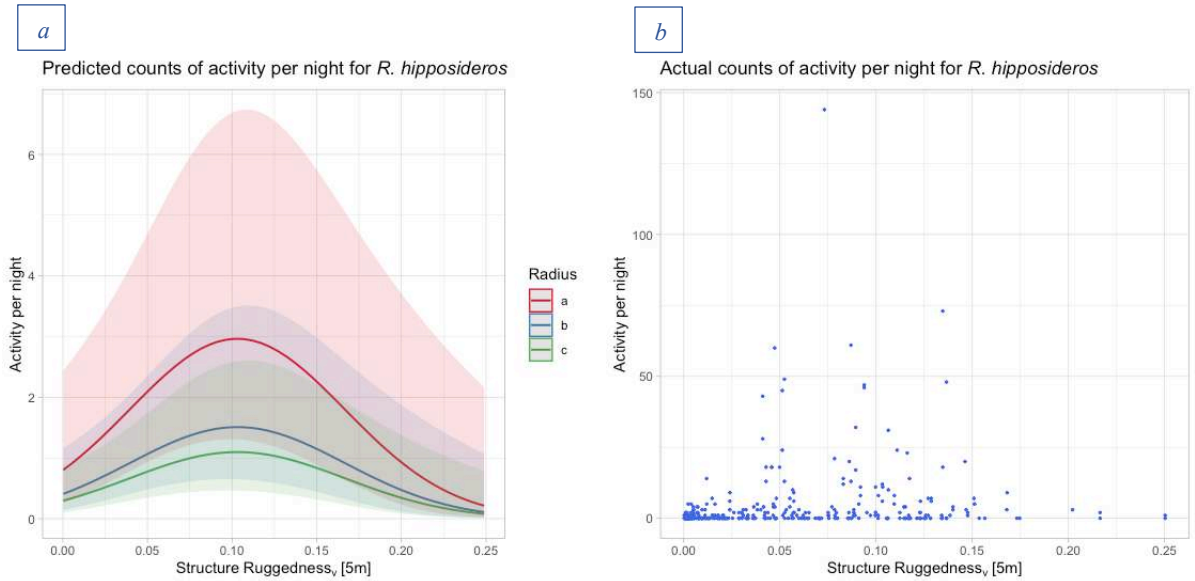

Figure 11: a) Model predicted relationship between commuting activity and structure ruggedness [5m] compared to b) actual counts of commuting activity

TERRAIN AND GROUND MEASURES

Along with the structure ruggedness variable, there are several terrain measures left in the model. All these ground parameters aren't significant in the model fit and confidence intervals reach beyond the zero threshold – meaning the assumption that the direction of the effect size is correctly translated onto the model fit is not supportable. However, both the linear and the quadratic open ground coefficient approximations lie considerably below zero on the log scale (-0.38 and -0.20) but with high standard errors (0.37 and 0.24). From 0 to 40% open ground cover, the model predicts an increase in commuting activity and a slightly stronger decrease for percentages above 40 (Figure 12a).

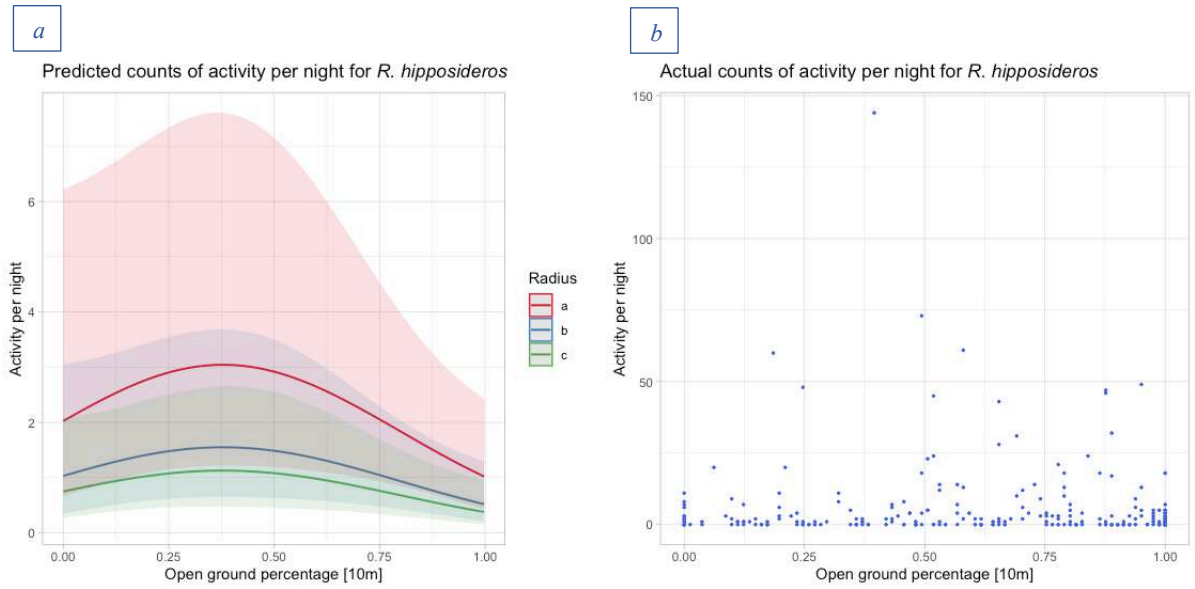

Figure 12: a) Model predicted relationship between commuting activity and percentage of open ground [5m] compared to b) actual counts of commuting activity

RADIUS

The radius variable represents distance to the roost. Increasing roost distance contributes significantly to bat activity. Radius c – which includes measurements furthest from the roost – has the strongest and highly significant negative effect on *R. hipposideros* in the model (β = -0.98 | $p < 0.01$). The also significantly negative coefficient for the middle radius b (β = 0.64 | $p < 0.05$) proposes a consistent activity decrease with increased distance from the roost (Appendix Figure_A 1).

LUX AND SPECTRAL BANDS

Comparing the model including my lightness predictor to the one with the lux variable, I found the lux model to fit the activity data slightly better (Δ AICc: 3.59). With a maximum AICc of 1449.11, the averaged lux model outperforms all other RHI models. Furthermore, the effect size of the lux variable is highly negative (β = -1.39). However, as the standard error for lux is very large (0.54), it is less significant in its model than the lightness variable (p = 0.01). Concerning spectral analysis, goodness of fit decreases with shorter wavelengths. The model with a long wavelength predictor (red band) outscores the one integrating the short wavelength spectral band (blue) (Δ AICc: 5.04). Red and green band models also perform better than the lightness model (Table 9).

However, when comparing modelled coefficients, the blue band variable has the highest effect on the model fit compared to all the other imagery-based variables. In summary, the variables retrieved from my drone imagery contribute similarly to their models with similar effect sizes and overall model performances. The prediction plots for the two extreme spectral outputs (red and blue) indicate a steeper declining curve for the blue band predictor (Figure 13a,c). This is in accord with the effect sizes.

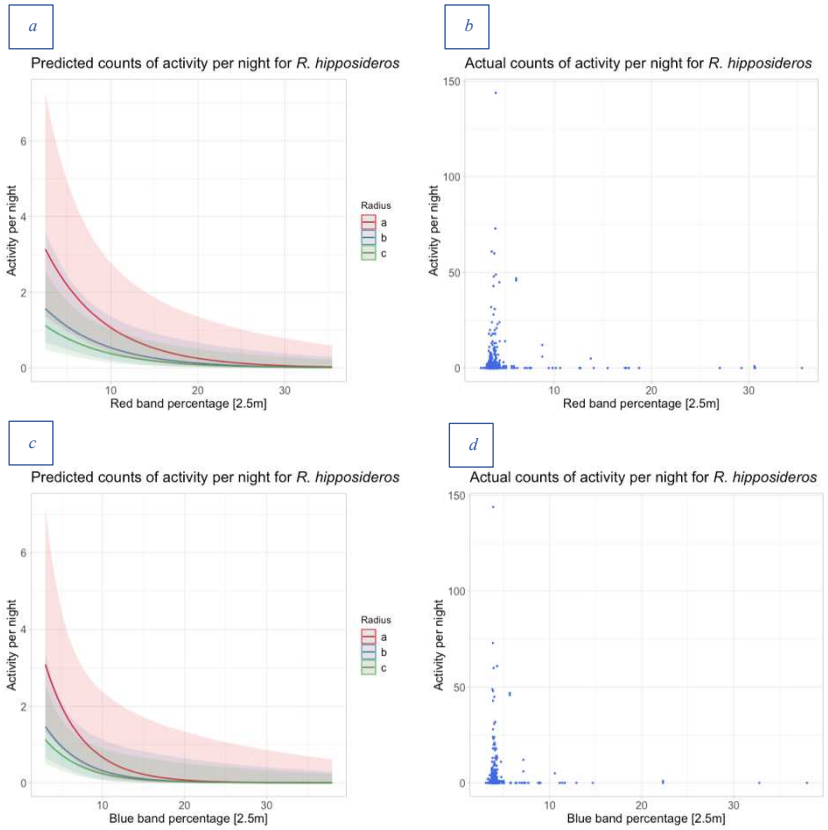

Figure 13: a) Model predicted relationship between commuting activity and percentage of red [2.5m] compared to b) actual counts of commuting activity

c) Model predicted relationship between commuting activity and percentage of red [2.5m] compared to d) actual counts of commuting activity

Table 9: Comparison of all averaged RHI models

Model (averaged)	Effect size of light/spectral predictor (β)	AICc	Rank
Lux	-1.40135	1393.27 – 1395.19	1
Red band	-0.58850	1398.10 – 1400.00	2
Green band	-0.55096	1398.64 – 1400.58	3
Lightness	**-0.58935**	**1399.08 – 1401.07**	**4**
Blue band	-0.62932	1401.68 – 1403.61	5
No Light	–	1407.53 – 1409.46	6

RANDOM EFFECTS

The random effects *Community* and *Location* were highly significant in my model. The recording day, however, didn't significantly improve the model fit (Table 10), but it represents the structure of my data and accounts for potential temporal autocorrelation (see sacrificial pseudoreplication issues mentioned above).

Table 10: ANOVA tables comparing the best model to models with single removed random variables

```
                        Df    AIC    BIC  logLik deviance  Chisq Chi Df Pr(>Chisq)
RHI_remove_Gemeinde     12 1406.6 1454.3 -691.31   1382.6
RHI_bestmodel_Lightness 13 1399.9 1451.5 -686.94   1373.9 8.7373      1   0.003118 **
---
Signif. codes:  0 '***' 0.001 '**' 0.01 '*' 0.05 '.' 0.1 ' ' 1
```

```
                         Df    AIC    BIC  logLik deviance  Chisq Chi Df Pr(>Chisq)
RHI_remove_Site_ID_Projekt 12 1440.2 1487.9 -708.13   1416.2
RHI_bestmodel_Lightness    13 1399.9 1451.5 -686.94   1373.9 42.365      1  7.573e-11 ***
---
Signif. codes:  0 '***' 0.001 '**' 0.01 '*' 0.05 '.' 0.1 ' ' 1
```

```
                        Df    AIC    BIC  logLik deviance  Chisq Chi Df Pr(>Chisq)
RHI_remove_Day          12 1398.3 1446.0 -687.18   1374.3
RHI_bestmodel_Lightness 13 1399.9 1451.5 -686.94   1373.9 0.4693      1     0.4933
```

Greater mouse-eared bat (*Myotis myotis*), MYM

For *M. myotis* model selection and averaging retained the following predictors in the model with respective effect sizes and Wald p-values:

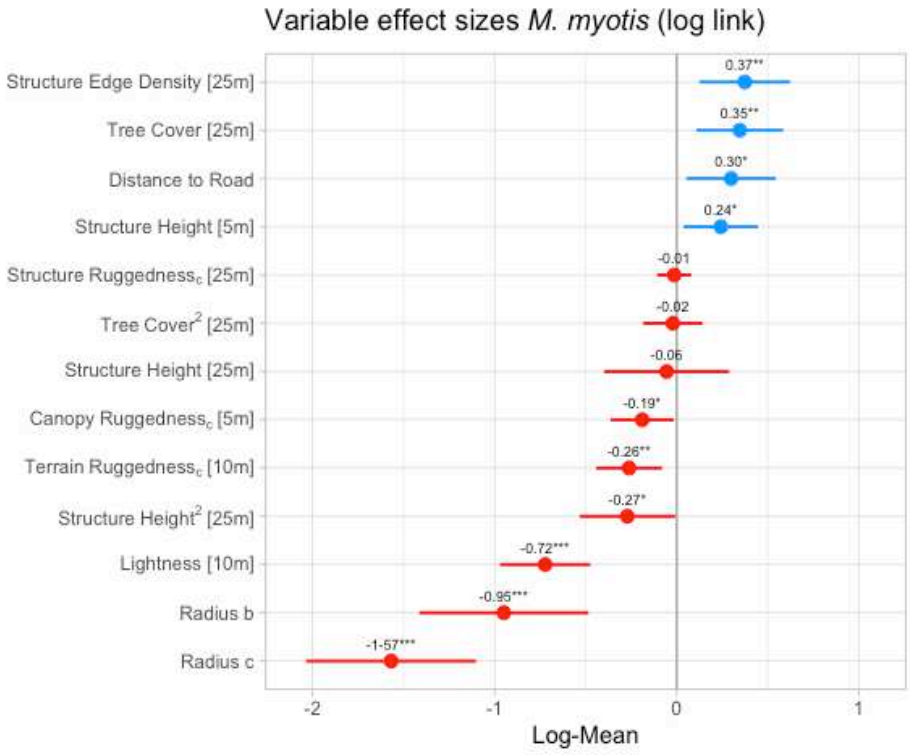

*Figure 14: Modelled variable effect sizes for M. myotis presented on the log link scale. Significance codes: $\alpha < 0.001$***, $\alpha < 0.01$**, $\alpha < 0.05$**

Table 11: MYM model summary table including coefficients, standard errors and p-values

Variable	Estimate	Std. Error	Adjusted SE	z value	Pr(>|z|)
Intercept	0.60676	0.33575	0.33675	1.80178	0.07158
Canopy Ruggedness$_c$ [5m]	-0.18962	0.08859	0.08886	2.13400	0.03284 *
Tree Cover [25m]	0.34658	0.12135	0.12168	2.84823	0.00440 **
Lightness [10m]	-0.72268	0.12634	0.12672	5.70289	< 2e-16 ***
Distance to Road	0.29882	0.12522	0.12560	2.37919	0.01735 *
Radius b (190/200m distance to roost)	-0.94964	0.23635	0.23706	4.00589	0.00006 ***
Radius c (350/400m distance to roost)	-1.56839	0.23752	0.23823	6.58347	< 2e-16 ***
Structure Edge Density [25m]	0.37375	0.12652	0.12689	2.94550	0.00322 **
Structure Height [5m]	0.24217	0.10395	0.10425	2.32286	0.02019 *
Structure Height [25m]	-0.05549	0.17485	0.17538	0.31641	0.75169
Structure Height^2 [25m]	-0.27137	0.13345	0.13385	2.02739	0.04262*
Terrain Ruggedness$_c$ [10m]	-0.26172	0.09215	0.09243	2.83161	0.00463**
Structure Ruggedness$_c$ [25m]	-0.01402	0.04789	0.04800	0.29213	0.77018
Tree Cover^2 [25m]	-0.02129	0.08299	0.08318	0.25599	0.79796
*Significance codes: $\alpha < 0.001$***, $\alpha < 0.01$**, $\alpha < 0.05$**					

LIGHTNESS

Similar to the *R. hipposideros* model, I found the lightness variable to be highly significant in the final averaged MYM model fit. The model estimates a strong negative effect of light on commuting activity of *M. myotis*. The effect is significant with a p-value far below 0.001 and an effect size of -0.72. Confidence intervals range from -0.91 to -0.42.

I also observe a significant improvement in goodness of fit from the averaged model without a light variable to the one including lightness. The fitted models contained in the averaged model with the light predictor range from 1977.37 to 1979.16 in AICc, while the ones including no light parameter lie between 2009.82 and 2011.80 (Δ AICc = 32.45). When comparing the two best models out of the model selection with LRT (Table 12), a highly significant improvement in model fit ($p < 0.001$) is detectable as well.

Table 12: ANOVA table comparing the best models with and without lightness

```
                         Df    AIC    BIC  logLik deviance  Chisq Chi Df Pr(>Chisq)
MYM_bestmodel_noLightness 10 2006.6 2047.0 -993.30   1986.6
MYM_bestmodel_Lightness   16 1973.1 2037.8 -970.54   1941.1 45.528      6  3.676e-08 ***
---
Signif. codes:  0 ‘***’ 0.001 ‘**’ 0.01 ‘*’ 0.05 ‘.’ 0.1 ‘ ’ 1
```

When looking at the R^2 values of the two models (Table 13), there is a significant increase in the marginal R^2 (no light: 0.212 | light: 0.335), while the difference in the approximated conditional coefficient is small. Above mentioned uncertainties in the computation of conditional R^2 also apply for *M. myotis*, directing the focus towards the marginal measure.

Table 13: Nakagawa and Schielzeth's marginal and conditional R2 measures for MYM

Best pre-average models	**Marginal R^2**	**Conditional R^2**
No lightness	0.212	0.788
Lightness	0.335	0.792

Like for the horseshoe bats, there is an exponential decrease in prediction of commuting activity with higher lightness values for *M. myotis* and there is visibly more commuting activity expected on the innermost radius. While the model predicts 0.42 counts at 20 percent lightness for radius b, there are still 1.1 counts per night expected for radius a. At 30 percent there are 0.3 Greater mouse-eared bats predicted to commute around radius a in a night. Compared to *R. hipposideros* the curve flattens more slowly, leading to higher activity at increased light intensities (Figure 15a).

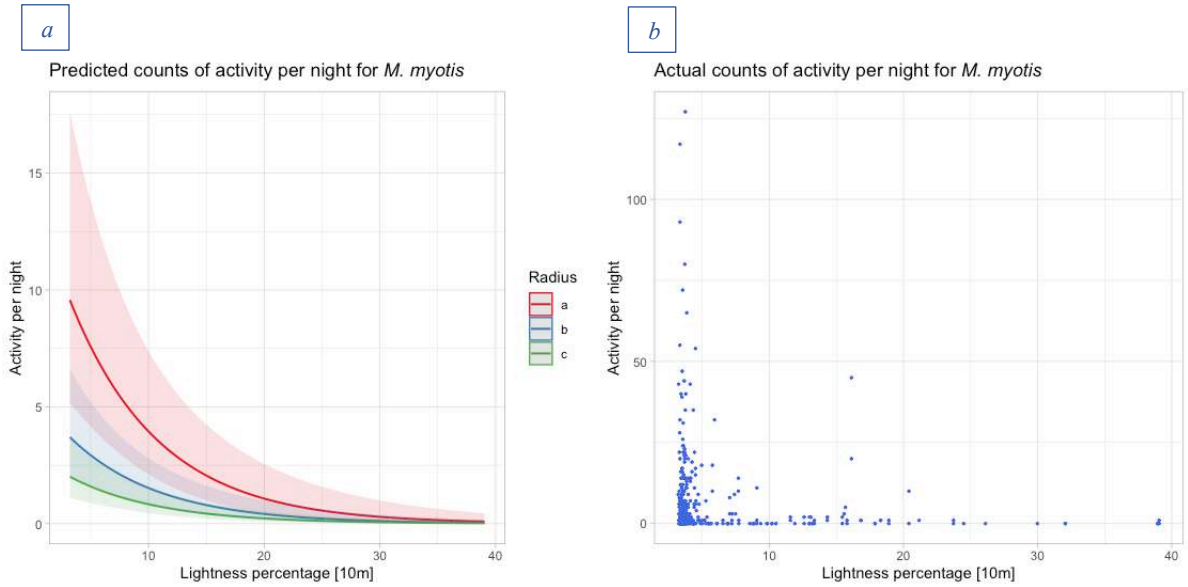

Figure 15: a) Model predicted relationship between commuting activity and lightness [10m] compared to b) actual counts of commuting activity

STRUCTURE MEASURES

The linear structure edge density predictor on a 25-meter scale is significantly positive in the model ($\beta = 0.37 \mid p < 0.01$). This variable includes various structures like hedgerows, buildings or trees above three meters in height. My model therefore suggests, that *M. myotis* favors an increased density of structure edges (Figure 16a).

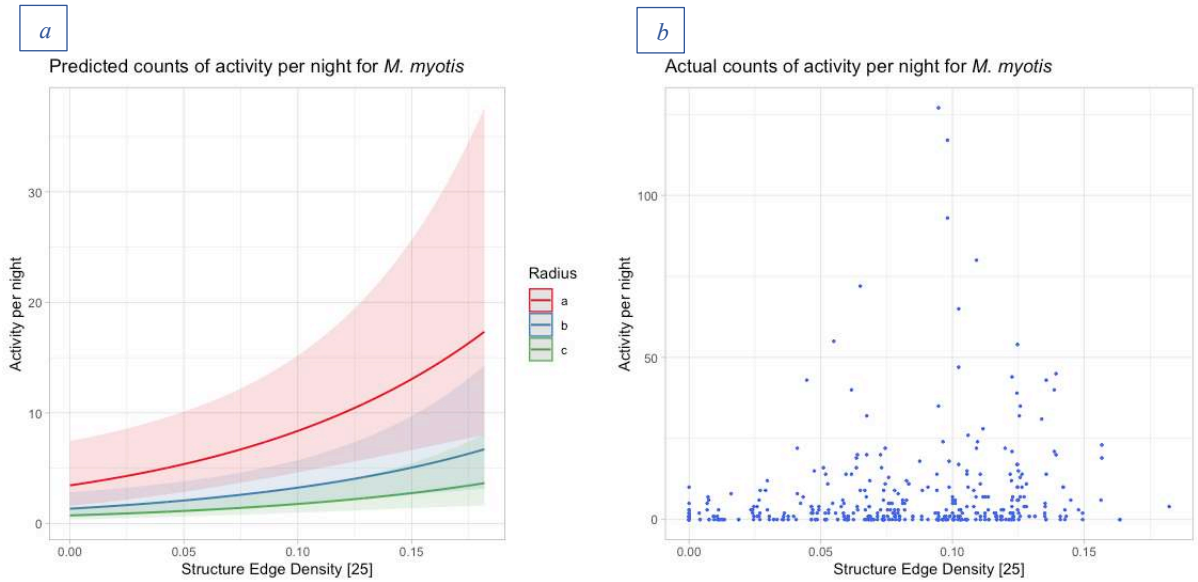

Figure 16: a) Model predicted relationship between commuting activity and structure edge density [25m] compared to b) actual counts of commuting activity

The structure height measure on a 25-meter scale is also significantly related to commuting counts, according to my model. In this case, both first and second order effect sizes show a negative direction. The quadratic term is significantly negative ($\beta = -0.27 \mid p < 0.05$) while the linear one is insignificantly negative ($\beta = -0.06$). Model prediction plots advocate for a bat activity increase with higher mean structure heights inside a 25-meter buffer. Above average heights of around 1.5 meters, however, counts are expected to decrease exponentially (Figure 17a). Uncertainty for these parameters – especially the linear one – are high, which leads to large confidence intervals around the predicted curve.

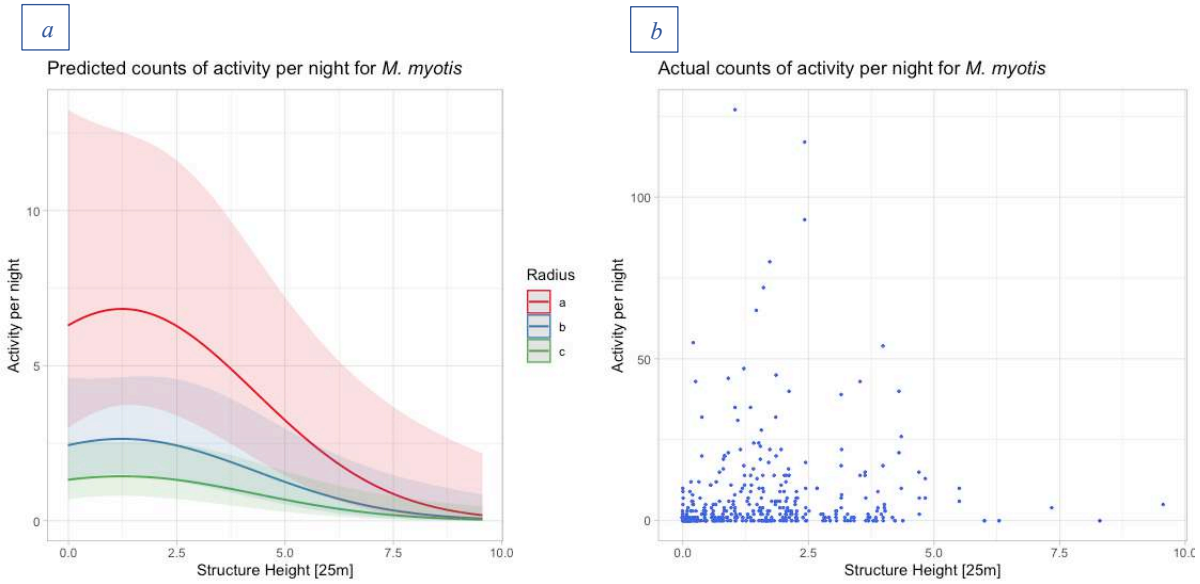

Figure 17: a) Model predicted relationship between commuting activity and structure height [25m] compared to b) actual counts of commuting activity

VEGETATION MEASURES

Unlike structure measures, vegetation variables solely include vegetation. Tree cover is calculated by computing the ground cover percentage of vegetation with height above three meters. Both the linear and the quadratic terms were retained in the model selection process. One can observe a significantly positive relationship between the linear tree cover variable and commuting counts. Very high commuting activity is predicted for high tree cover percentages, even though the curve is predicted to flatten after around 60% land coverage due to the slightly negative quadratic term (Figure 18). When 70% of the 25m area is covered by trees, there are 16.9 counts expected per night on the radius closest to the roost.

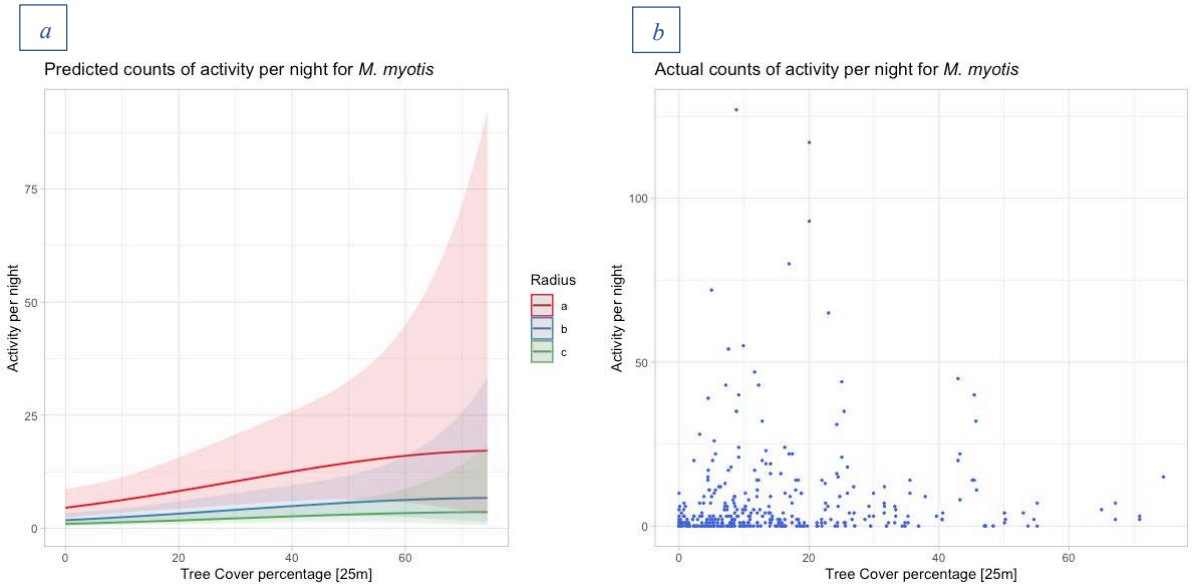

Figure 18: a) Model predicted relationship between commuting activity and structure height [25m] compared to b) actual counts of commuting activity

The canopy ruggedness measure – computed with the curvature method on a 5-meter scale – was also retained in the model selection. It represents the ruggedness of tree canopy surfaces above 3 meters. The variable significantly contributes to commuting counts of *M. myotis* with a negative coefficient of -0.19 ($p < 0.05$), leading to an expected fairly linear decrease in commuting counts with increased canopy ruggedness (Figure_A 2).

TERRAIN MEASURES

There is one parameter of terrain ruggedness remaining in the final model. It is calculated using the curvature technique for a mean ruggedness value at ground level inside a 10-meter buffer. The relationship between terrain ruggedness and commuting activity is significantly negative ($\beta = -0.26 \mid p < 0.01$). This is evident in the predicted activity curve, which decreases with increased terrain ruggedness (Figure_A 3).

DISTANCE TO ROAD

There is a highly positive relationship between the distance to road variable and commuting activity of *M. myotis*. The effect size of 0.30 ($p < 0.05$) indicates, that *M. myotis* prefers to commute away from roads and streets. However, there is still a lot of bat activity detectable close to streets (Figure_A 4b). This is also expected by the model, still predicting 5.6 counts per night for a one meter distance to road on radius a (Figure_A 4a). On radius b it expects only 2.2 counts per night.

RADIUS

As for *R. hipposideros,* roost distance contributes negatively to commuting activity of *M. myotis.* The effects on *M. myotis* are even larger and more significant. Radius c – including measurements furthest from the roost – has the biggest effect size in the model ($\beta = -1.57 \mid p < 0.001$) followed by the middle radius b ($\beta = -0.95 \mid p < 0.001$). Prediction plots indicate an exponential activity decrease with further distance to the roost (Figure_A 5).

LUX AND SPECTRAL BANDS

For *M. myotis* the blue band model (shorter wavelengths) accounts for most of the variability in my commuting count data. The model including the red band variable (longer wavelengths) on the other hand performs worst. The best blue band model fits the data better than the best lightness model with a difference of 6.96 in AICc. The lightness model outperforms the red band model by another 3.54. Unlike for *R. hipposideros*, the model integrating the manual lux measurements gives a poorer fit compared to the lightness and all spectral band models.

Comparing effect sizes, the different model outputs indicate, that short wave emissions (blue band) have a more negative effect on commuting activity of *M. myotis* than long wave emissions (red band) (Table 14). The green band model performs in the same range of AICc as the one including lightness. The prediction plots for short and long wave model representations, show a very steep decline in bat commuting activity with an increase of short-wave radiation. As the model predicts 7.4 counts of *M. myotis* per night on radius a with 5 percent of the blue channel, it expects only 1.4 counts for 10 percent blue portion. The predicted curve for the red band parameter is more flattened – 7.9 counts for 5 percent and 5.4 counts for 10 percent of red portion (Figure 19). Please mind the different scaling of the x-axis for red and blue bands.

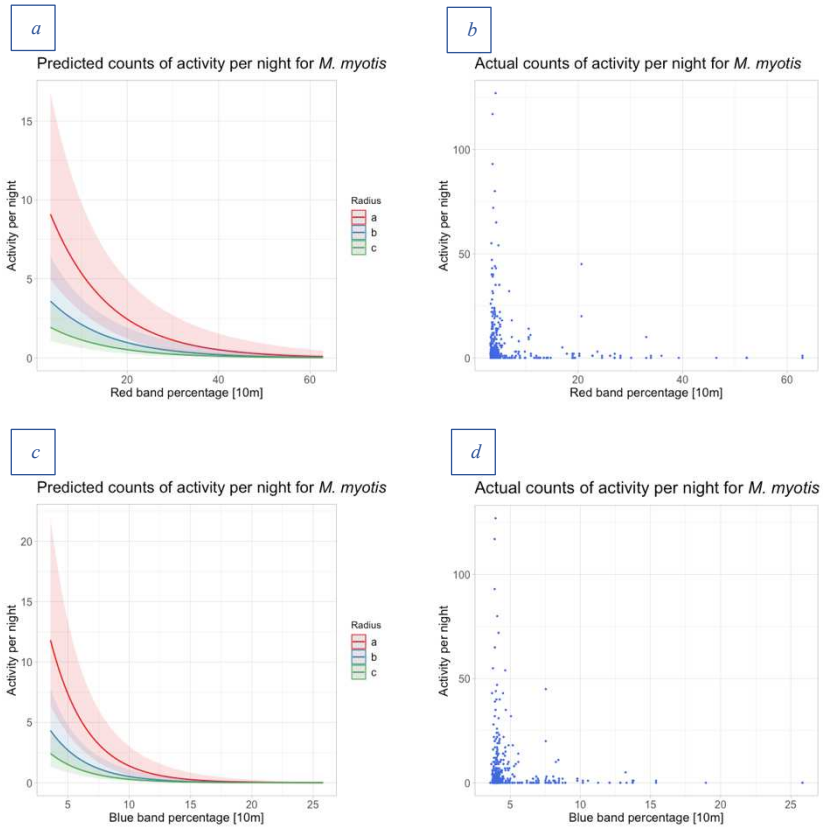

Figure 19: a) Model predicted relationship between commuting activity and percentage of red [2.5m] compared to b) actual counts of commuting activity

c) Model predicted relationship between commuting activity and percentage of red [2.5m] compared to d) actual counts of commuting activity

Table 14: Comparison of all averaged models MYM

Model (averaged)	Effect size of light/spectral predictor (β)	AICc	Rank
Blue band	-0.87355	1970.41 – 1972.40	1
Green band	-0.76656	1976.25 – 1978.12	2
Lightness	**-0.72268**	**1977.37 – 1979.16**	**3**
Red band	-0.66288	1980.91 – 1982.87	4
Lux	-0.70718	1981.84 – 1983.67	5
No Light	–	2009.82 – 2011.80	6

RANDOM EFFECTS

All the random effects show significant contributions to the explanation of the variance in commuting counts of *M. myotis* (Table 15). Especially the identification of all the single locations is highly significant along with the measurement day.

Table 15: ANOVA tables comparing the best model to models with single removed random variables

```
                        Df    AIC    BIC  logLik deviance  Chisq Chi Df Pr(>Chisq)
MYM_remove_Gemeinde     15 1976.4 2037.0 -973.19   1946.4
MYM_bestmodel_Lightness 16 1973.1 2037.8 -970.54   1941.1 5.3035      1    0.02128 *
---
Signif. codes:  0 ‘***’ 0.001 ‘**’ 0.01 ‘*’ 0.05 ‘.’ 0.1 ‘ ’ 1
```

```
                         Df    AIC    BIC  logLik deviance  Chisq Chi Df Pr(>Chisq)
MYM_remove_Site_ID_Projekt 15 2020.9 2081.5 -995.43   1990.9
MYM_bestmodel_Lightness    16 1973.1 2037.8 -970.54   1941.1 49.785      1  1.715e-12 ***
---
Signif. codes:  0 ‘***’ 0.001 ‘**’ 0.01 ‘*’ 0.05 ‘.’ 0.1 ‘ ’ 1
```

```
                       Df    AIC    BIC  logLik deviance  Chisq Chi Df Pr(>Chisq)
MYM_remove_Day         15 1983.3 2044.0 -976.65   1953.3
MYM_bestmodel_Lightness 16 1973.1 2037.8 -970.54   1941.1 12.232      1  0.0004698 ***
---
Signif. codes:  0 ‘***’ 0.001 ‘**’ 0.01 ‘*’ 0.05 ‘.’ 0.1 ‘ ’ 1
```

Spatial modelling - GIS

The spatial modelling approach has generated significant output for some sites and less valuable results for others. I focus on Veltheim (*M. myotis*) due to the availability of data on actual commuting corridors derived from local experts (Nater, 2019). Additionally, Veltheim suits well as a verification site as it was not included into the statistical models. I furthermore present the models of two sites which contain highly valuable information (Burgdorf and Surcasti; one site for each species) and one exemplary site where the models generated less significant output (Sachseln, *M. myotis*). The computed maps of all remaining sites are found in the appendix.

VELTHEIM (M. myotis)

Nater (2019) visualized commuting corridors in Veltheim derived from expert knowledge and the old model without lightness (Figure 20). Validating with her recorded activity data, she detected shortcomings in the modelled corridors. Especially, the predicted commuting paths into eastern and western direction were shown to be inaccurate. In the west, the recorded data revealed little to no activity and experts were also not aware of any commuting corridors. In the east, the old model predicted the bats to immediately cross the illuminated street. The activity data and experts, however, suggest a preference towards the darker and longer paths into north-eastern direction, where the bats then cross the street at a darker location (Figure 21).

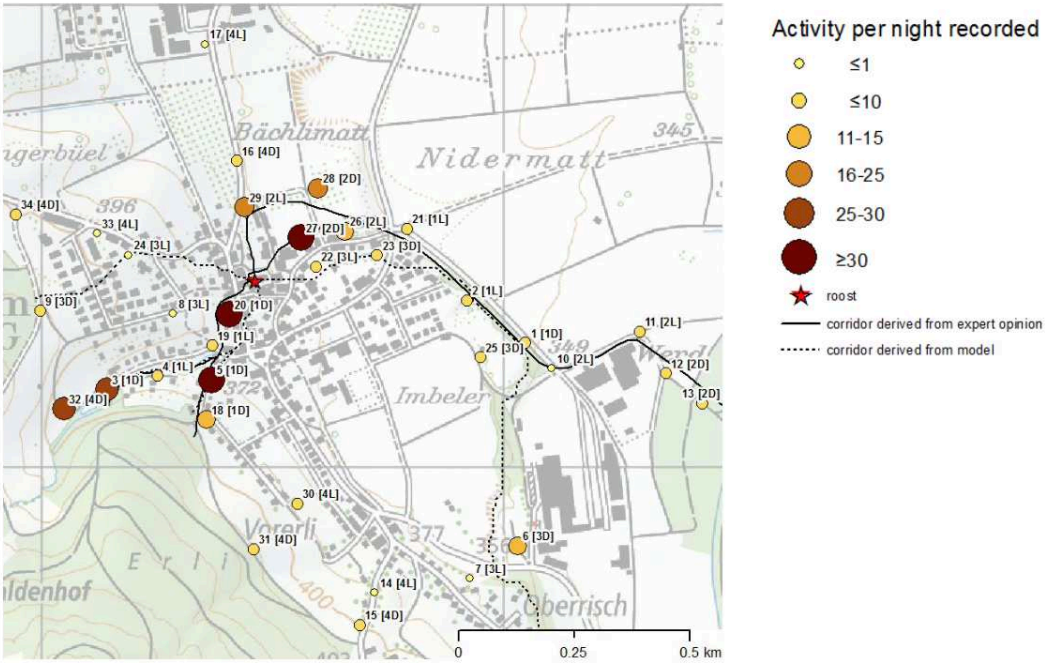

Figure 20: Illustration of sampling locations in Veltheim, showing sampled mean commuting activity of M. myotis per night, represented by size and color of bubble. Additionally, the corridors derived from expert knowledge and predicted by the model without lightness are visualized (Nater, 2019).

The two least cost paths (LCP) don't differ. both follow into south-western direction. This predicted corridor of highest commuting flow coincides with the recorded activity data.

Figure 21: Least cost paths for MYM in Veltheim with the slightly transparent lightness layer underneath, and the aerial image as the bottom layer

The flow density maps allow a broader picture on the less frequently used corridors of interest (Figure 22). Clearly, the new lightness model predicts significantly less commuting flow density in the west of the roost. The previously predicted corridor in western direction disappears in my new lightness model. This coincides with the lack of recorded activity and corridors predicted by experts. When looking at the current flow in the east, however, differences in the two model outputs are less conclusively detectable.

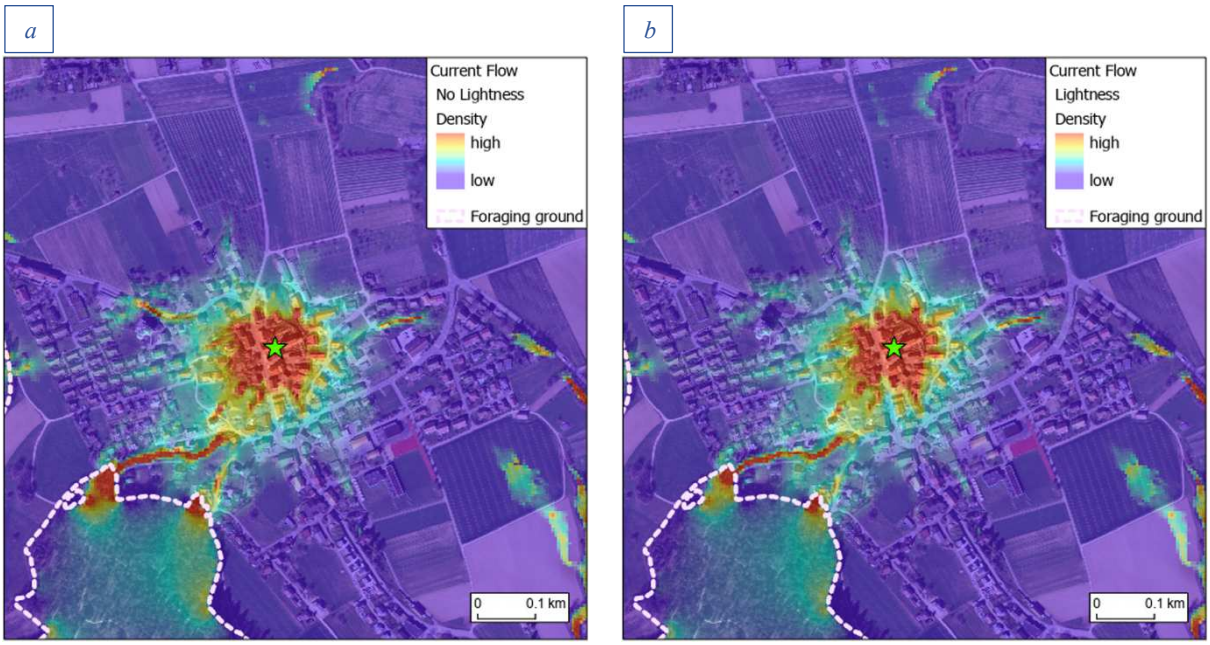

Figure 22: Current flow maps of MYM commuting in Veltheim predicted with a) no lightness and b) lightness

The difference map hereby gives more insights on distinct changes in predicted current flows when lightness is included into the model (Figure 23). As a reminder: The current flow map predicted by the model with no light predictor was subtracted from the one of the lightness model. Pixels of positive values (red) therefore represent areas, into which the bats elude due to light avoidance. Negative values (blue) on the other hand are areas where they are driven out by nocturnal illuminance. In conclusion, the bats relocate from blue to red areas under the impact of ALAN.

The difference map additionally emphasizes the findings from the current flow maps, as many bats leave the corridor along the highly illuminated main street in the west. Also, commuting into south-western direction is constrained by ALAN. However, when looking at the current flow maps, the highest absolute densities are still found along these corridors, which is in accord with the activity data and expert knowledge.

The absence of predicted activity in the west and south-west leads to a higher flow density into the north-eastern direction, where experts and recording data have also suggested increased commuting activity. However, the model still expects the bats to cross the road east of the roost early and follow along a corridor south of the street. In these areas, the model prediction appears to still be inferior to expert knowledge.

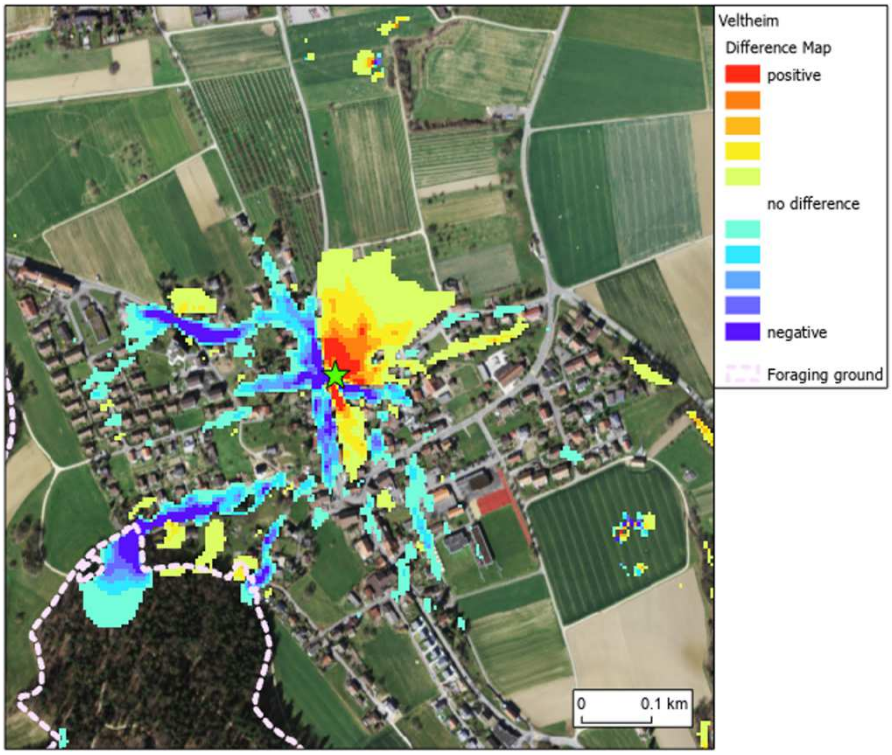

Figure 23: Difference map of Veltheim for MYM, depicting the difference in predicted current flow densities from a model with a lightness predictor to one including no light variable

BURGDORF (M. myotis)

The two calculated LCPs differ for *M. myotis* in Burgdorf (Figure 24). The model including lightness predicts the commuting route in the south-west to go around the illuminated street, while the model without lightness expects a more direct path. On the other hand, the lightness LCP in the north is expected to take a more direct route passing in between two streetlamps, while the model with no light predicts a longer path across a more illuminated part of the street.

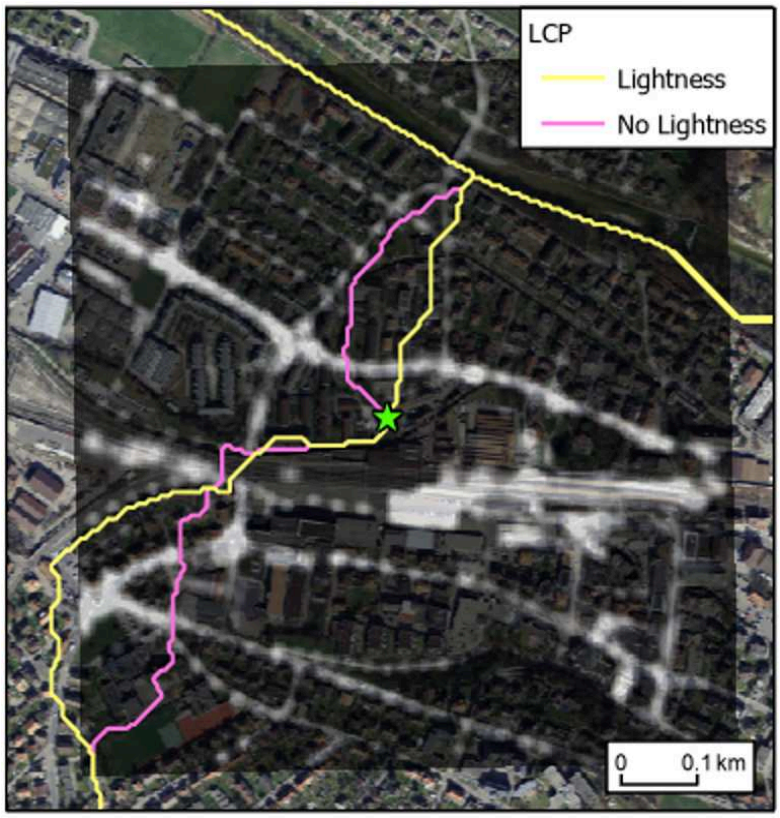

Figure 24: Least cost paths for MYM in Burgdorf with the slightly transparent lightness layer underneath, and the aerial image as the bottom layer

The current flow map from Burgdorf (Figure 25) including the lightness variable reveals the avoidance of the highly illuminated railway station in the south-east of the roost. Additionally, there appears to be less northwards commuting and a higher flow density in east and west direction.

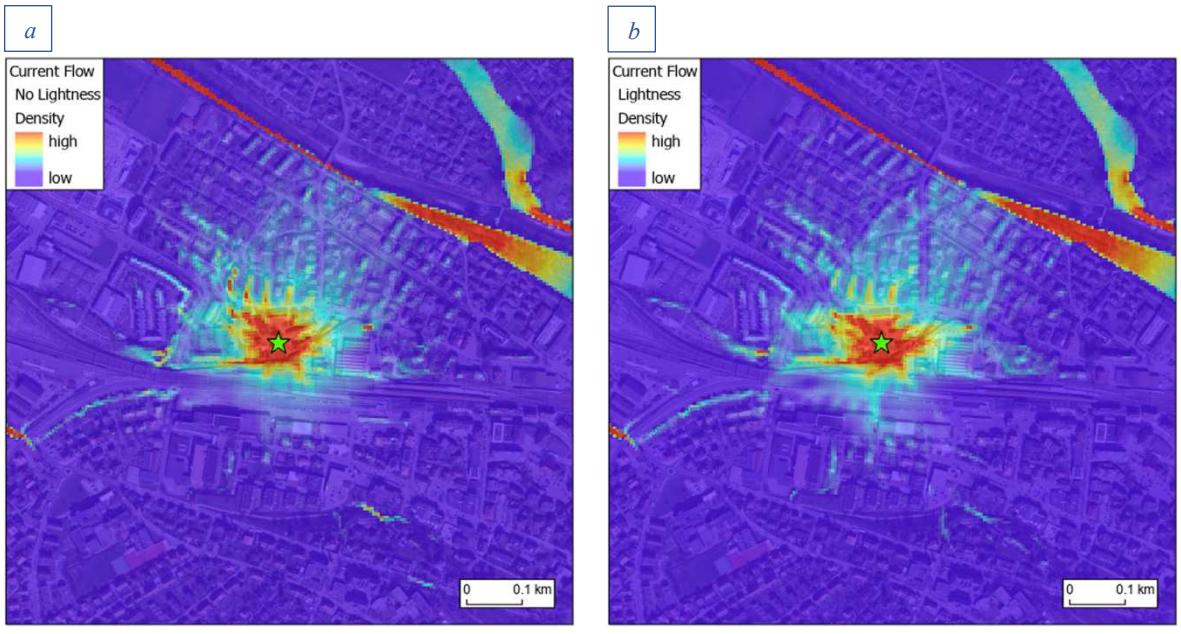

Figure 25: Current flow maps of MYM commuting in Burgdorf predicted with a) no lightness and b) lightness

Looking at the difference map of the two current flows (Figure 26), I detect the same tendency. The model without a light predictor, expects more commuting in the north direction and towards the railway station. The lightness model however predicts the bats to cross the rails at darker areas or commute along the northern side of the railway station, while the northern street in latitudinal direction is visibly less frequently crossed.

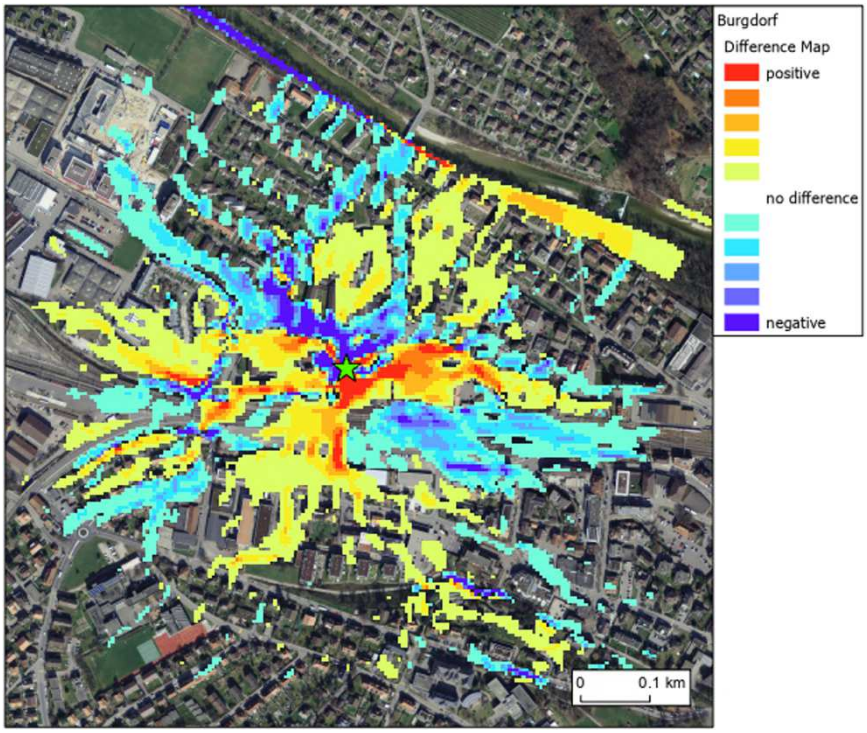

Figure 26: Difference map of Burgdorf for MYM, depicting the difference in predicted current flow densities from a model with a lightness predictor to one including no light variable

LUMNEZIA – SURCASTI (R. hipposideros)

The predicted least cost paths for Surcasti show great disparity (Figure 27). The model without lightness expects the most favorable route for *M. myotis* to follow along the settlement houses towards the northern forest. This path leads over two illuminated streetlights. The LCP computed with the lightness model, however, predicts lower costs for *R. hipposideros* when targeting the eastern forest and commuting over open pastureland.

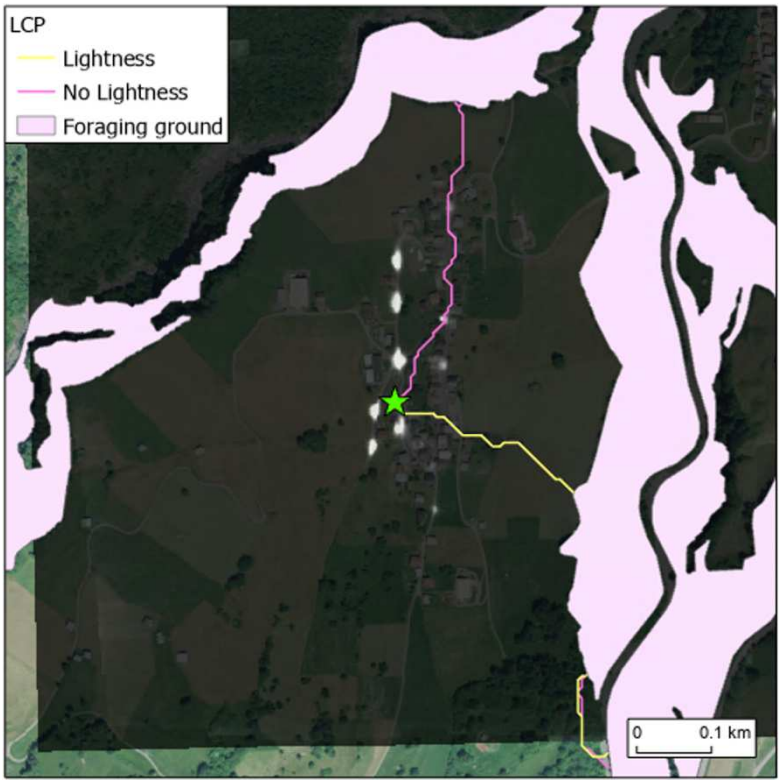

Figure 27: Least cost paths for RHI in Surcasti with the slightly transparent lightness layer underneath, and the aerial image as the bottom layer

The current flow maps emphasize the bat's higher likelihood to fly eastwardly when taking ALAN into account. I additionally recognize more activity in the opposite westward direction. As already illustrated in the LCP map, commuting towards the northern forest is highly constrained in the lightness model.

a

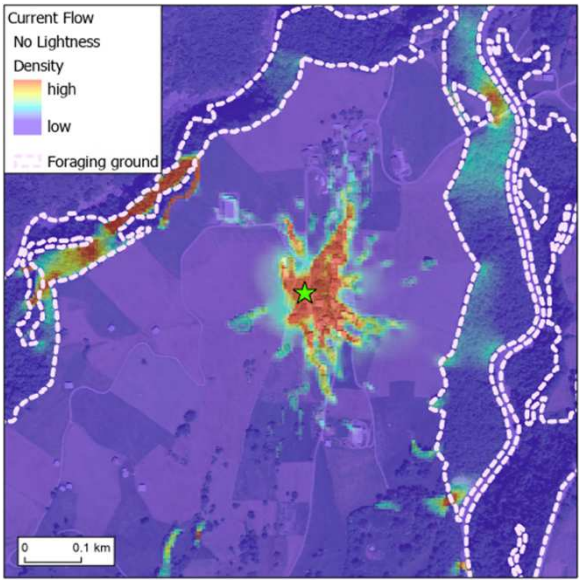

b

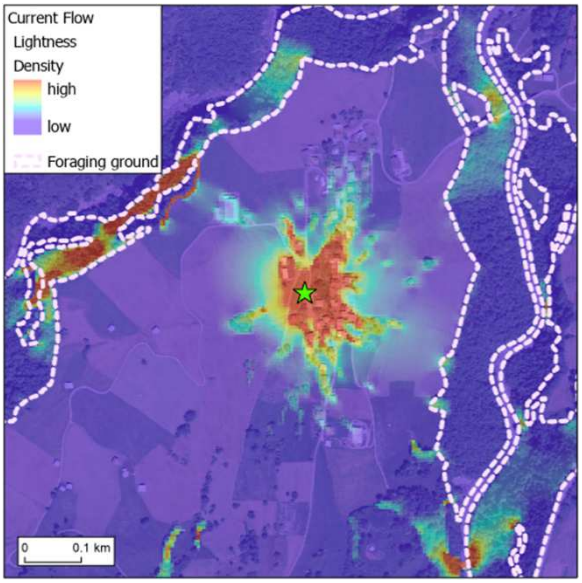

Figure 28: Current flow maps of RHI commuting in Surcasti predicted with a) no lightness and b) lightness

Analysis of the difference map (Figure 29) once again underlines the findings above. While the model with no lightness predictor expects more longitudinal movement (north-south), the model including lightness assumes increased commuting in latitudinal directions (east-west). ALAN drives the bats away from the more structured areas into more open grounds.

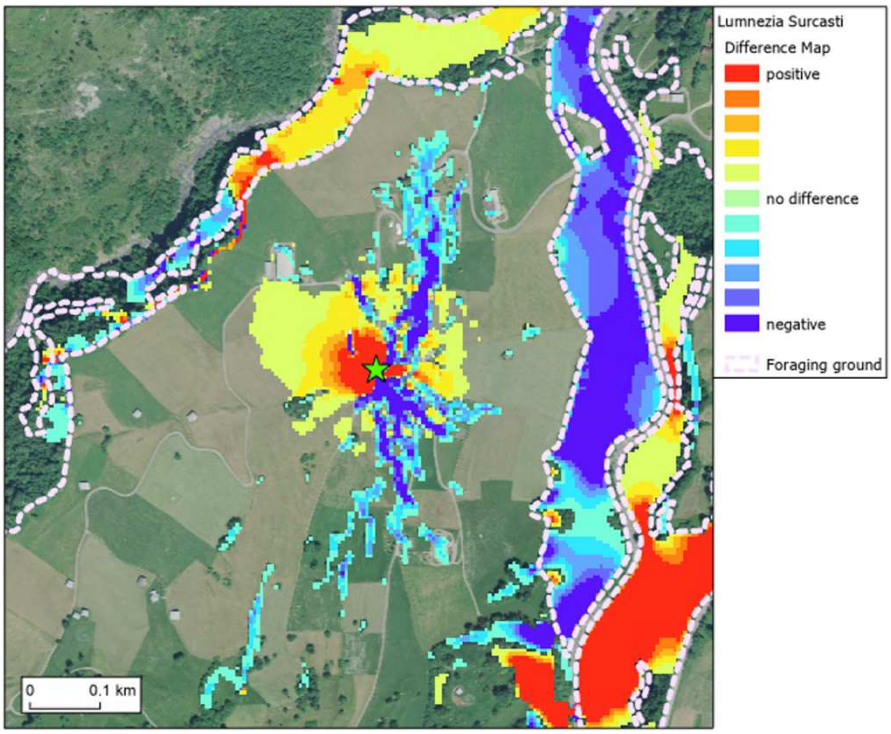

Figure 29: Difference map of Surcasti for RHI, depicting the difference in predicted current flow densities from a model with a lightness predictor to one including no light variable

SACHSELN (M. myotis)

In Sachseln there are very little alterations detectable between the model predicted with light to the one without. The LCPs are expected to follow practically along the same route (Figure 30). Also, the current flow models look very similar (Figure 31). However, especially the two illuminated streets south-west from the roost are clearly expected to be less commuted in the lightness model.

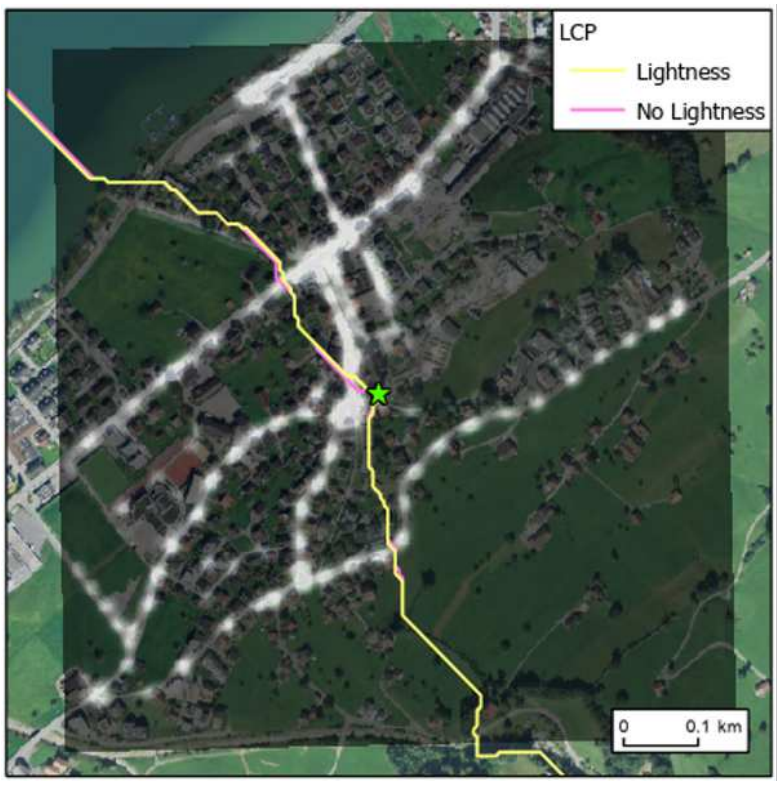

Figure 30: Least cost paths for MYM in Sachseln with the slightly transparent lightness layer underneath, and the aerial image as the bottom layer

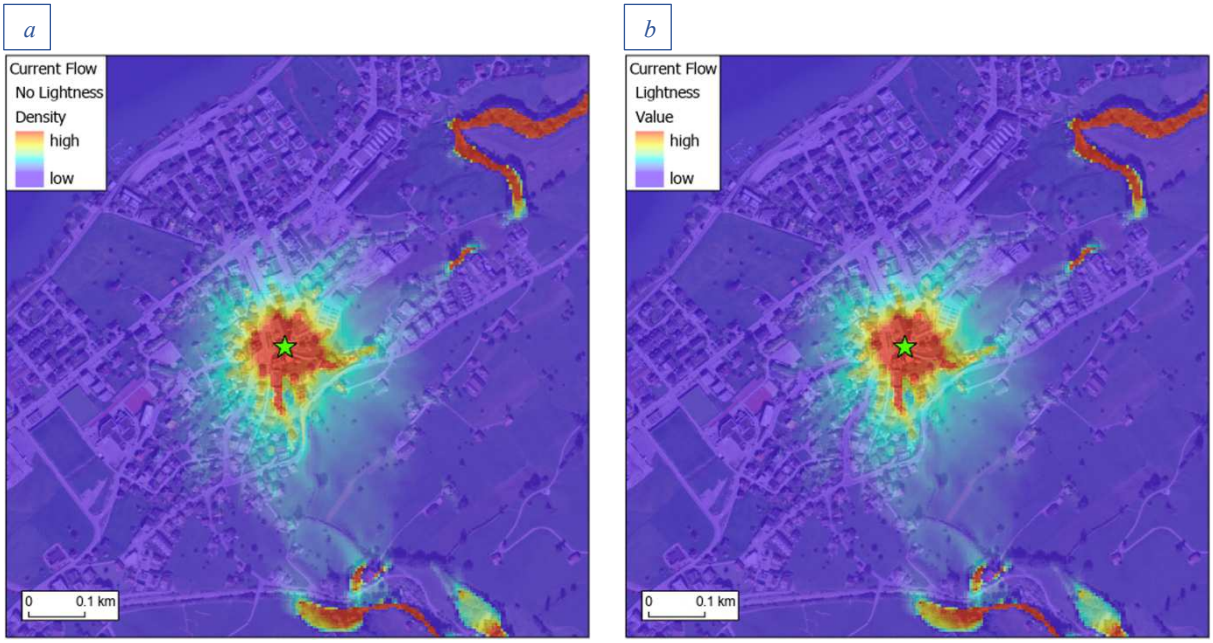

Figure 31: Current flow maps of MYM commuting in Sachseln predicted with a) no lightness and b) lightness

The difference map gives some more insight, revealing, that the lightness model predicts more bats flying out into north eastern direction, where there is less illuminance (Figure 32). The two streets mentioned above appear negative, meaning that the bats are driven out of these areas.

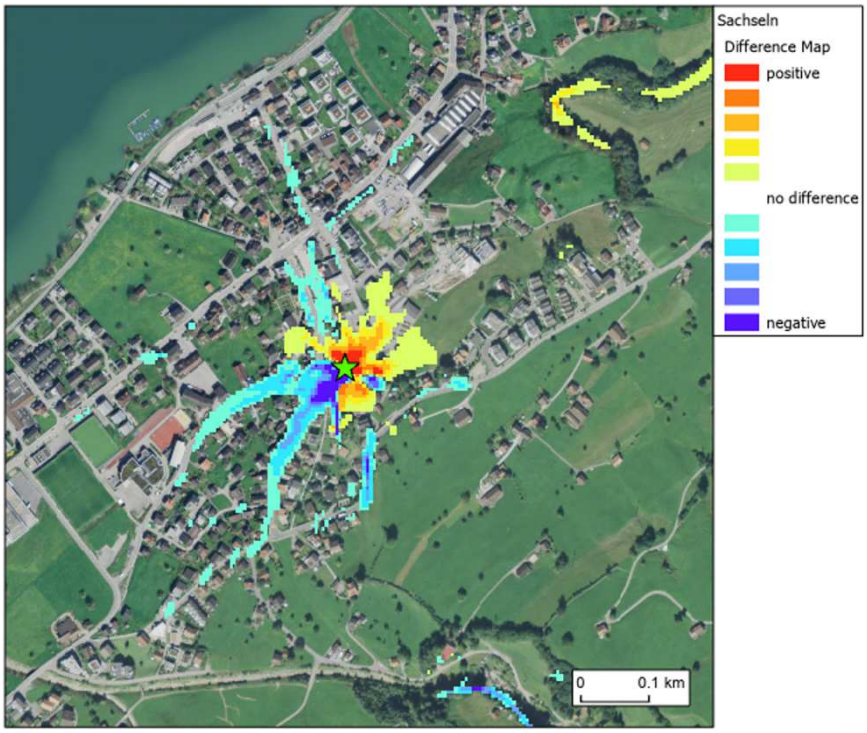

Figure 32: Difference map of Sachseln for MYM, depicting the difference in predicted current flow densities from a model with a lightness predictor to one including no light variable

Discussion

The UAV retrieved lightness variable as a light predictor in bat commuting activity modelling

I found the lightness variable obtained by drone photography to perform well in the representation of a lux measure on a more global, spatially explicit scale, hence offering the possibility of continuous data for corridor modelling. The strong and significant correlation between the aerial drone-captured data and my ground truth measurements supports such statements (R^2 = 0.84). The implementation of aerial nocturnal imagery may therefore contribute significantly to the ecological research on light pollution and the study of the effect of ALAN on nocturnal animals. The more global scale enables GIS analysis and spatial modelling of light at night. As there is still shortage in satisfactory nocturnal satellite data, I believe that the utilization of commercial UAVs poses a low-cost alternative with very highly resolved outputs. The computation of a layer representing ALAN from RGB images is quick and simple.

A possible restriction in my lightness variable, however, is that the amount of light intensity received by the drone sensor is highly dependent on the albedo (reflectance) of the reflecting surfaces. Therefore, my lightness variable might suffer some drawbacks compared to hand measurements, as it can't represent the genuine illuminance landscape. However, my study doesn't support this hypothesis, as the aerially obtained variable could easily compete with a manually measured Lux predictor for model fitting. It even has the potential to analyze possible differences in the animal's perception of light pollution. Some higher-flying species might be more affected by reflected light while low-flying species are more susceptible to direct illuminance. In the future, research on the bat's perception of light pollution could also help to selectively modify the vicinity of specific species based on their individual adaptions.

Model implementations

GLMM

LIGHTNESS

My results show that the UAV-retrieved lightness predictor elevates model suitability significantly. Based on various indicators (Wald Z-Test, LRT, R^2 and AICc) I can reject the

null hypothesis of no significant effect of ALAN for both *R. hipposideros* and *M. myotis*. The significantly negative lightness predictors in both models suggest that the Lesser horseshoe bats as well as the Greater mouse-eared bats are strongly susceptible to artificial light at night and avoid commuting near illuminated areas. This underlines the existing knowledge on both species and confirms the results of previous work discussing the negative impact of ALAN on *R. hipposideros and M. myotis* (Azam et al., 2018; Hale & Arlettaz, 2019; Stone et al., 2009, 2012).

In my study however, the lightness parameter is a less significant predictor for *R. hipposideros* commuting activity. Following corresponding literature, there is strong evidence for *R. hipposideros* to be extremely sensitive to light sources and potentially even more so than *M. myotis* (Stone, 2013). This difference in variable significance could result from the highly rural and barely light polluted areas in which the few remaining roosts are located. The very scarce light sources might just not be enough for a luminance gradient to allow for a better model fit. As my data shows (Figure 10b), there is hardly any *R. hipposideros* activity left at already minimal light intensities. This coincides with Stone et al. (2009), who show that the Lesser horseshoe bat already avoids light intensities of 0.1 Lux.

Examining the older manually obtained lux variable and my lightness variable in the model, one detects resembling outcomes. Model fits perform similarly well and effect sizes are comparable. The slightly better overall fit for *R. hipposideros* may therefore be explained with a different light perception among the two species. As the drone camera sensor measures reflected light, the luxmeter receives direct light radiation from under the light source. Even though, both species are known to fly low above the ground, the Lesser horseshoe bats commute at even lower heights (Roemer et al., 2017), leading to potentially higher sensitivity to direct lighting. *M. myotis* on the other hand could possibly be more susceptible to indirect lighting as it also flies above light sources, similar to the drone.

The difference between the effects of lux and lightness might also arise from the high light sensitivity of *R. hipposideros*. As the hand-measured variable is able to represent light at a very local scale, it may possibly prove to be more fitting for descriptive modelling of *R. hipposideros* commuting counts. Differences in parameter scale are also detectable for the lightness variable itself. *M. myotis* was most impacted by lightness averaged over a 10-meter buffer, while *R. hipposideros* was more strongly affected by lightness at the smallest scale available (buffer = 2.5m), hinting towards different scales of perception, which would coincide with the differences in echolocation distances.

STRUCTURE AND TERRAIN MEASURES

There is evidence, that both species rely on vertical structures for orientation as they commute along hedgerows or tree lines to the foraging grounds (Ravessoud, 2017; Stone et al., 2009). However, especially *R. hipposideros* depends on linear landscape features for increased insect abundance, shelter from wind and rain, acoustic orientation and predator avoidance (Motte & Libois, 2002; Stone et al., 2009; Zahn et al., 2008). As its wing morphology and echolocation with short detection range are adapted to a finely structured environment (Ravessoud, 2017), it predominantly avoids open areas. My modelling results endorse these findings. They suggest the Lesser horseshoe bats to strongly depend on ruggedness features for orientation. If there is too much height variation in the structures, however, they are avoided. As the computed structures variable includes buildings, high structure ruggedness could also arise near densely constructed settlements, which might be shun. The retention of the second order (quadratic) open ground variable additionally underlines the bats' preference towards lightly structured commuting routes and their avoidance of open areas (Stone et al., 2009).

M. myotis is better adapted to such open areas due to the characteristics of its echolocation signal. It is believed to identify background features at quite long distances (Boonman & Schnitzler, 2005) and therefore be able to commute in more open areas. Nevertheless, two structure variables were significant in the model. The positive effect of structure edge density on *M. myotis* commuting activity shows, that this species also depends on vertical features for its corridors. My model predicts a constant increase of activity with increase of edge density. Fitting a smaller model including only the linear and the quadratic term, however, I detect a more parabolic relationship (Figure 33), which also better aligns with the activity distribution (Figure 16b). Hence, even though model selection only retained the linear predictor, and the model predicts a linear relationship on the log-link scale, it is likely that *M. myotis* avoids too highly clustered structures.

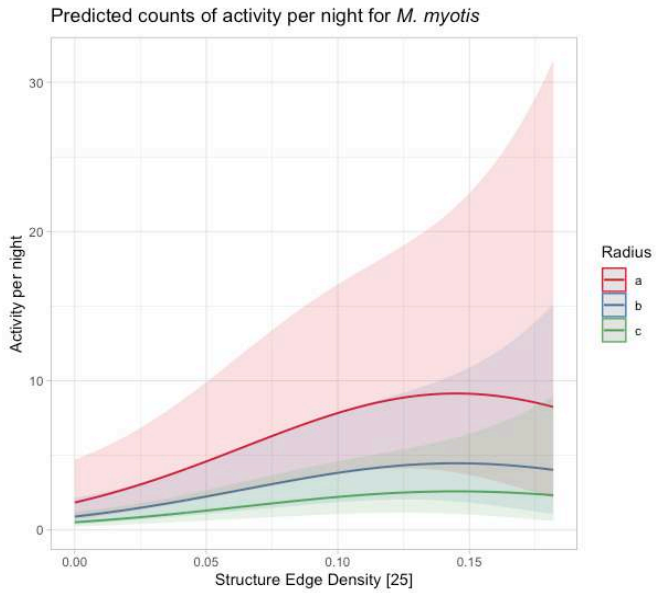

Figure 33: Model predicted relationship between commuting activity and structure edge density [25m] based on a small model with only the linear and the quadratic terms as fixed effects

The similar relationship between structure height inside a 25-meter buffer and commuting activity furthermore suggests, that the mouse-eared bats prefer commuting along structures of medium height. Possibly, the bats tend to fly over features with significant edges for better detection. As *M. myotis* is also a rather low-flying species, it might avoid high buildings and trees, as it can't view their top and therefore fails to detect their upper edges.

The predicted negative relationship between ground level ruggedness and commuting activity is difficult to interpret as it would suggest that *M. myotis* prefers smooth open grounds to coarse ground surfaces. By once again fitting a smaller model and integrating the quadratic terrain ruggedness variable, I tried to obtain a clearer picture on this relationship. However, integrating the second order term doesn't help much in this case (Figure_A 6) and suggests the model not to have missed out on important additional information. Nevertheless, this result emphasizes the Greater mouse-eared bats' better adaption to open grounds with smooth surfaces. Compared to *R. hipposideros*, Greater mouse-eared bats are faster flyers with a considerably longer foraging range. Thus, the preference for open ground might permit them to reach their foraging grounds quicker.

DISTANCE TO ROAD

The strong positive relationship between the distance to road variable and *M. myotis* commuting activity suggests, that the bats tend to avoid roads and streets on their nightly commuting routes. Distance to roads could also correlate negatively with lightness, as streetlamps make up for a high percentage of luminance at night. However, I found the two variables not to be correlated (R^2 = -0.16). Interestingly, at one meter road distance the model still predicts quite a lot of activity on the radius closest to the roost. This might be due to the roosts often being very centrally located inside the villages. Therefore, the bats are often forced to commute closely along or over roads and streets, leaving them more susceptible to streetlights and other street related barriers.

VEGETATION MEASURES

The vegetation measures for *M. myotis* underline, that the ruggedness of surfaces is less essential to the Greater mouse-eared bats than to the Lesser horseshoe bats. Seemingly, for *M. myotis* it is more important, that there are enough vertical structures (see structure edge density) and trees (tree cover) along their commuting routes than the surface texture of the like (see structure ruggedness$_c$, terrain ruggedness$_c$ or canopy ruggedness$_c$). While the tree cover variable is significantly positive, the canopy ruggedness variable is significantly negative. The predicted flattening of the curve for tree covers above 60 percent is in accord with the assumption that bats tend to follow treelines and hedgerows, but don't favor dense forests while commuting.

I would have expected the canopy ruggedness measure to also have a quadratic relationship to commuting activity. Fitting the small quadratic model didn't provide better understanding, however (Figure_A 7). It suggests high commuting activity either for high or low canopy ruggedness, which is ecologically inexplainable.

RADIUS

The decrease in commuting activity of both species with increased roost distance could be expected, even though they are believed to follow along certain corridors and not evenly spread in all directions. The model may suggest some sort of "leaky pipeline" where individuals are lost during commuting due to deviation from the expected corridors, which leads to a thinning in bat activity with increasing distance from the roost.

RGB BANDS FOR ADDITIONAL SPECTRAL INFORMATION

Validating the spectral information of UAV imagery through ground truth measurements proved to be challenging, as the spectrometer wasn't sensitive enough to collect data on light reflected from the ground. Despite the different sensor perceptions, the red band correlated with the red peak and the blue band correlated with the blue peak of my measurements. Nevertheless, especially the correlations for blue light were not very strong. Maybe an increased sample size could have better validated the spectral data.

Concerning the RGB variables in bat activity modelling, I detected that especially for *M. myotis* spectral indices seem to play a large role in their selection of commuting routes. Based on effect size and full model goodness of fit, my model suggests, that short wavelength light radiation has a more negative effect on bat activity than long wavelength radiation. My results concerning *M. myotis* follow older research on the subject (Stone et al., 2015), highlighting the heavily negative influence of short-wave LED light sources on bat activity. For the Lesser horseshoe bat model, the results weren't as obviously interpretable. The model coefficients suggest that the blue band also has the highest negative effect on their commuting counts of *R. hipposideros*. Assessment of the full model fits, however, suggests a better fit for the red band model, which represents longer wavelengths.

As prediction plots are based upon the model coefficients, predicted commuting activities decline the steepest with an increase in blue band percentage for both species. Slightest increases in blue band percentages lead to drastic plummets in expected commuting counts. I suggest to further study issues on the influence of spectral indices of ALAN on bats. Implementations for new LED streetlamps progresses quickly. As they are widely deemed to be exclusively environmentally friendly, my study proposes that it's important to be critical towards these new light technologies and at least promote the installment of LEDs with longer wavelength emissions (amber).

GIS

My spatial prediction models visualize the results from the mixed model fit. Using Veltheim as a validation site has shown, that when compared to the activity data and corridors predicted by experts, my new corridor models prove to be much better representations of reality. Previous falsely predicted corridors have dissipated or shifted to other areas in the lightness model. Our Veltheim models point out an increased commuting away from the actual path of least cost.

The highly illuminated main street seems to force many bats to take the alternative longer routes into north-eastern directions. These model-predicted movements were also observed by the local experts. However, east of the roost one can still detect some shortcomings of the modelled corridors compared to the ones derived from expert knowledge.

The Burgdorf example clearly highlights the possible barrier effects of ALAN on the commuting habits of *M. myotis*. The highly illuminated railway station is avoided while the bats seem to search for dark passages over the rails to get to the southern forest. The LCP additionally demonstrates that they are sometimes forced to take detours around lit areas. These extra expenses due to increased flight time can potentially be harmful to the bats' survival and reproductive success, as stress and cortisol levels may increase (Stone et al., 2009). Comparing the Burgdorf models with and without a light predictor, I detect the bats to be driven away from the highly illuminated spaces (see blue areas on the difference map) to elude into more obscure areas (red areas). The railroad in the south and the illuminated street in the north constrict the bats to more latitudinal commuting, leading to potential bottleneck effects when crossing streets or rails. Such effects seem most probable in the west, where most individuals appear to follow the computed least cost path over the railway through a narrow, slightly darker corridor. Keeping such passages in the dark may prove to be of great value to the bats and must be prioritized in the conservation process.

In Surcasti, I also observed a stronger tendency towards latitudinal commuting when including lightness as a predictor. Taking a closer look at the LCP modelled without light, one detects, that it expects the bats to fly directly over two illuminated streetlamps. These lights most probably account for the shift in the expected path of least resistance. The newly modelled corridors predict the bats to commute over open grounds. This constrains their ability of landmark generation for orientation through the detection of vertical structures. *R. hipposideros* hereby also uses such landscape features for higher abundance of insects and protection from wind and predators. As they are forced into open areas through light barriers, they are more exposed to such threats. As a conservation measure, the plantation of a hedge across the easterly meadow could alleviate this problem.

The example of Sachseln shows, that some differences in the spatial models with and without lightness may not immediately be observable, as there are not many indicators suggesting a difference in the two models. LCPs as well as current flow densities look very similar. However, when looking at the difference map of the two models, my new lightness model clearly proposes the bats to shy away from the illuminated south-west into the opposite direction.

Some extremely dark sites – such as Buttisholz (Figure_A 14-16) – naturally show no change in commuting prediction at all. However, for most sites there are observable shifts in the predicted corridors after the inclusion of lightness. These shifts often indicate barrier effects of ALAN, leading to bottle necks in the bat's commuting corridors and potential evasion into less natural and more risky areas. This shows the great potential of the visualization of such predictive models. The newly modelled corridor maps may serve in the implementation of increased conservation efforts on bat commuting paths. They can aid in the communication with local agencies and decision makers as light regimes have to be locally assessed and examined by local experts in order to conserve the commuting corridors of *R. hipposideros* and *M. myotis*.

Potential future improvements

In an earlier variable selection process, the categorical radius variable was selected over the discrete distance to roost variable measured in meters (Ravessoud, 2017). Re-fitting the current best models by replacing the radius with the distance to roost variable showed, that the two predictors contribute similarly to the model. While the re-fitted *M. myotis* model is a slightly worse fit (ΔAICc = 3.357), the *R. hipposideros* model with the discrete roost distance variable fits the data negligibly better than the one with the radius variable (ΔAICc = 1.384). In both new models, distance to roost is highly significant (RHI: 0.01 | MYM: 0.001) and the coefficients (RHI: β = -0.3786 | MYM: β = -0.56591) emphasize the strong negative relationship between roost distance and the commuting activity of both species. As the categorical radius variable couldn't be integrated into the spatial models, an inclusion of the discrete distance to roost could potentially increase the visualizations of the commuting corridors.

Another potential restriction in my model is the lack of an aspect variable, which would represent the cardinal direction of each sampling point relative to the roost. As this factor is strongly related to the levels of community (Gemeinde), there might be some spatial patterns as commuting direction could potentially not be independent. Nation-wide factors such as wind or simple random patterning due to the small number of levels for site could lead to spatial autocorrelation. The assessment of such an aspect variable could be a future modelling step to further improve the existing model.

Conclusion and outlook

My research emphasizes, that the implementation of drone imagery can constitute a valuable technique in the visualization of artificial light at night. The inclusion of a UAV retrieved lightness variable significantly increased the model goodness of fit compared to a model with no light variable for both species. As my lightness predictor is a continuous data layer in a 400-meter radius around the 20 roosts, I was able to spatially predict commuting routes of *R. hipposideros* and *M. myotis*. The new GIS outputs provide new area-wide quantifiable corridor models that predominantly show significant visual transformations compared to old maps predicted without an ALAN parameter. As my recent model is statistically a better fit to the activity data, I believe the newly computed commuting routes to provide a more suitable representation of reality. The modelled corridors for Veltheim explicitly visualize the expected improvements.

Such corridor maps are useful tools in the dialogue with municipalities and other decision makers, as they highlight potential constrictions in the commuting corridors (bottlenecks and pinpoints). I hope that my research accentuates the potential barrier effects of artificial light at night on the commuting of my two study species and that local lighting regimes are adapted accordingly. The lack of such adaptions can potentially have highly negative impacts on the demographics of bat populations, altering the community composition of their prey and decreasing their survival and reproduction rates (Stone et al., 2009). High illumination of the bat's flight paths especially close to the roost can even lead to them not emerging from their roost at all. I strongly believe that the ecological and conservational value of similarly framed models exceeds the studied species. Modelling ALAN as continuous data using drone imagery may assist conservation objectives for various other nocturnal species.

The models integrating the spectral bands red, green and blue also showed promising results. Especially, for *M. myotis* I showed that short-wave radiation emitted by modern LED-streetlamps has a higher negative influence on commuting activity than the long-wave radiation emitted by the traditional lamps. For *R. hipposideros* results were less transparent. Effect sizes pointed to the same conclusion, but overall goodness of fits proposed the red model to explain the most variance. However, the spectral models for the Lesser horseshoe bat were difficult to compare, as differences in AICc were overall small. I believe that multispectral imagery can additionally serve in the detection of barriers for nocturnal species and the customization of artificial light sources.

Acknowledgements

I want to especially thank my main supervisors, Dr. Marin Obrist (WSL) and Dr. Eva Knop (Agroscope and UZH), for the possibility to be a part of this long-term project at the Swiss Federal Institute for Forest, Snow and Landscape Research (WSL). I am very grateful for their guidance and expertise in the construction of the overall study design and for their professional feedbacks along the work process.

My gratitude also goes out to Dr. Klaus Ecker (WSL) who substantially contributed to the structuring of the model with his inputs and support. Additionally, he guided me in the generation of the lightness layers and computed the current flow and least cost maps. I further acknowledge Dr. Ruedi Bösch, who instructed me in the handling of the drone and provided advice on general issues in the field of remote sensing.

I also want to thank Agroscope (Swiss Federal research into agriculture, nutrition and the environment) and SWILD (research and consulting association, Zurich) for the provision of the Spectrometer and the Luxmeter, respectively.

Finally, I want to thank all my friends and family who accompanied and assisted me during field work in the middle of the night.

References

Akaike, H. (2011). *Akaike's Information Criterion BT - International Encyclopedia of Statistical Science* (M. Lovric (ed.); p. 25). Springer Berlin Heidelberg.

Arlettaz, R. (1996). Feeding behaviour and foraging strategy of free-living mouse-eared bats, Myotis myotis and Myotis blythii. *Animal Behaviour*, *51*(1), 1–11.

Audet, D. (1990). Foraging Behavior and Habitat Use by a Gleaning Bat, Myotis myotis (Chiroptera: Vespertilionidae). *Journal of Mammalogy*, *71*(3), 420–427.

Azam, C., Le Viol, I., Bas, Y., Zissis, G., Vernet, A., Julien, J. F., & Kerbiriou, C. (2018). Evidence for distance and illuminance thresholds in the effects of artificial lighting on bat activity. *Landscape and Urban Planning*.

Bartoń, K. (2020). *MuMIn: Multi-Model Inference*. https://cran.r-project.org/package=MuMIn

Bliss, C. I., & Fisher, R. A. (1953). Fitting the Negative Binomial Distribution to Biological Data. *Biometrics*, *9*(2), 176–200.

Bohnenstengel, T., Krättli, H., Obrist, M., Bontadina, F., Jaberg, C., Ruedi, M., & Moeschler, P. (2014). *Rote Liste Fledermäuse. Gefährdete Arten der Schweiz, Stand 2011*.

Bolker, B. M. (2019). *Generalized linear mixed models in R: nitty-gritty*. https://bbolker.github.io/goettingen_2019/notes/glmm_details.html

Bolker, B. M. (2021). *GLMM FAQ*.

Bolker, B. M., Brooks, M. E., Clark, C. J., Geange, S. W., Poulsen, J. R., Stevens, M. H. H., & White, J. S. S. (2009). Generalized linear mixed models: a practical guide for ecology and evolution. In *Trends in Ecology and Evolution* (Vol. 24, Issue 3, pp. 127–135). Elsevier Current Trends.

Boonman, A., & Schnitzler, H. (2005). Frequency modulation patterns in the echolocation signals of two vespertilionid bats. *Journal of Comparative Physiology. A, Neuroethology, Sensory, Neural, and Behavioral Physiology*, *191*, 13–21.

Braaker, S., Moretti, M., Boesch, R., Ghazoul, J., Obrist, M. K., & Bontadina, F. (2014). Assessing habitat connectivity for ground-dwelling animals in an urban environment. *Ecological Applications*, *24*(7), 1583–1595.

Brooks, M. E., Kristensen, K., van Benthem, K. J., Magnusson, A., Berg, C. W., Nielsen, A., Skaug, H. J., Maechler, M., & Bolker, B. M. (2017). {glmmTMB} Balances Speed and Flexibility Among Packages for Zero-inflated Generalized Linear Mixed Modeling. *The R Journal*, *9*(2), 378–400. https://journal.r-project.org/archive/2017/RJ-2017-

066/index.html

Burnham, K. P., & Anderson, D. R. (2004). Multimodel Inference: Understanding AIC and BIC in Model Selection. *Sociological Methods & Research*, *33*(2), 261–304.

Burnham, K. P., Anderson, D. R., & Huyvaert, K. P. (2011). AIC model selection and multimodel inference in behavioral ecology: some background, observations, and comparisons. *Behavioral Ecology and Sociobiology*, *65*(1), 23–35.

DJI Entertainment Technology. (2021). *No Title*. https://www.dji.com/ch/mavic-2

Drescher, C. (2004). Radiotracking of Myotis myotis (Chiroptera, Vespertilionidae) in South Tyrol and implications for its conservation. *Mammalia*, *68*, 387–395.

Esri Inc. (2018). *ArcGIS Desktop 10.6.1*.

Esri Inc. (2019). *ArcGIS Pro 2.4.3*.

FOCA. (2020). *FAQs about drone regulations – Version 3.0*. Federal Office of Civil Aviation. https://www.bazl.admin.ch/bazl/en/home/good-to-know/drones-and-aircraft-models/allgemeine-fragen-zu-drohnen.html

Gallo, J. A., & Greene, R. (2018). *Connectivity analysis software for estimating linkage priority*.

Gaston, K. J., Bennie, J., Davies, T. W., & Hopkins, J. (2013). The ecological impacts of nighttime light pollution: a mechanistic appraisal. *Biological Reviews*, *88*(4), 912–927.

Graham, M. H. (2003). Confronting multicollinearity in ecological multiple regression. *Ecology*, *84*(11), 2809–2815.

Groll, A. (2017). *glmmLasso: Variable Selection for Generalized Linear Mixed Models by L1-Penalized Estimation*. https://cran.r-project.org/package=glmmLasso

Hale, J., & Arlettaz, R. (2019). *Artificial lighting and Biodiversity in Switzerland - Technical Report V4*.

Hartig, F. (2020). *DHARMa: Residual Diagnostics for Hierarchical (Multi-Level / Mixed) Regression Models*. https://cran.r-project.org/package=DHARMa

Hurlbert, S. H. (1984). Pseudoreplication and the Design of Ecological Field Experiments. *Ecological Monographs*, *54*(2), 187–211.

Hurvich, C. M., & Tsai, C.-L. (1989). Regression and time series model selection in small samples. *Biometrika*, *76*(2), 297–307.

Hutson, A., Marnell, F., & Torv, T. (2015). *A guide to the implementation of the Agreement on the Conservation of Populations of European Bats (EUROBATS)*.

Johnson, J. B., & Omland, K. S. (2004). Model selection in ecology and evolution. In *Trends in Ecology and Evolution* (Vol. 19, Issue 2, pp. 101–108). Elsevier Ltd.

Kullback, S., & Leibler, R. A. (1951). On Information and Sufficiency. *The Annals of Mathematical Statistics*, *22*(1), 79–86. http://www.jstor.org/stable/2236703

Lewanzik, D., & Voigt, C. C. (2014). Artificial light puts ecosystem services of frugivorous bats at risk. *Journal of Applied Ecology*, *51*(2), 388–394.

Lüdecke, D. (2018). ggeffects: Tidy Data Frames of Marginal Effects from Regression Models. *Journal of Open Source Software*, *3*(26), 772.

Lüdecke, D., Makowski, D., Waggoner, P., & Patil, I. (2020). performance: Assessment of Regression Models Performance. *CRAN*.

Malakoutikhah, S., Fakheran, S., & Soffianian, A. (2014). Applying Circuitscape Theory to Identify Migration Corridors Between Mooteh and Ghamishloo Wildlife Refuges in Isfahan Province-Iran TT - استفاده از تئوری مدارهای الکتریکی جهت شناسایی کریدورهای مهاجرتی بین پناهگاه‌های حیات وحش موته و قمشلو در استان اصفها. *IJAE*, *2*(5), 77–89. http://ijae.iut.ac.ir/article-1-386-en.html

McRae, B. H., Shah, V. B., & Mohapatra, T. (2013). *Circuitscape 4 User Guide*. *The Nature Conservancy*. *http://www.circuitscape.org*.

McRae, B., & Shah, V. (2009). *Circuitscape User Guide*.

Meier, T. (2019). *Challenging the predictive power of flight corridor models for bats*. ETH Zürich.

Motte, G., & Libois, R. (2002). Conservation of the lesser horseshoe bat (Rhinolophus hipposideros Bechstein, 1800) (Mammalia: Chiroptera) in Belgium. A case study of feeding habitat requirements. *Belgian Journal of Zoology*, *132*.

Nakagawa, S., & Schielzeth, H. (2013). A general and simple method for obtaining R2 from generalized linear mixed-effects models. *Methods in Ecology and Evolution*, *4*(2), 133–142.

Nater, A. (2019). *Evaluating methods to predict commuting flyways of Greater mouse-eared bats (Myotis myotis): Do corridors represent ecological infrastructure networks?* ETH Zürich.

Nishad, P., & Chezian, R. (2013). Various colour spaces and colour space conversion algorithms. *Journal of Global Research in Computer Science*, *4*, 44–48.

Obrist, M. (2019). *Projekt Implementation nachdunkler Fledermaus-Flugkorridore Zwischenbericht 2019*.

Pauwels, J., Le Viol, I., Azam, C., Valet, N., Julien, J.-F., Bas, Y., Lemarchand, C., Sanchez de Miguel, A., & Kerbiriou, C. (2019). Accounting for artificial light impact on bat activity for a biodiversity-friendly urban planning. *Landscape and Urban Planning*, *183*,

12–25.

Peixoto, J. L. (1990). A Property of Well-Formulated Polynomial Regression Models. *The American Statistician*, *44*(1), 26–30.

R Core Team. (2020). *R: A Language and Environment for Statistical Computing*. https://www.r-project.org/

Ravessoud, T. (2017). *Finding a method to predict the commuting activity of bats*. Unuversity of Lausanne.

Riley, S., Degloria, S., & Elliot, S. D. (1999). A Terrain Ruggedness Index that Quantifies Topographic Heterogeneity. *Internation Journal of Science*, *5*, 23–27.

Roemer, C., Disca, T., Coulon, A., & Bas, Y. (2017). Bat flight height monitored from wind masts predicts mortality risk at wind farms. *Biological Conservation*, *215*, 116–122.

Rowse, E. G., Lewanzik, D., Stone, E. L., Harris, S., & Jones, G. (2016). *Dark Matters: The Effects of Artificial Lighting on Bats BT - Bats in the Anthropocene: Conservation of Bats in a Changing World* (C. C. Voigt & T. Kingston (eds.); pp. 187–213). Springer International Publishing.

RStudio Team. (2019). *RStudio: Integrated Development Environment for R*. http://www.rstudio.com/

Rydell, J., Entwistle, A., & Racey, P. A. (1996). Timing of Foraging Flights of Three Species of Bats in Relation to Insect Activity and Predation Risk. *Oikos*, *76*(2), 243–252.

Sappington, J. M., Longshore, K. M., & Thompson, D. B. (2007). Quantifying Landscape Ruggedness for Animal Habitat Analysis: A Case Study Using Bighorn Sheep in the Mojave Desert. *The Journal of Wildlife Management*, *71*(5), 1419–1426.

Speakman, T. D. J. (2003). Physiological ecology and energetics of bats. *Bat Ecology*, 430–490. http://ci.nii.ac.jp/naid/20001124006/en/

Stone, E. L. (2013). *Bats and lighting: Overview of current evidence and mitigation*.

Stone, E. L., Harris, S., & Jones, G. (2015). Impacts of artificial lighting on bats: A review of challenges and solutions. In *Mammalian Biology* (Vol. 80, Issue 3, pp. 213–219). Elsevier GmbH.

Stone, E. L., Jones, G., & Harris, S. (2009). Street Lighting Disturbs Commuting Bats. *Current Biology*.

Stone, E. L., Jones, G., & Harris, S. (2012). Conserving energy at a cost to biodiversity? Impacts of LED lighting on bats. *Global Change Biology*, *18*(8), 2458–2465.

Tibshirani, R. (1996). Regression Shrinkage and Selection Via the Lasso. *Journal of the Royal Statistical Society: Series B (Methodological)*, *58*(1), 267–288.

Tilman, D., May, R. M., Lehman, C. L., & Nowak, M. A. (1994). Habitat destruction and the extinction debt. *Nature*, *371*(6492), 65–66.

Voigt, C. C., & Kingston, T. (2016). *Bats in the Anthropocene BT - Bats in the Anthropocene: Conservation of Bats in a Changing World* (C. C. Voigt & T. Kingston (eds.); pp. 1–9). Springer International Publishing.

Wagenmakers, E.-J., & Farrell, S. (2004). AIC model selection using Akaike weights. *Psychonomic Bulletin & Review*, *11*(1), 192–196.

Yoon, E.-J., Kim, Y., Kim, Y., Lee, K., Lee, D. K., 국립환경연구원일본, 대학원서울대학교, & 조경지역시스템 공학부서울대학교. (2019). Connectivity Assessment Based on Circuit Theory for Suggestion of Ecological Corridor. *Journal of Environmental Impact Assessment*, *28*(3), 275–286.

Zahn, A., Holzhaider, J., Kriner, E., Maier, A., & Kayikcioglu, A. (2008). Foraging activity of Rhinolophus hipposideros on the Island of Herrenchiemsee, Upper Bavaria. *Mammalian Biology*, *73*(3), 222–229.

Appendix

Prediction Plots

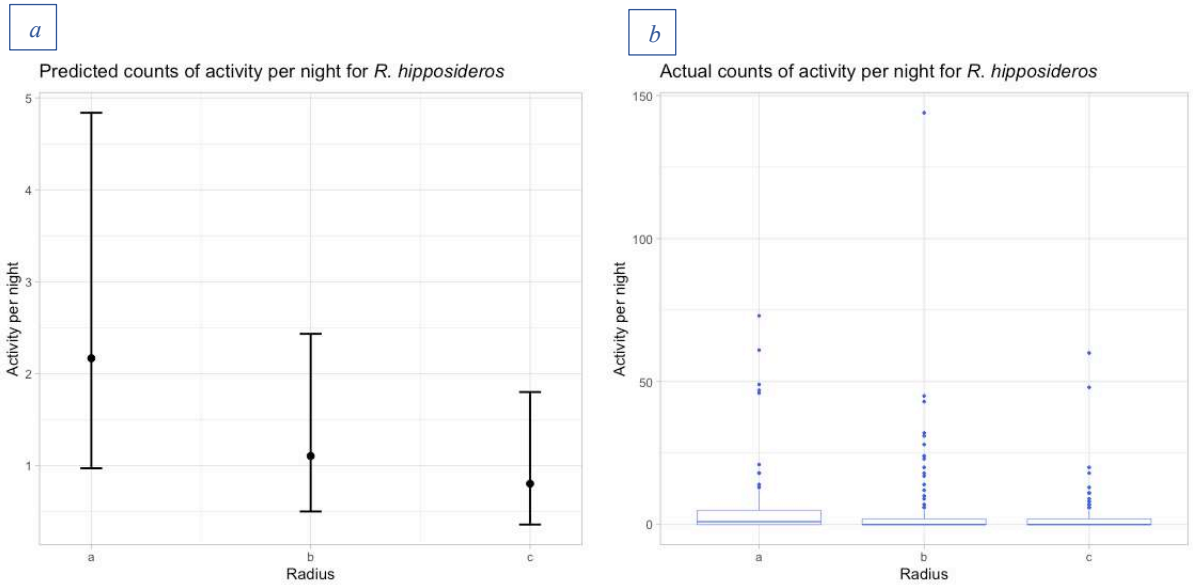

Figure_A 1: a) Model predicted relationship between commuting activity and Radius compared to b) actual counts of commuting activity

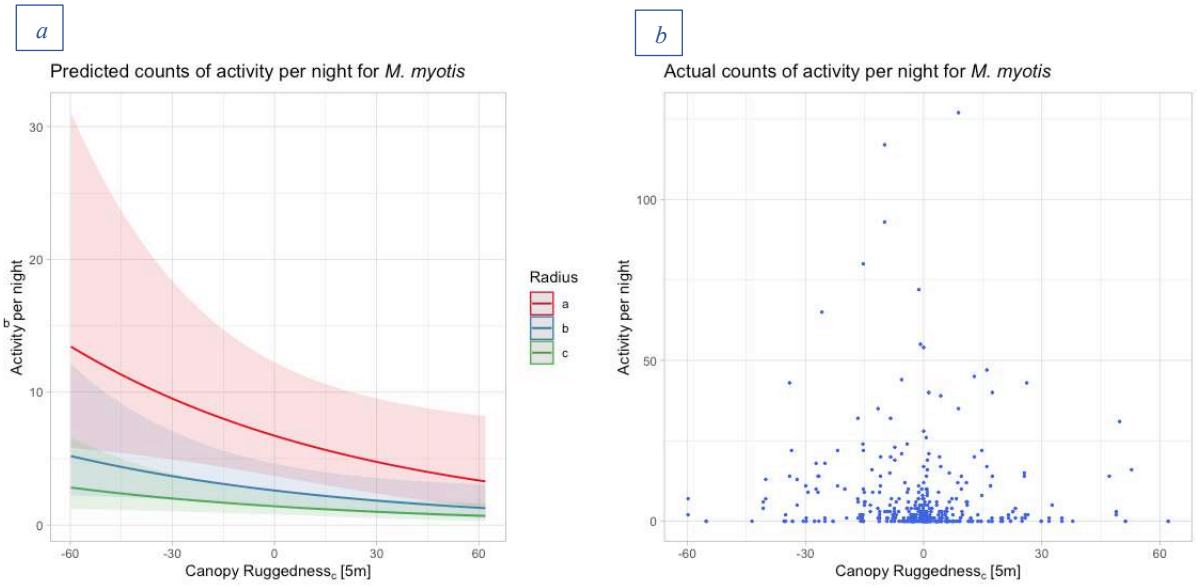

Figure_A 2: a) Model predicted relationship between commuting activity and canopy ruggedness$_c$ [5m] compared to b) actual counts of commuting activity

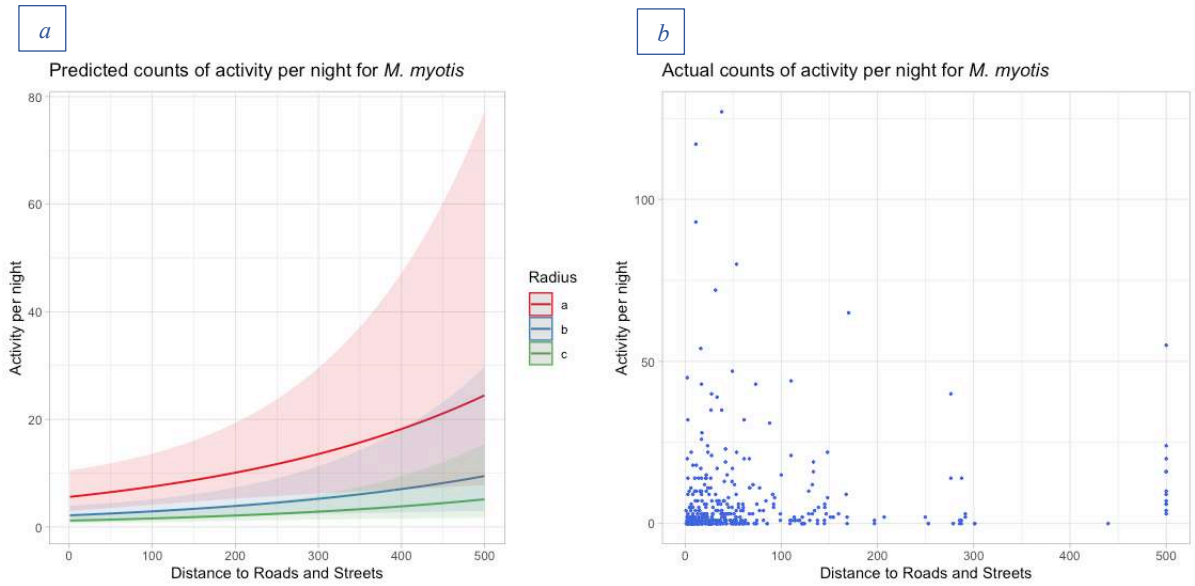

Figure_A 3: a) Model predicted relationship between commuting activity and distance to roads compared to b) actual counts of commuting activity

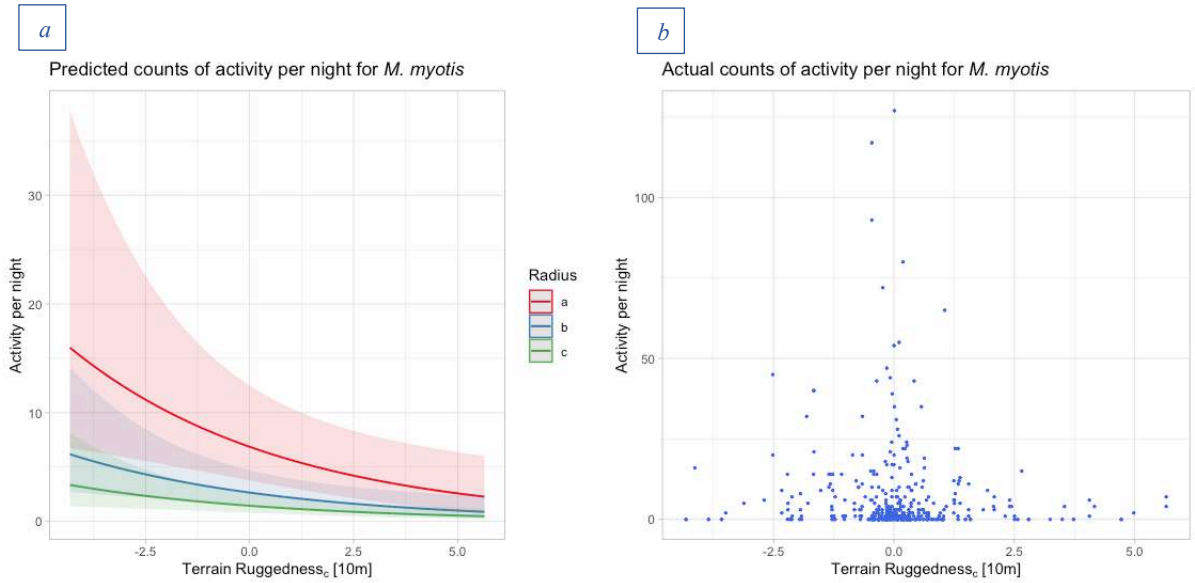

Figure_A 4: a) Model predicted relationship between commuting activity and terrain ruggedness$_c$ [10m] compared to b) actual counts of commuting activity

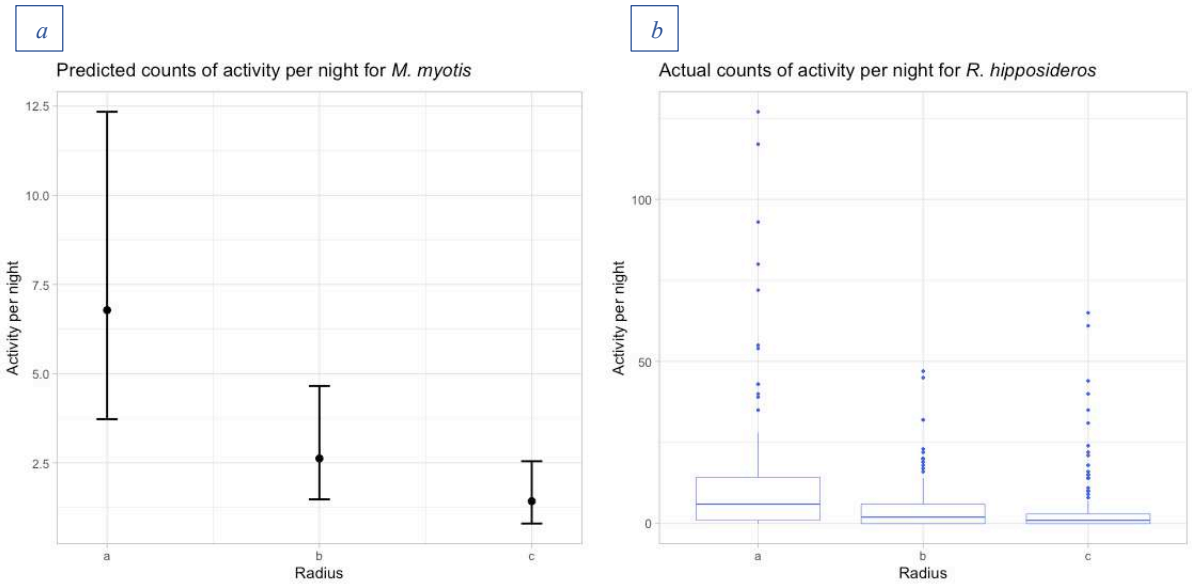

Figure_A 5: a) Model predicted relationship between commuting activity and Radius compared to b) actual counts of commuting activity

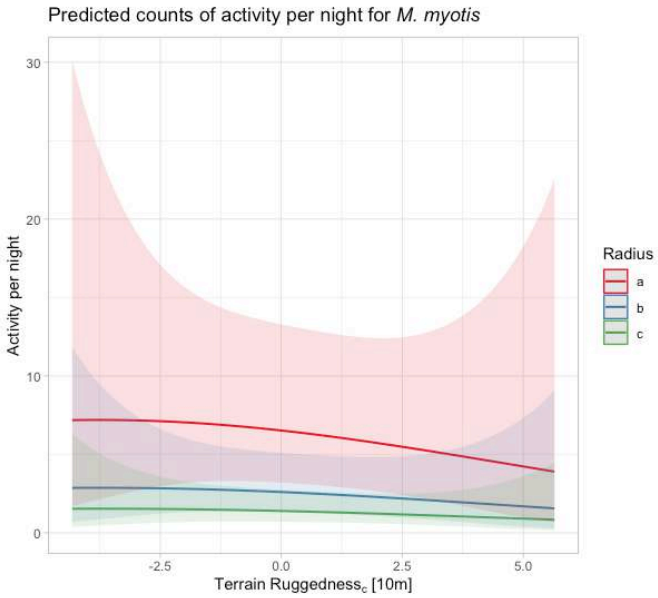

Figure_A 6: Model predicted relationship between commuting activity and terrain ruggedness$_c$ [10m] based on a small model with only the linear and the quadratic terms as fixed effects

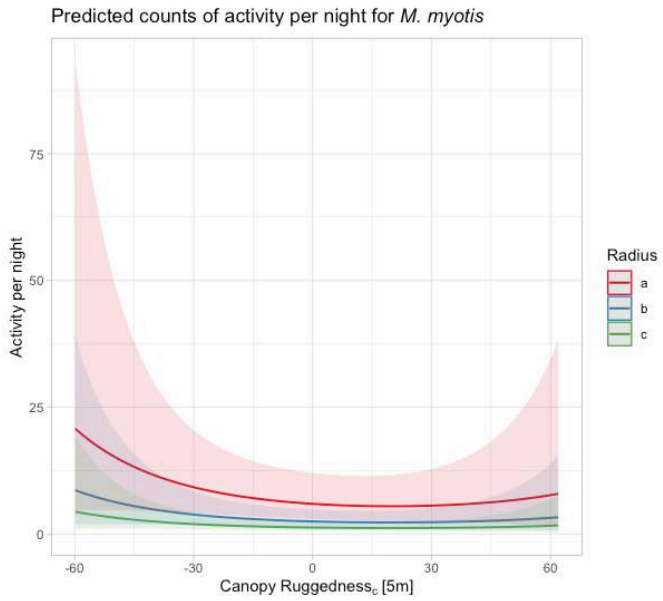

Figure_A 7: Model predicted relationship between commuting activity and canopy ruggedness$_c$ [5m] based on a small model with only the linear and the quadratic terms as fixed effects

Spatial modelling outputs

Myotis myotis – MYM

ALTENDORF

Figure_A 8: Least cost paths for MYM in Altendorf with the slightly transparent lightness layer underneath, and the aerial image as the bottom layer

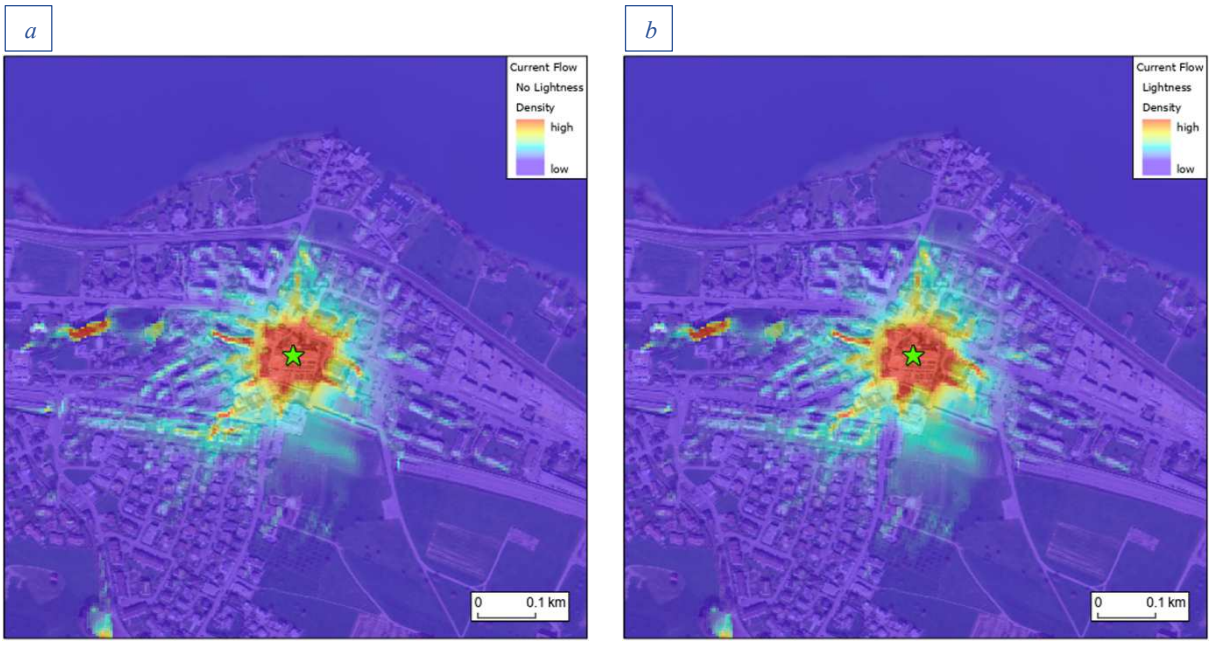

Figure_A 9: Current flow maps of MYM commuting in Altendorf predicted with a) no lightness and b) lightness

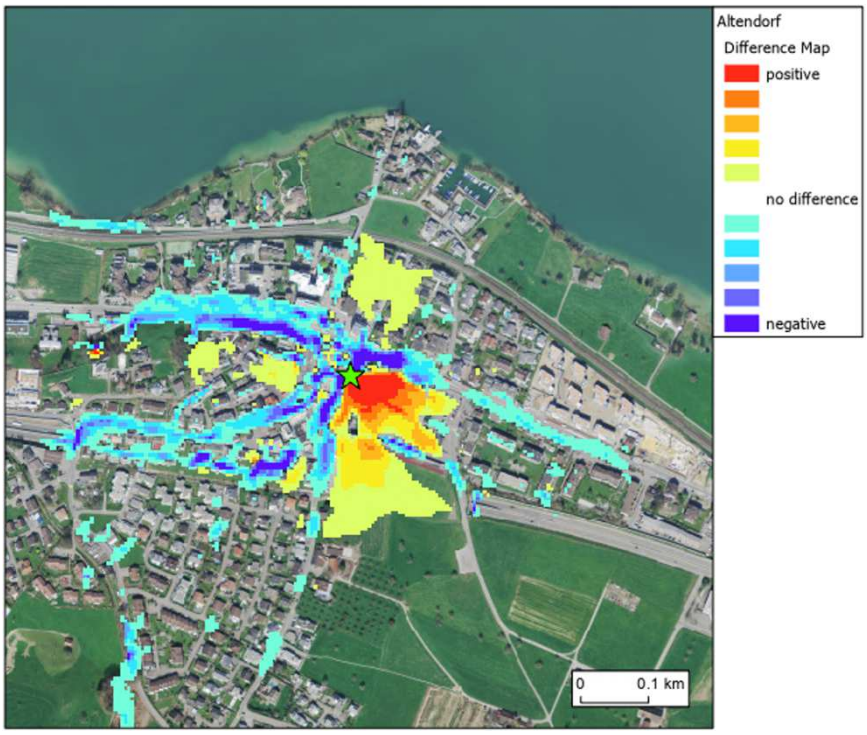

Figure_A 10: Difference map of Altendorf for MYM, depicting the difference in predicted current flow densities from a model with a lightness predictor to one including no light variable

BEGGINGEN

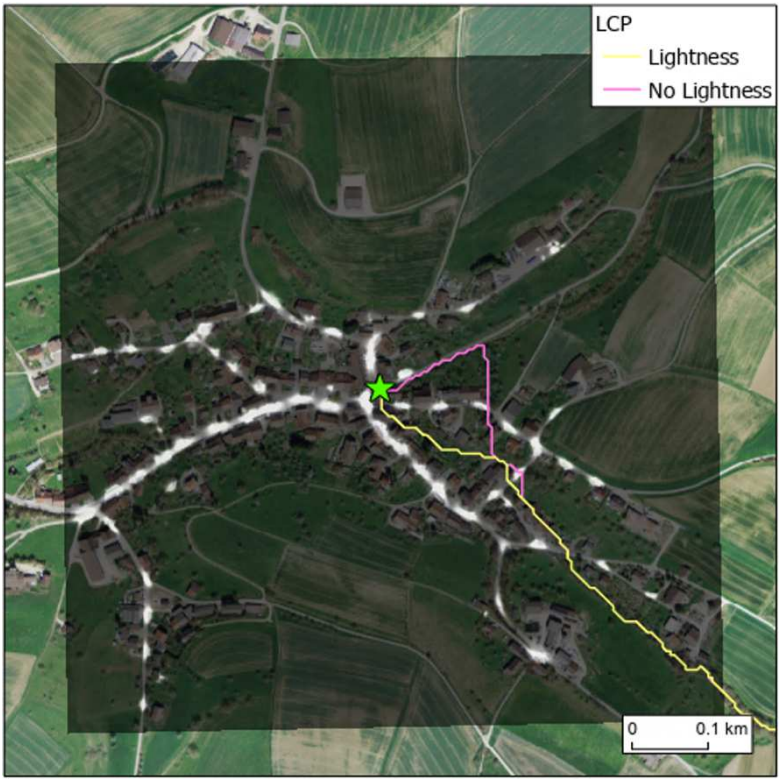

Figure_A 11: Least cost paths for MYM in Beggingen with the slightly transparent lightness layer underneath, and the aerial image as the bottom layer

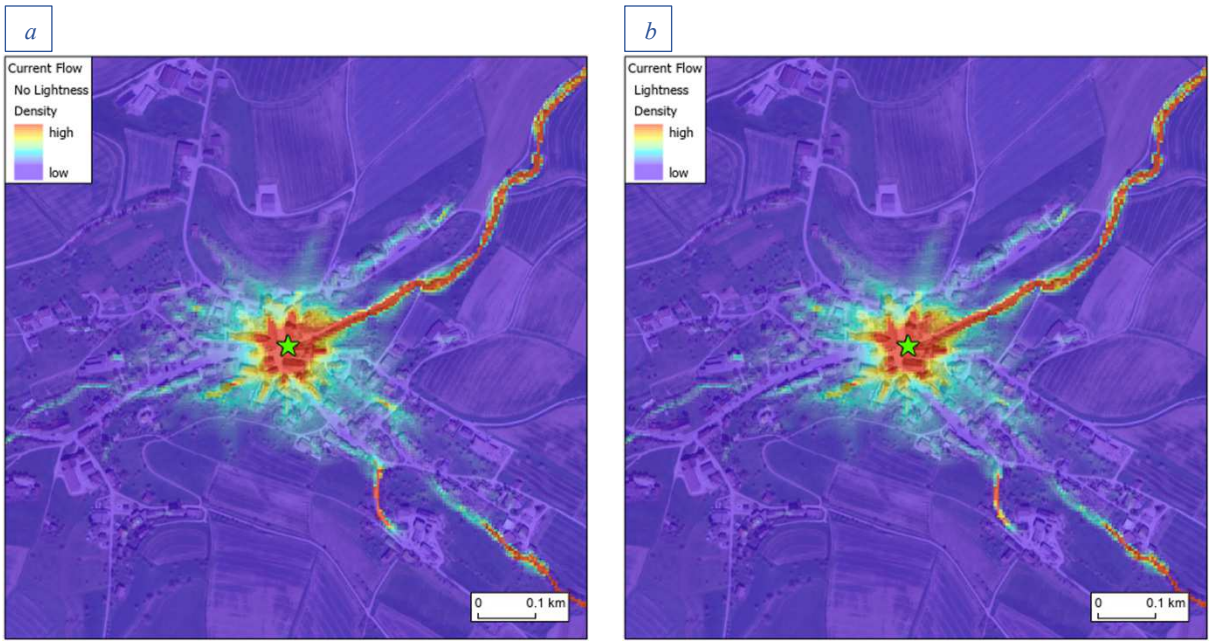

Figure_A 12: Current flow maps of MYM commuting in Beggingen predicted with a) no lightness and b) lightness

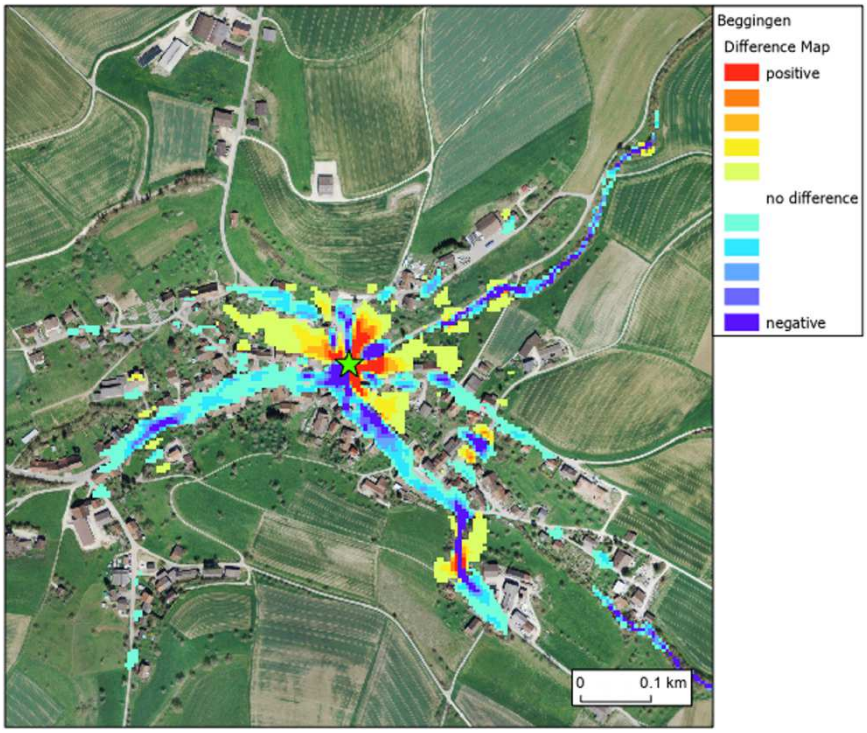

Figure_A 13: Difference map of Beggingen for MYM, depicting the difference in predicted current flow densities from a model with a lightness predictor to one including no light variable

BUTTISHOLZ

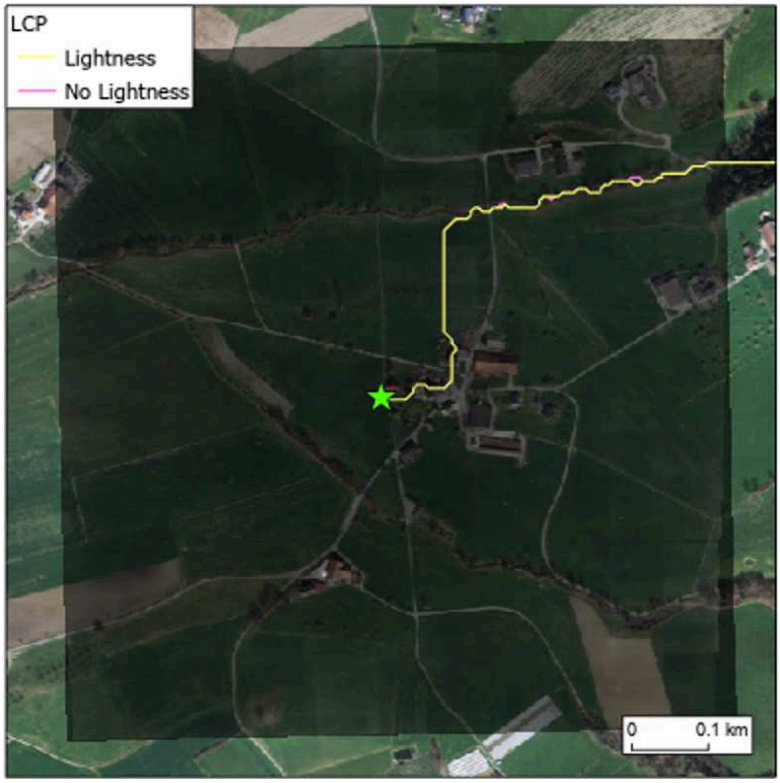

Figure_A 14: Least cost paths for MYM in Buttisholz with the slightly transparent lightness layer underneath, and the aerial image as the bottom layer

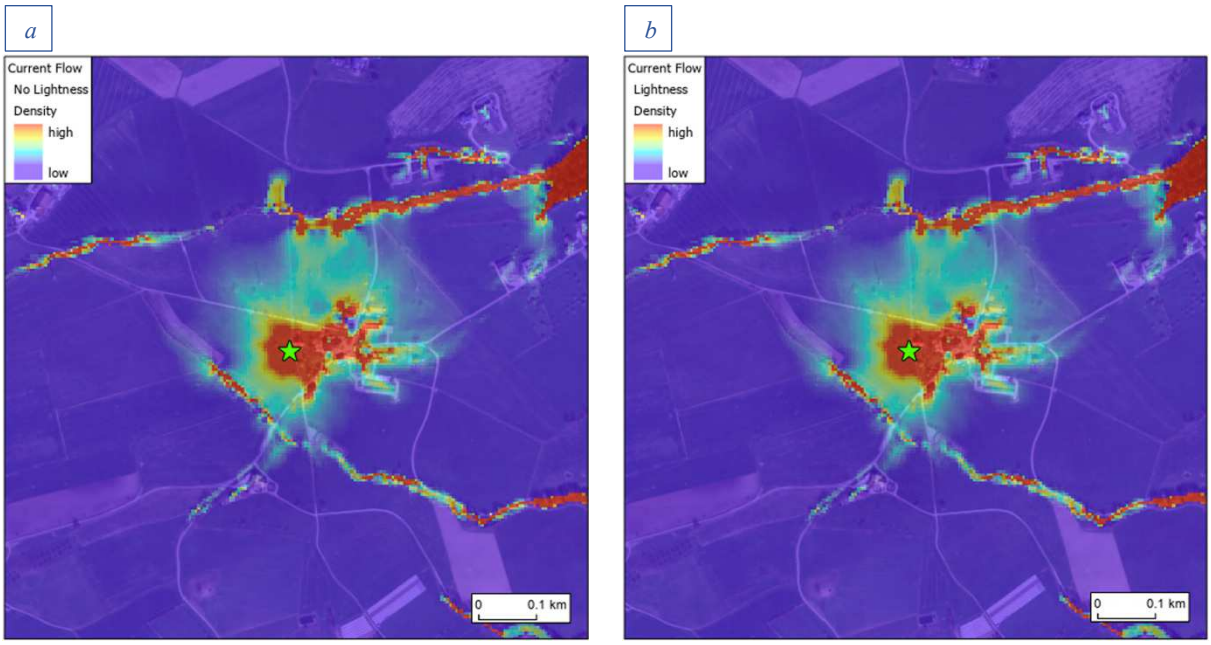

Figure_A 15: Current flow maps of MYM commuting in Buttisholz predicted with a) no lightness and b) lightness

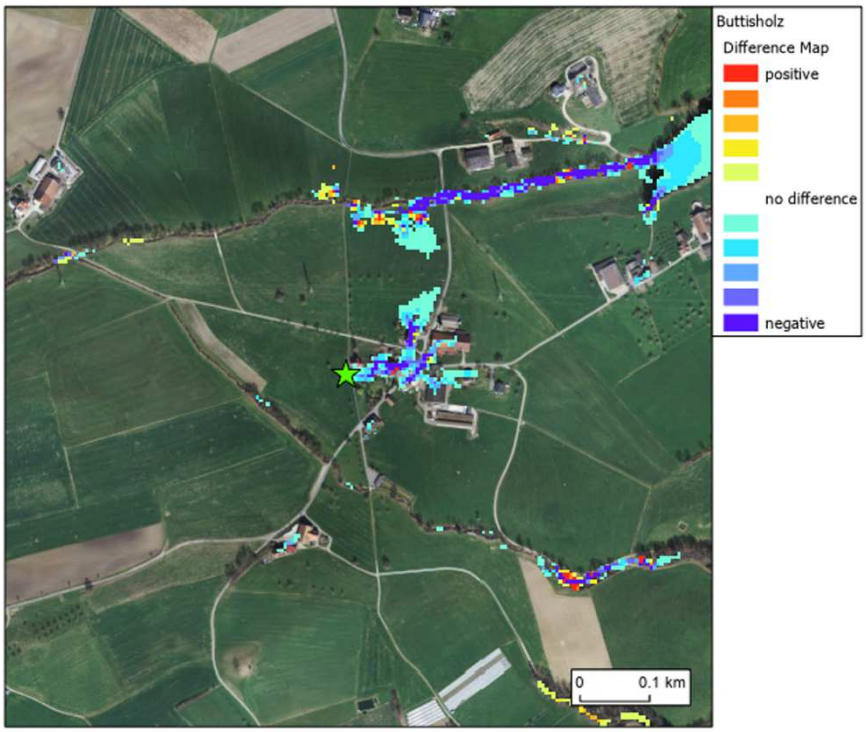

Figure_A 16: Difference map of Buttisholz for MYM, depicting the difference in predicted current flow densities from a model with a lightness predictor to one including no light variable

COURTÉTELLE

Figure_A 17: Least cost paths for MYM in Courtételle with the slightly transparent lightness layer underneath, and the aerial image as the bottom layer

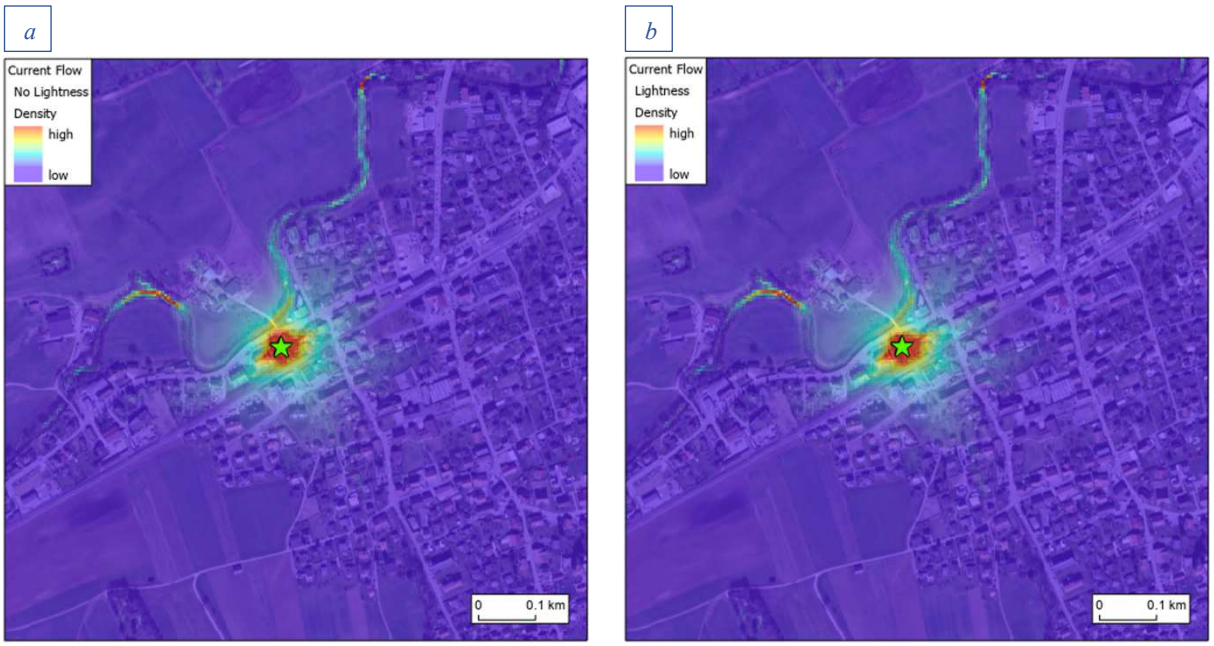

Figure_A 18: Current flow maps of MYM commuting in Courtételle predicted with a) no lightness and b) lightness

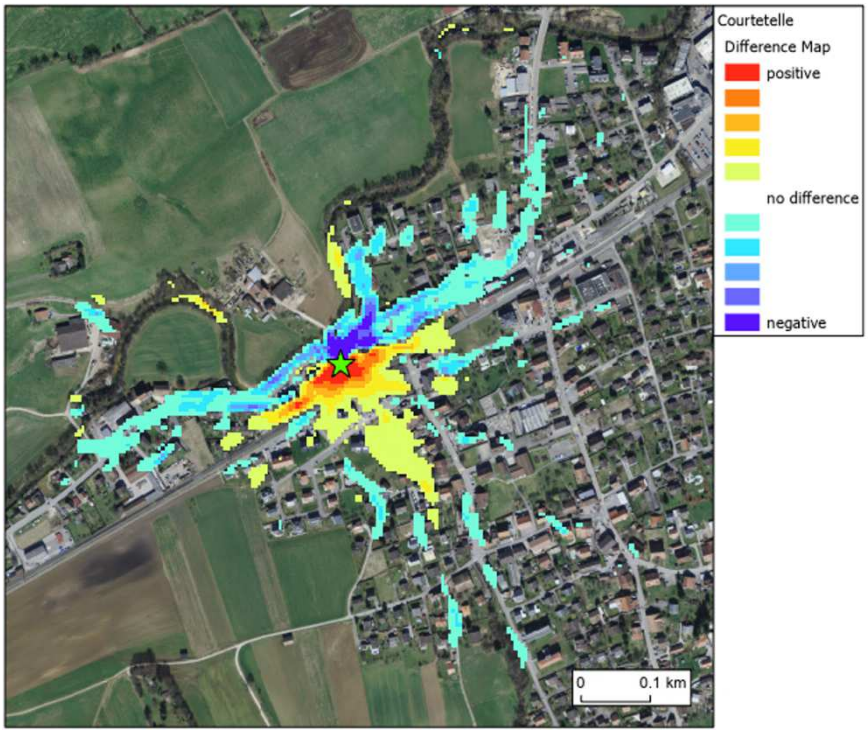

Figure_A 19: Difference map of Courtételle for MYM, depicting the difference in predicted current flow densities from a model with a lightness predictor to one including no light variable

EYSINS

Figure_A 20: Least cost paths for MYM in Eysins with the slightly transparent lightness layer underneath, and the aerial image as the bottom layer

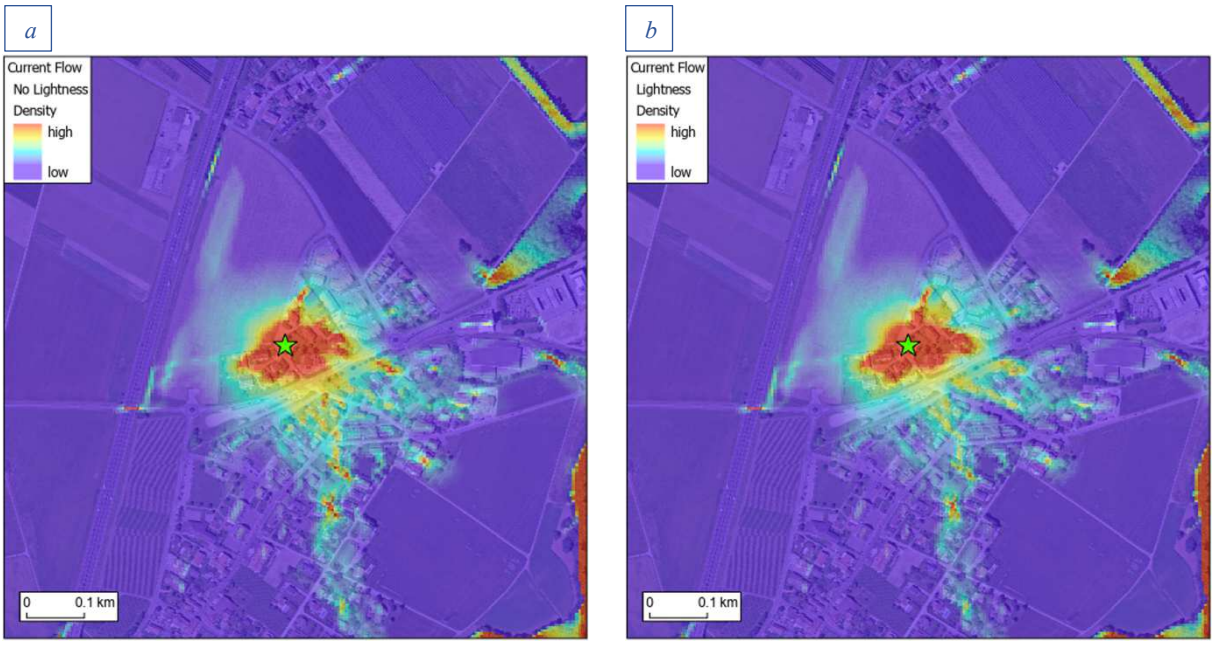

Figure_A 21: Current flow maps of MYM commuting in Eysins predicted with a) no lightness and b) lightness

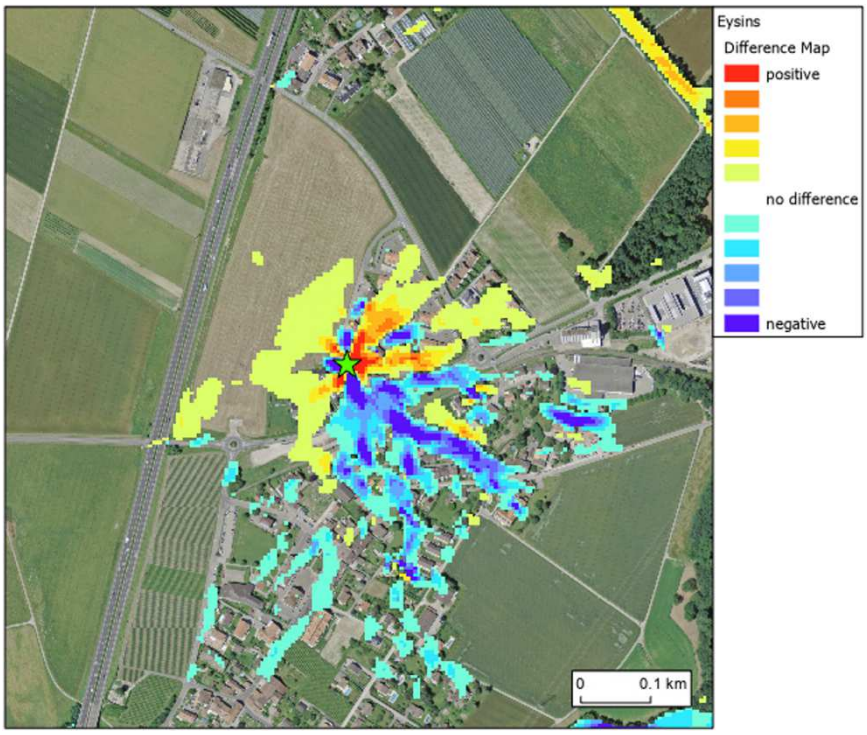

Figure_A 22: Difference map of Eysins for MYM, depicting the difference in predicted current flow densities from a model with a lightness predictor to one including no light variable

KALLNACH

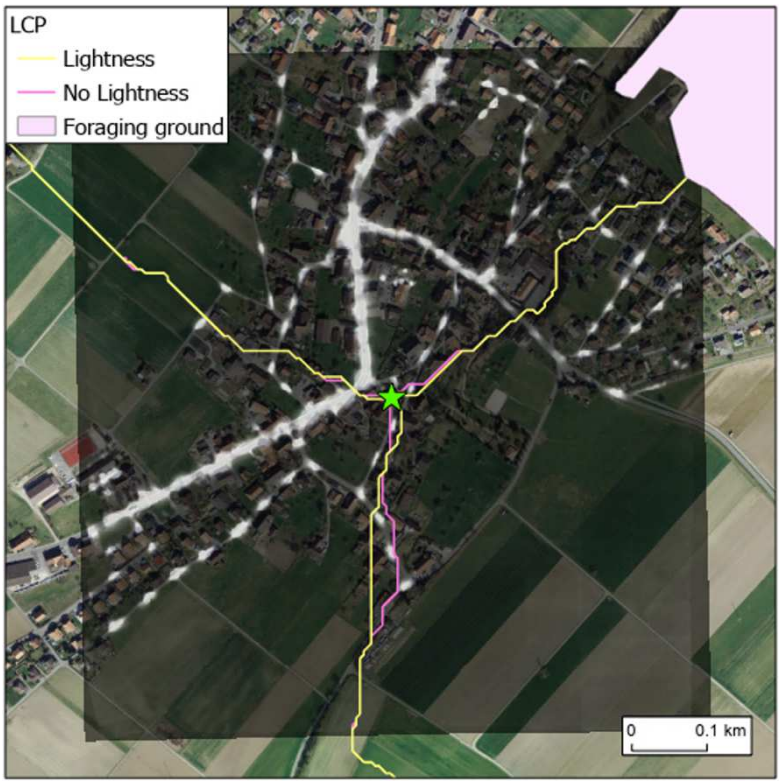

Figure_A 23: Least cost paths for MYM in Kallnach with the slightly transparent lightness layer underneath, and the aerial image as the bottom layer

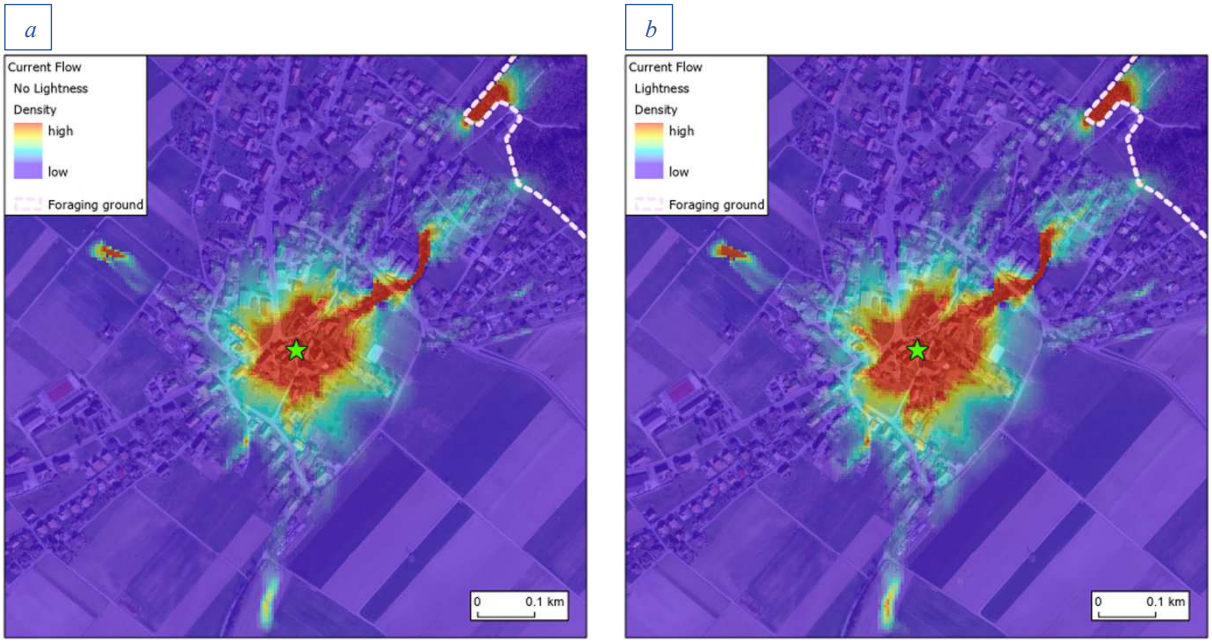

Figure_A 24: Current flow maps of MYM commuting in Kallnach predicted with a) no lightness and b) lightness

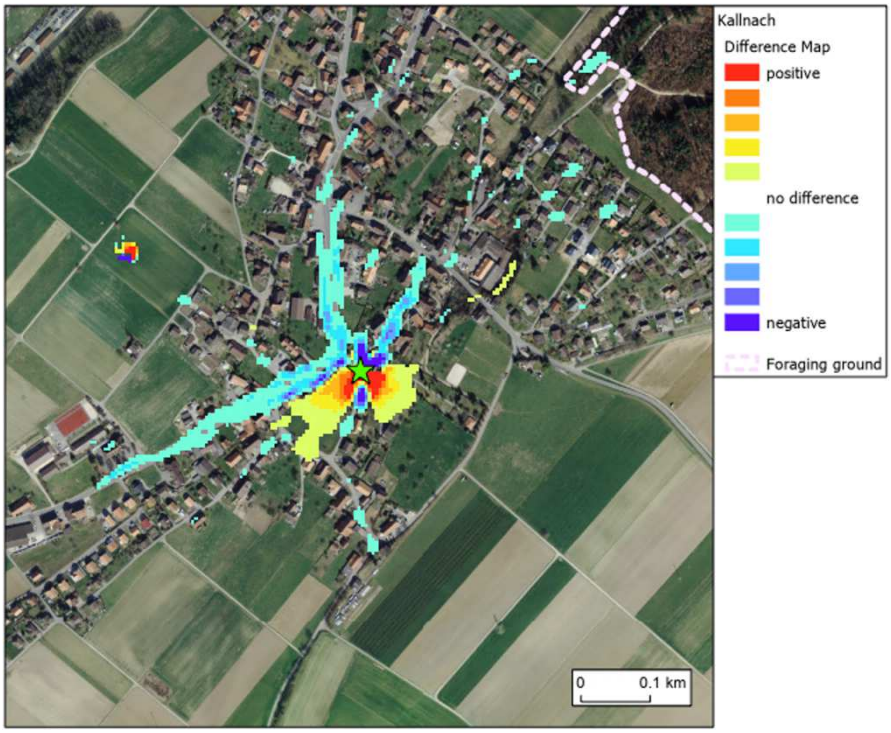

Figure_A 25: Difference map of Kallnach for MYM, depicting the difference in predicted current flow densities from a model with a lightness predictor to one including no light variable

LIPPERSWIL

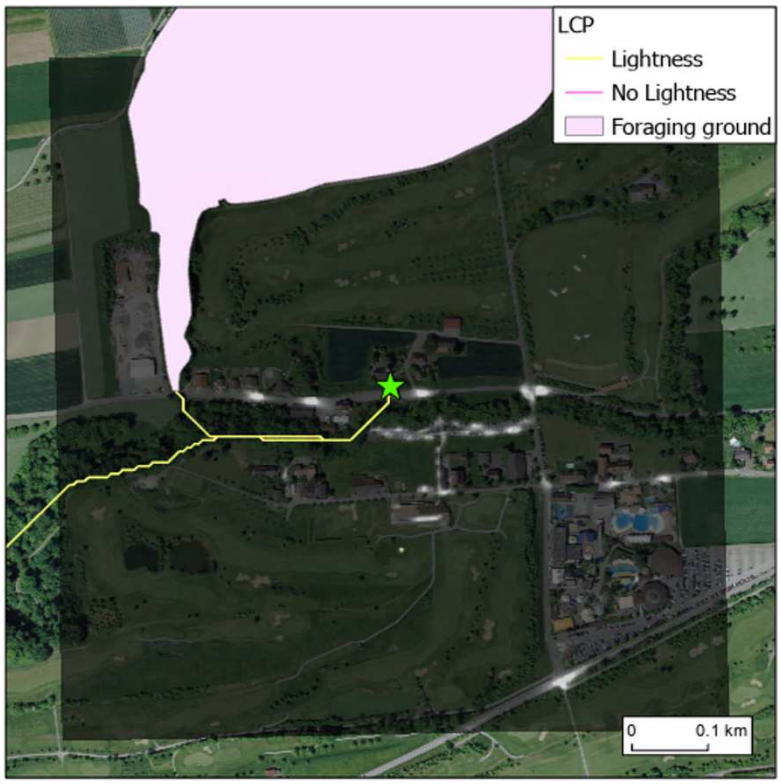

Figure_A 26: Least cost paths for MYM in Lipperswil with the slightly transparent lightness layer underneath, and the aerial image as the bottom layer

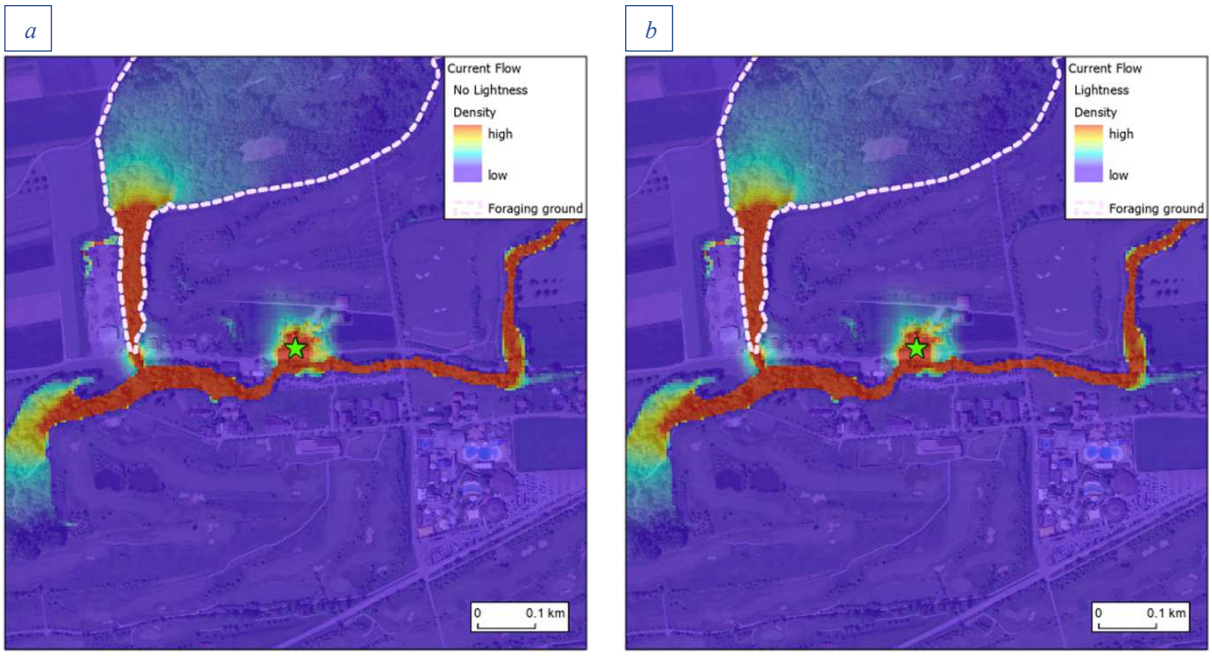

Figure_A 27: Current flow maps of MYM commuting in Lipperswil predicted with a) no lightness and b) lightness

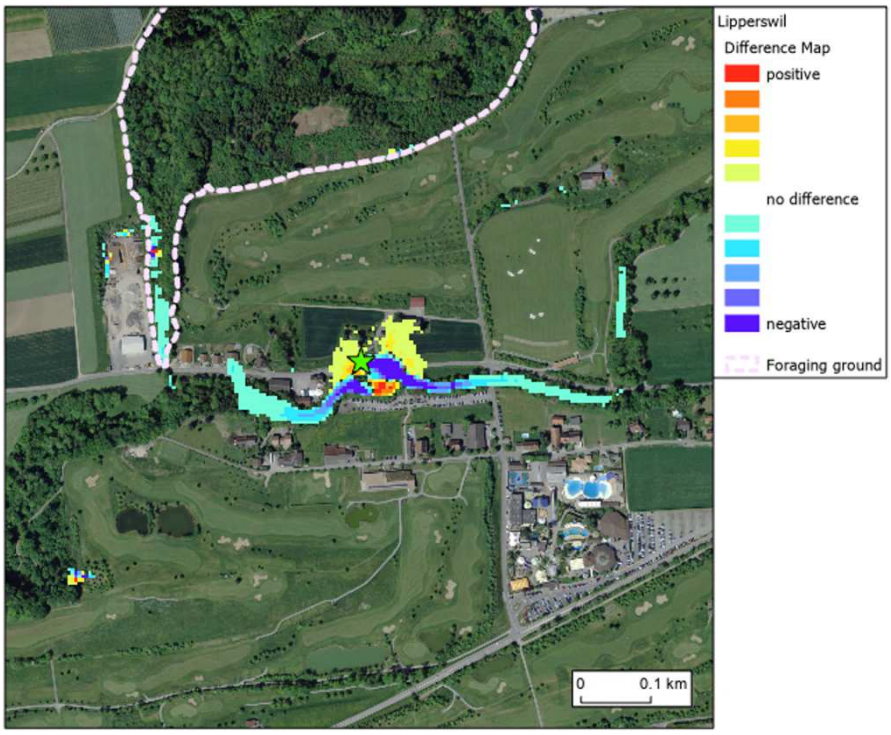

Figure_A 28: Difference map of Lipperswil for MYM, depicting the difference in predicted current flow densities from a model with a lightness predictor to one including no light variable

MÜHLAU

Figure_A 29: Least cost paths for MYM in Mühlau with the slightly transparent lightness layer underneath, and the aerial image as the bottom layer

a

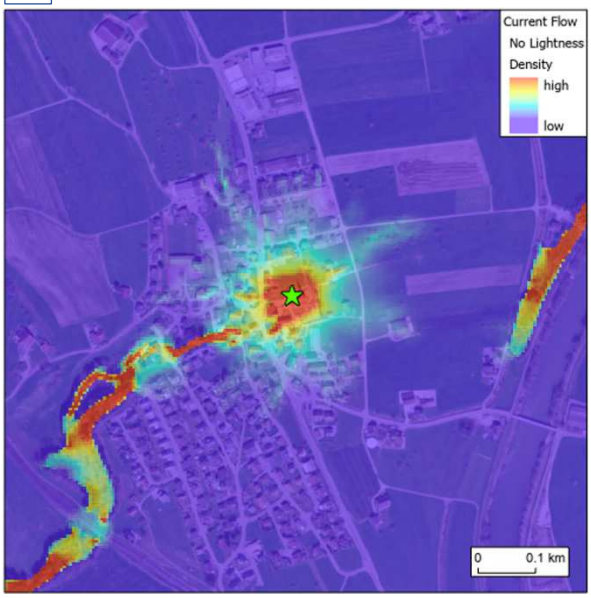

b

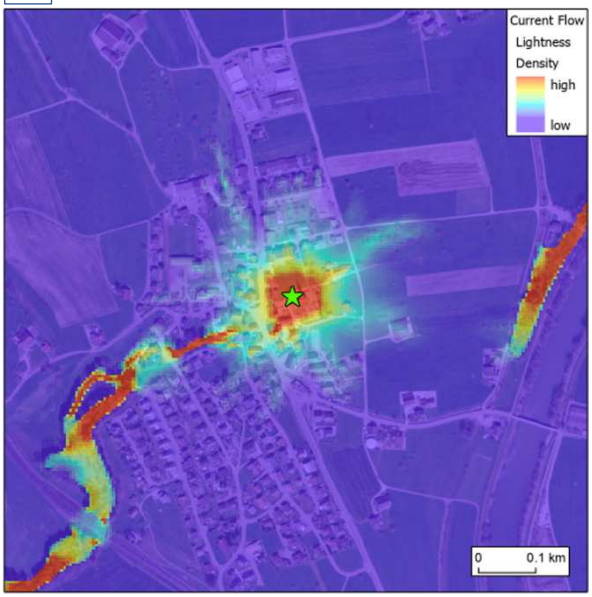

Figure_A 30: Current flow maps of MYM commuting in Mühlau predicted with a) no lightness and b) lightness

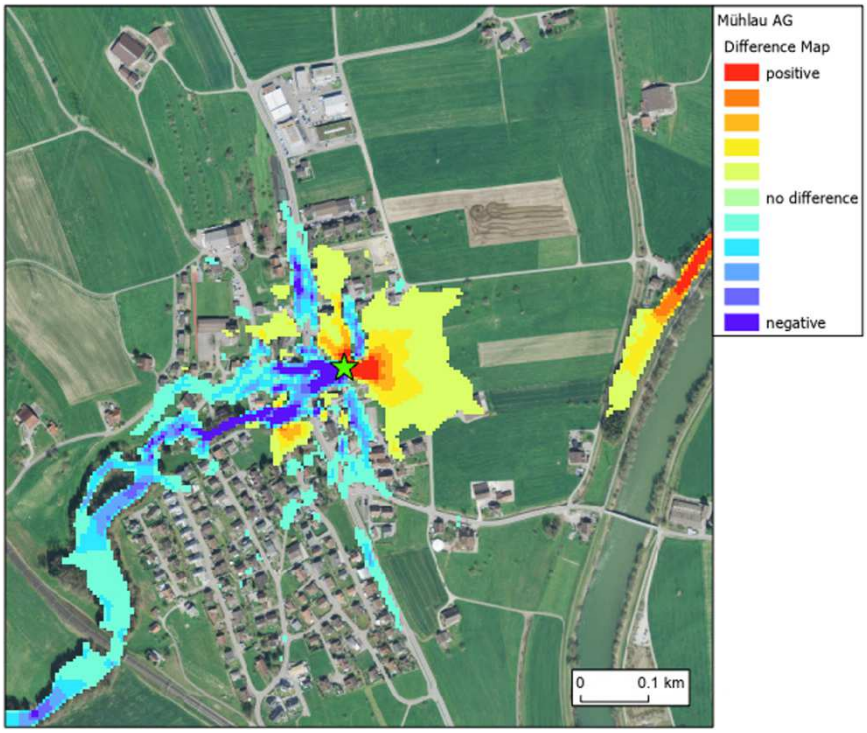

Figure_A 31: Difference map of Mühlau for MYM, depicting the difference in predicted current flow densities from a model with a lightness predictor to one including no light variable

STEINEN

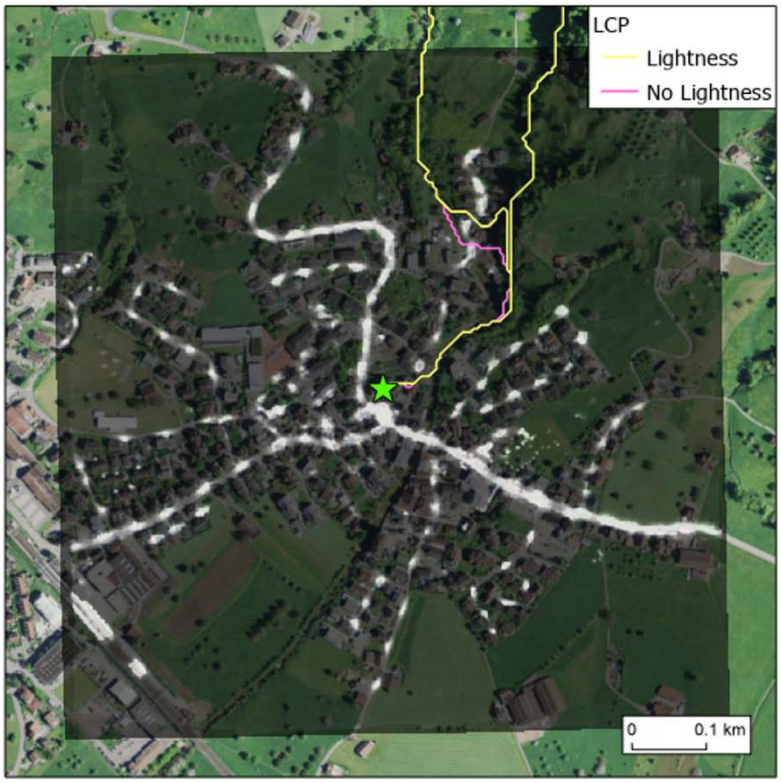

Figure_A 32: Least cost paths for MYM in Steinen with the slightly transparent lightness layer underneath, and the aerial image as the bottom layer

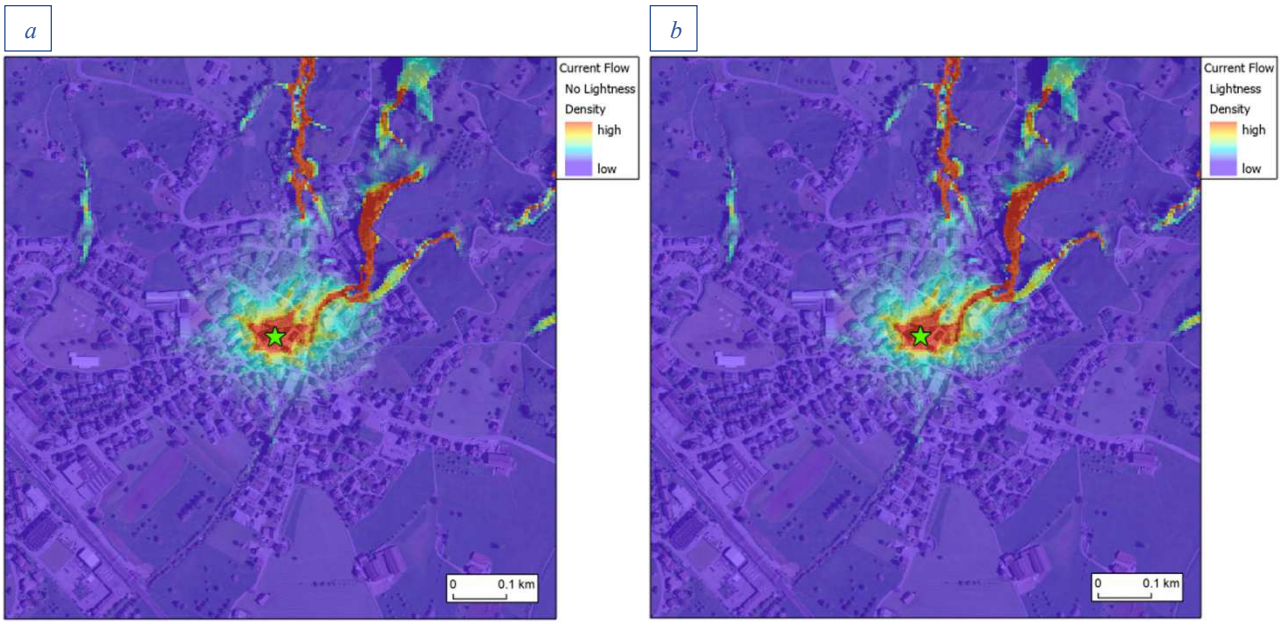

Figure_A 33: Current flow maps of MYM commuting in Steinen predicted with a) no lightness and b) lightness

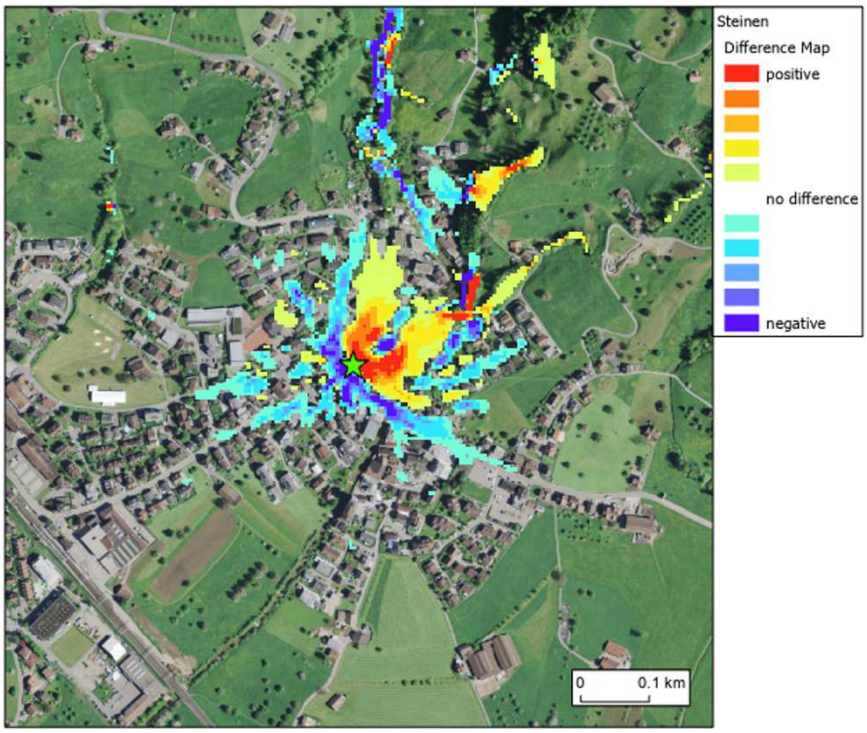

Figure_A 34: Difference map of Steinen for MYM, depicting the difference in predicted current flow densities from a model with a lightness predictor to one including no light variable

Rhinolophus hipposideros – RHI

AMSOLDINGEN

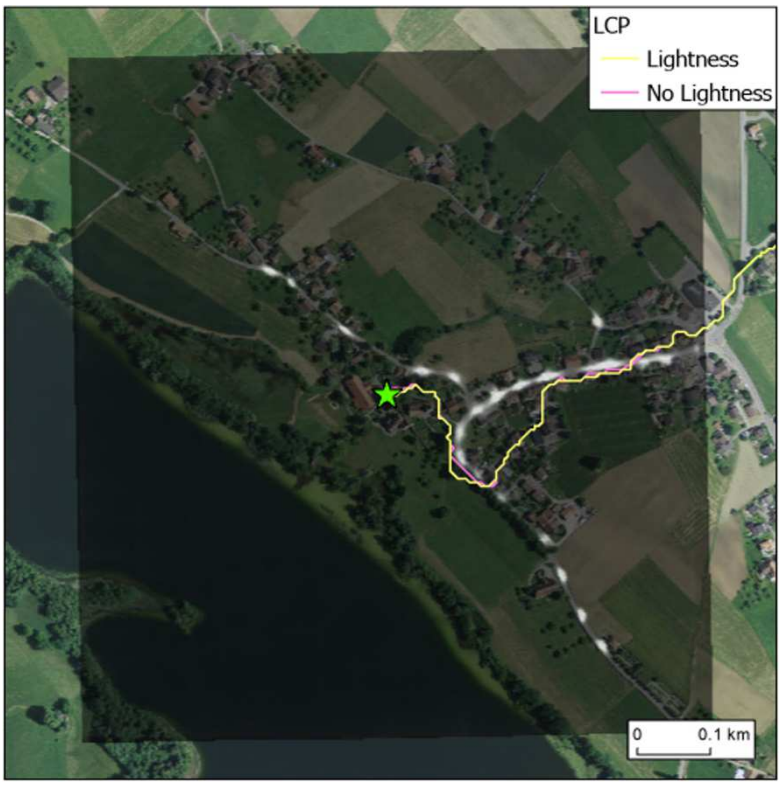

Figure_A 35: Least cost paths for RHI in Amsoldingen with the slightly transparent lightness layer underneath, and the aerial image as the bottom layer

a

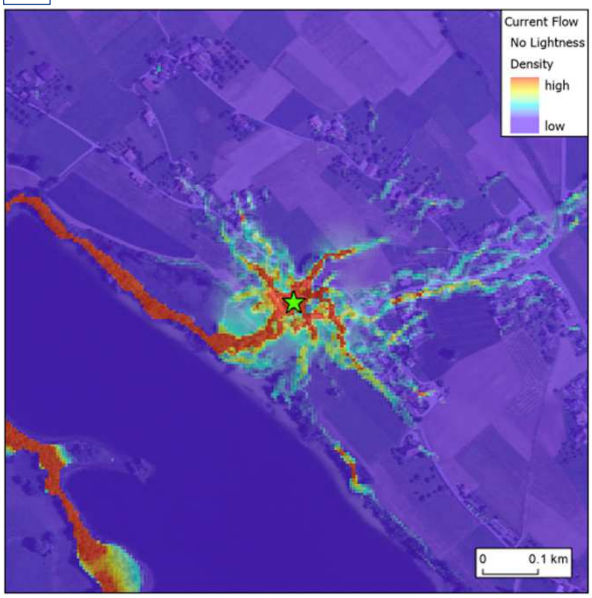

b

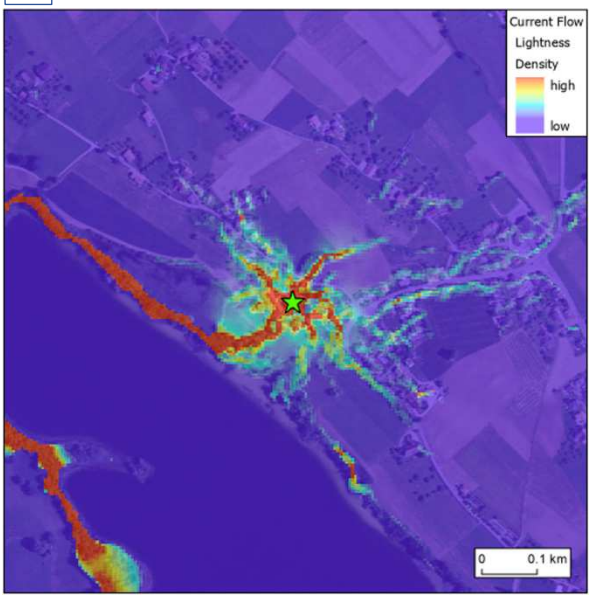

Figure_A 36: Current flow maps of RHI commuting in Amsoldingen predicted with a) no lightness and b) lightness

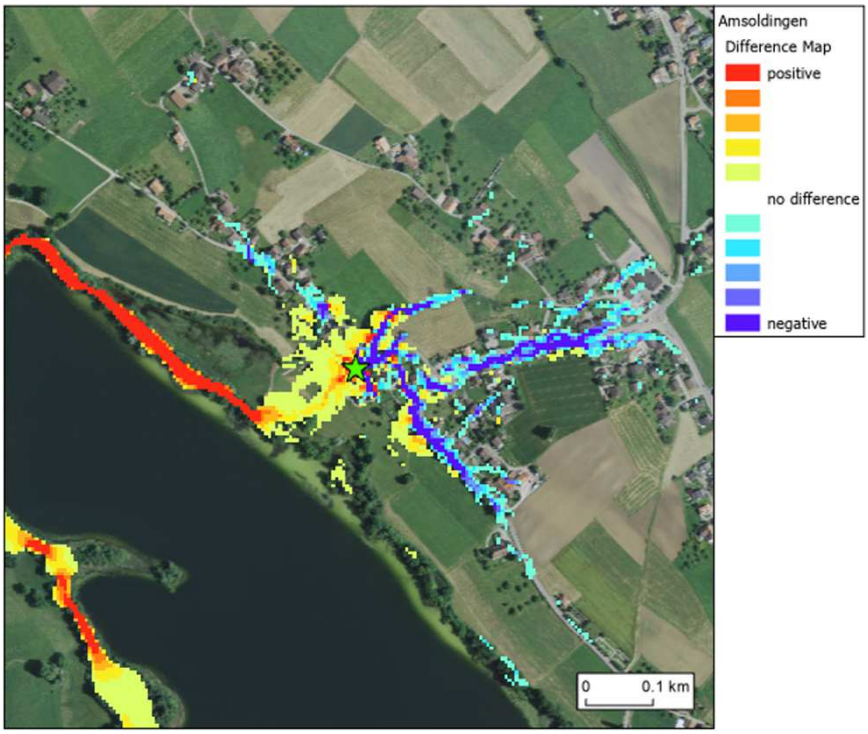

Figure_A 37: Difference map of Amsoldingen for RHI, depicting the difference in predicted current flow densities from a model with a lightness predictor to one including no light variable

CASTIEL

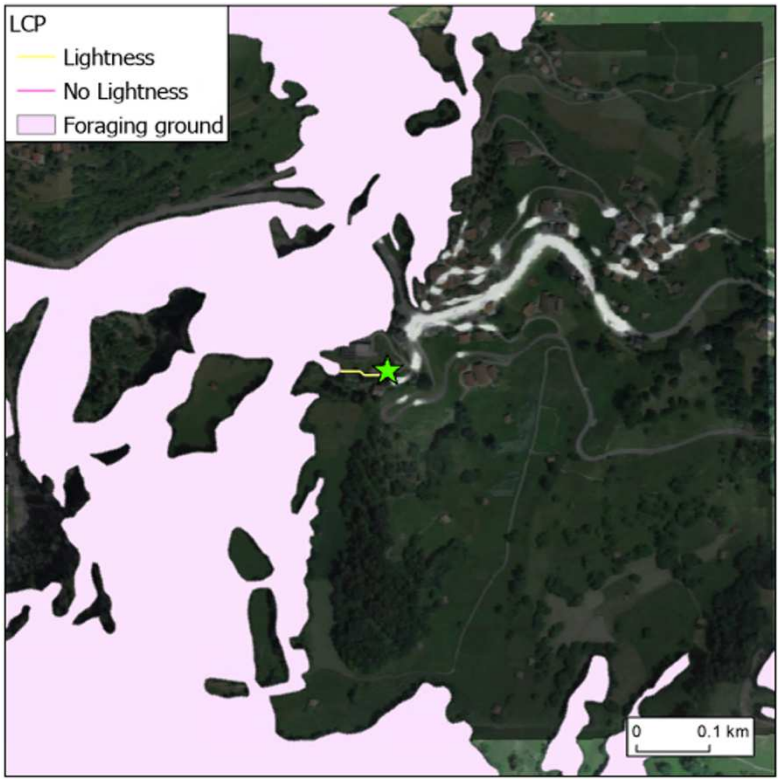

Figure_A 38: Least cost paths for RHI in Castiel with the slightly transparent lightness layer underneath, and the aerial image as the bottom layer

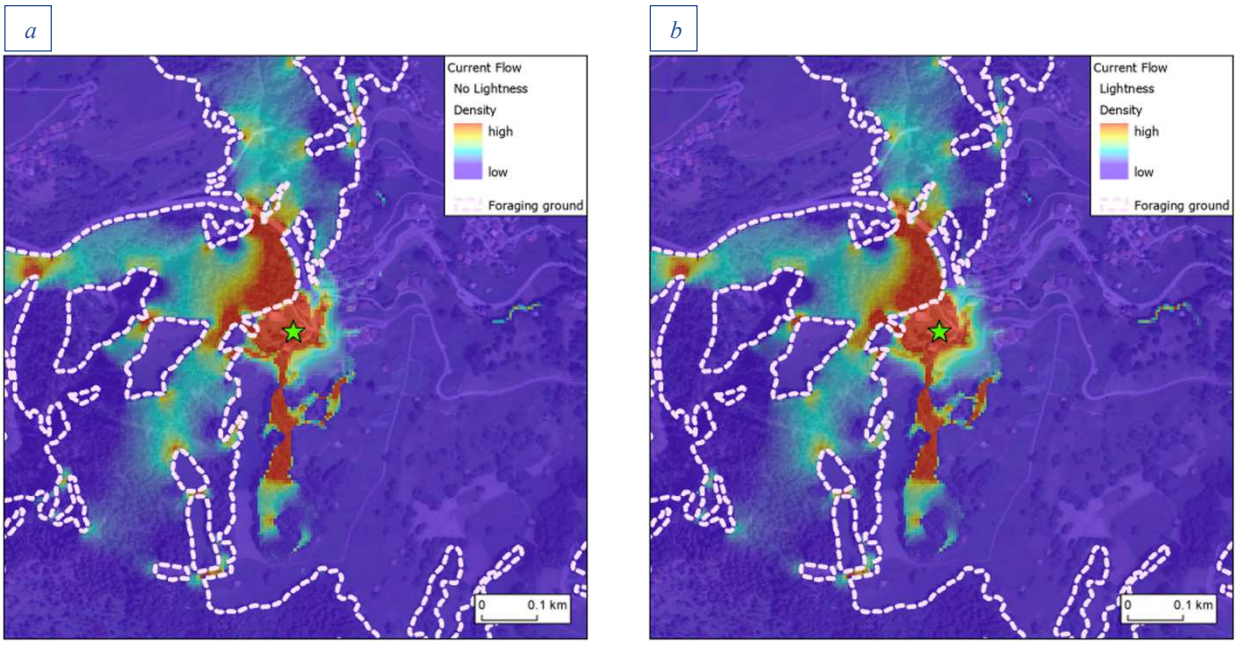

Figure_A 39: Current flow maps of RHI commuting in Castiel predicted with a) no lightness and b) lightness

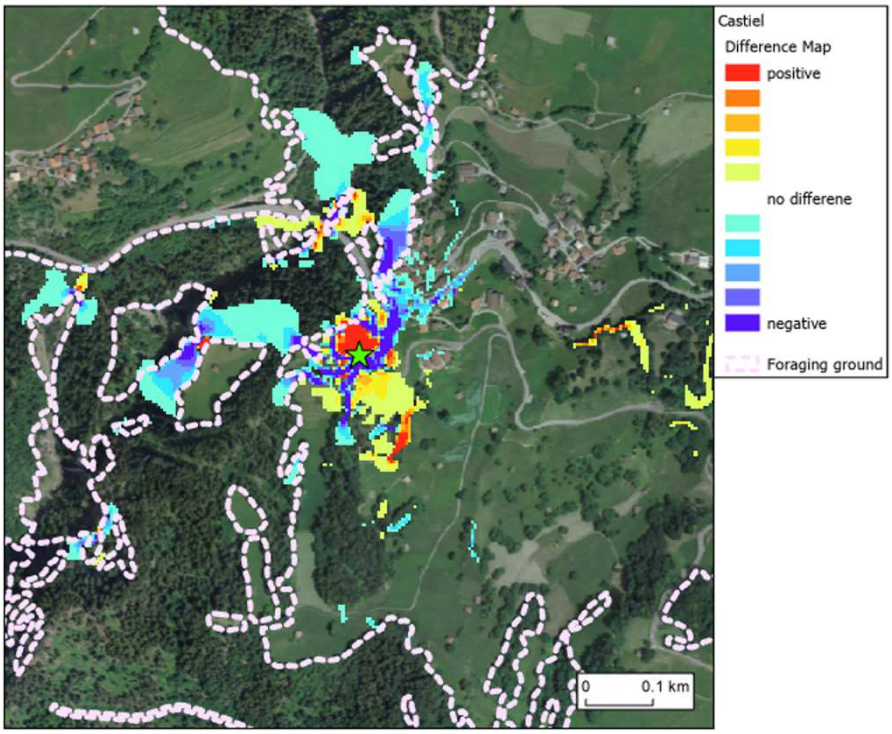

Figure_A 40: Difference map of Castiel for RHI, depicting the difference in predicted current flow densities from a model with a lightness predictor to one including no light variable

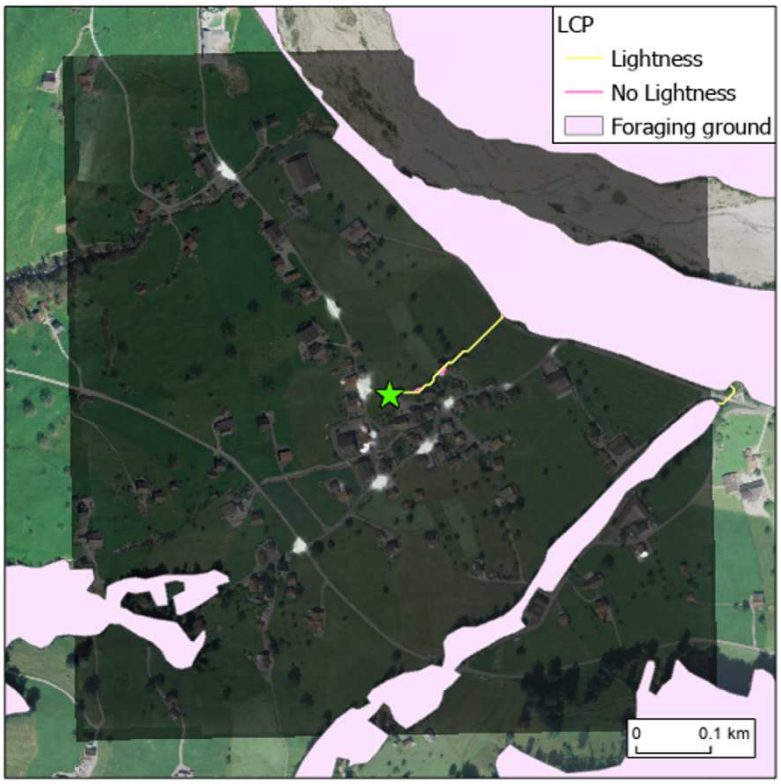

Figure_A 41: Least cost paths for RHI in Giswil with the slightly transparent lightness layer underneath, and the aerial image as the bottom layer

a

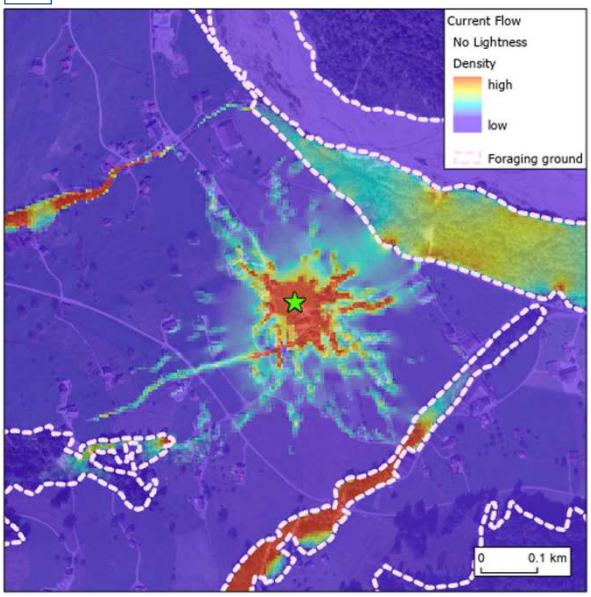

b

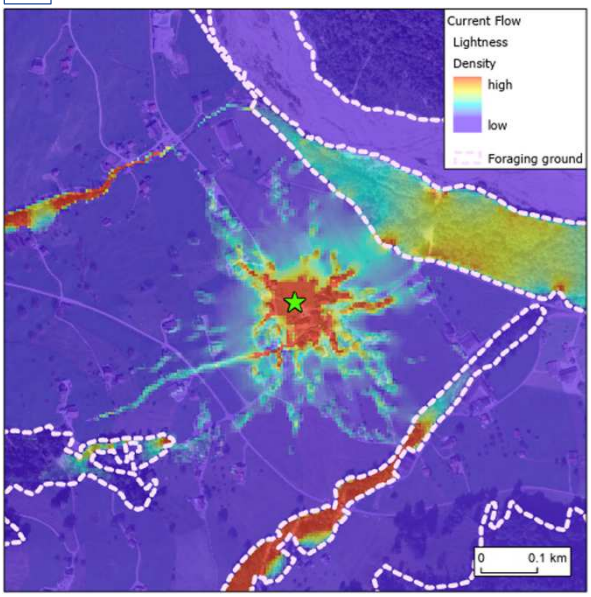

Figure_A 42: Current flow maps of RHI commuting in Giswil predicted with a) no lightness and b) lightness

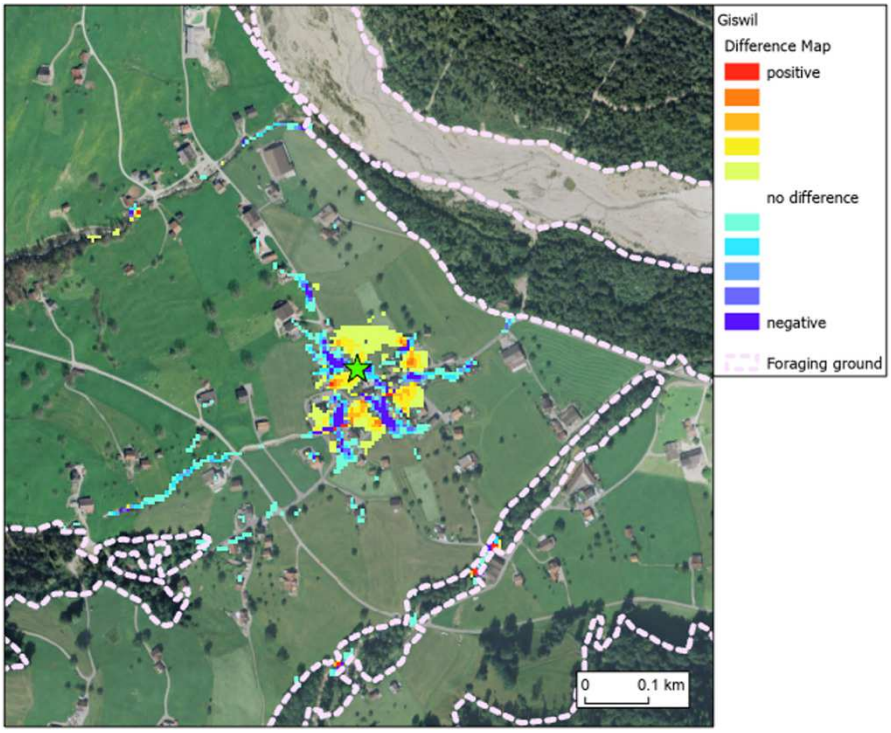

Figure_A 43: Difference map of Giswil for RHI, depicting the difference in predicted current flow densities from a model with a lightness predictor to one including no light variable

METZERLEN – MARIASTEIN

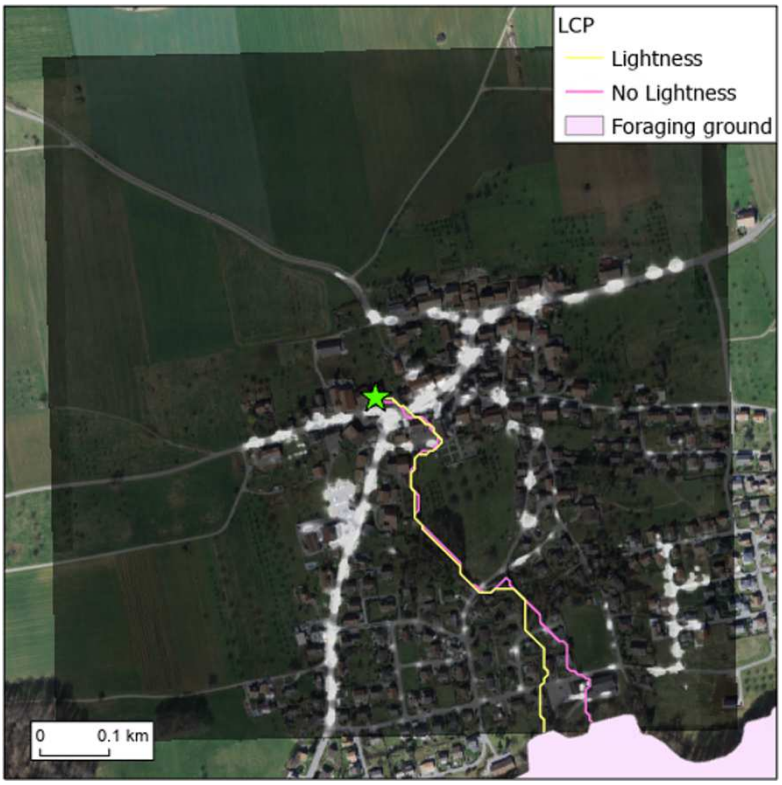

Figure_A 44: Least cost paths for RHI in Metzerlen with the slightly transparent lightness layer underneath, and the aerial image as the bottom layer

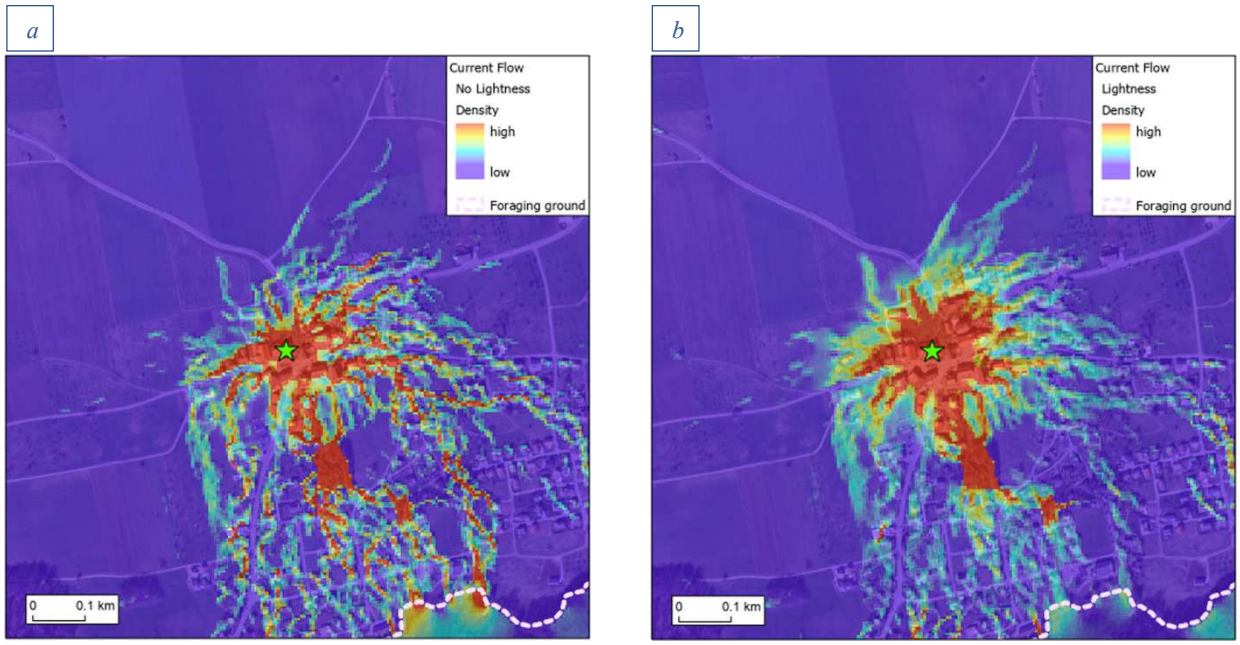

Figure_A 45: Current flow maps of RHI commuting in Metzerlen predicted with a) no lightness and b) lightness

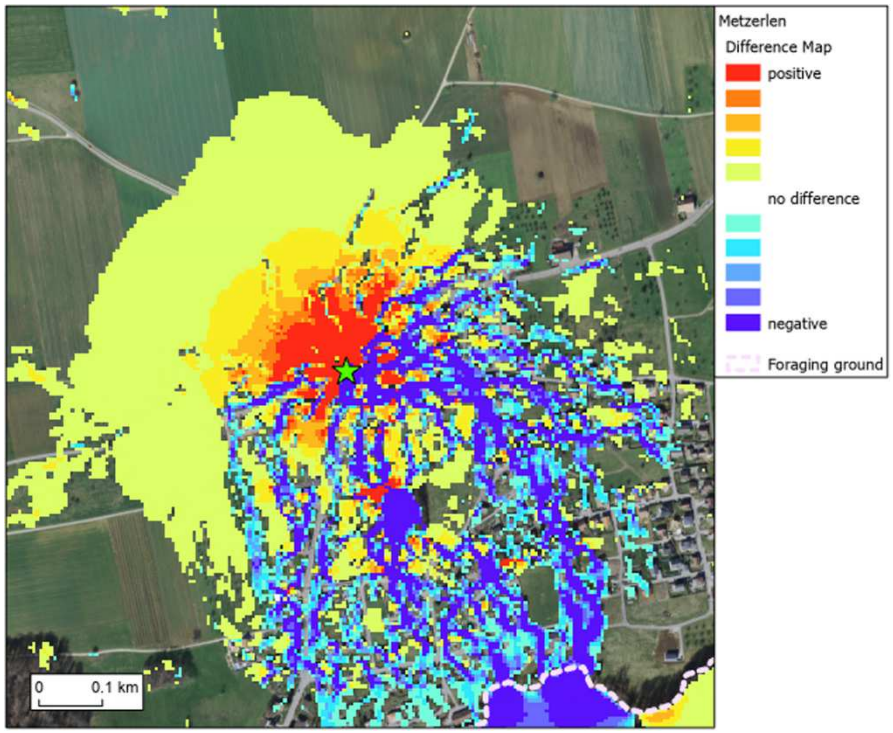

Figure_A 46: Difference map of Metzerlen for RHI, depicting the difference in predicted current flow densities from a model with a lightness predictor to one including no light variable

SACHSELN

Figure_A 47: Least cost paths for RHI in Sachseln with the slightly transparent lightness layer underneath, and the aerial image as the bottom layer

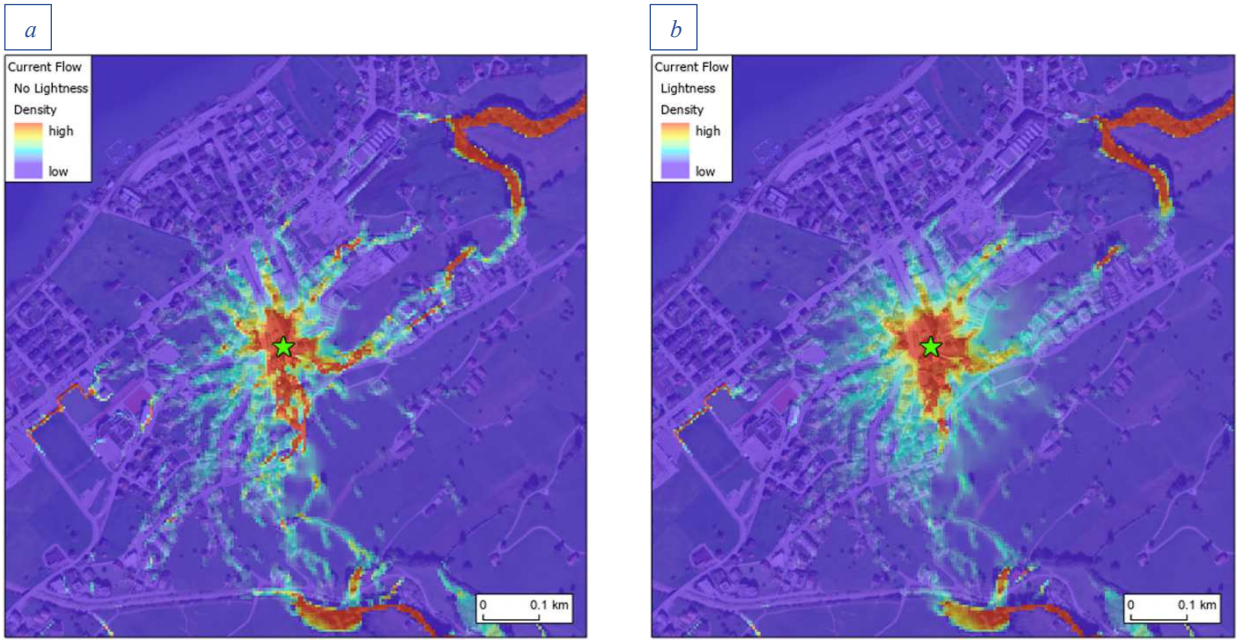

Figure_A 48: Current flow maps of RHI commuting in Sachseln predicted with a) no lightness and b) lightness

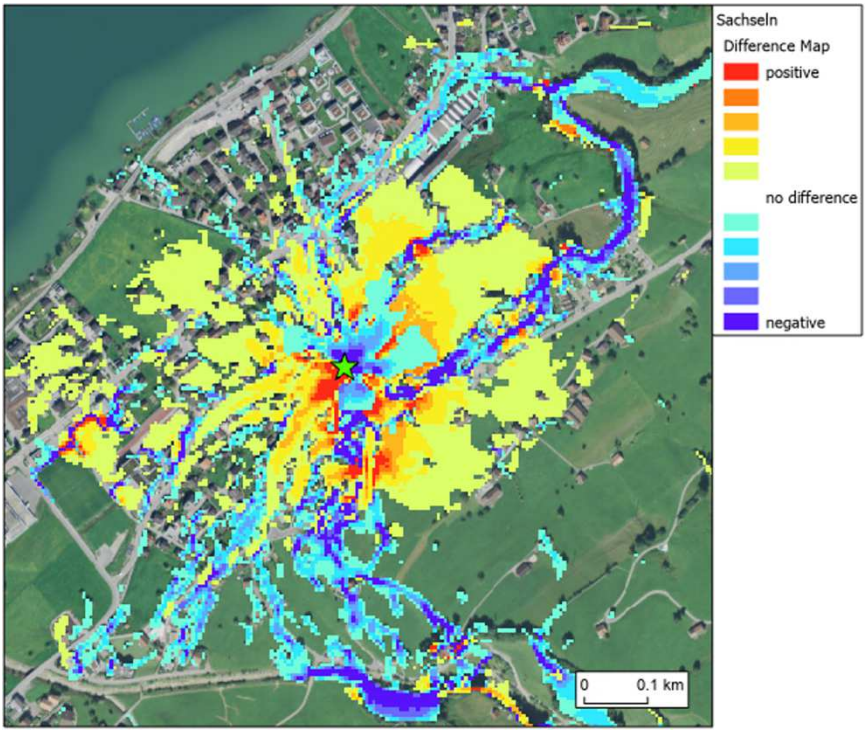

Figure_A 49: Difference map of Sachseln for RHI, depicting the difference in predicted current flow densities from a model with a lightness predictor to one including no light variable

SARNEN – WILEN

Figure_A 50: Least cost paths for RHI in Sarnen with the slightly transparent lightness layer underneath, and the aerial image as the bottom layer

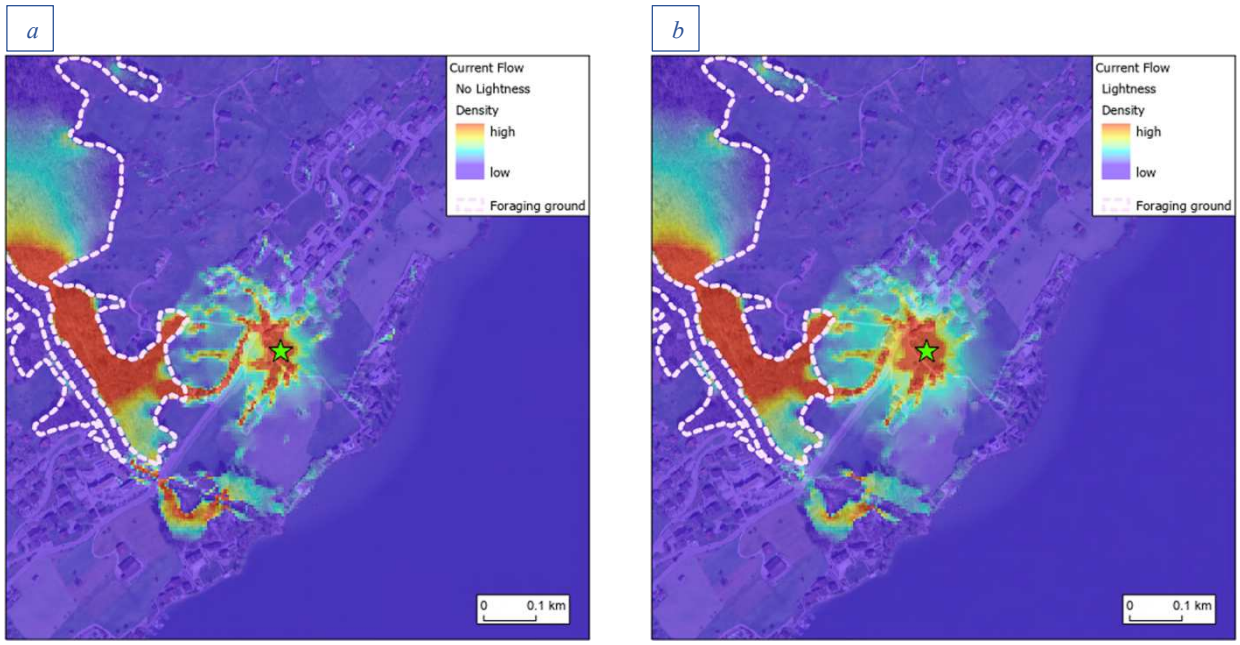

Figure_A 51: Current flow maps of RHI commuting in Sarnen predicted with a) no lightness and b) lightness

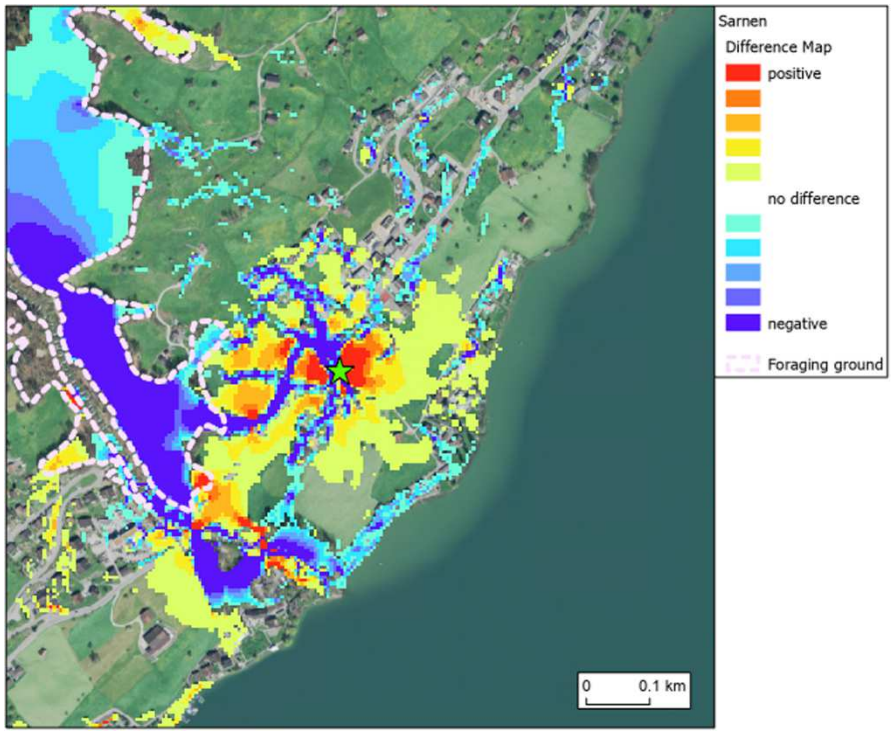

Figure_A 52: Difference map of Sarnen for RHI, depicting the difference in predicted current flow densities from a model with a lightness predictor to one including no light variable

LUMNEZIA – UORS

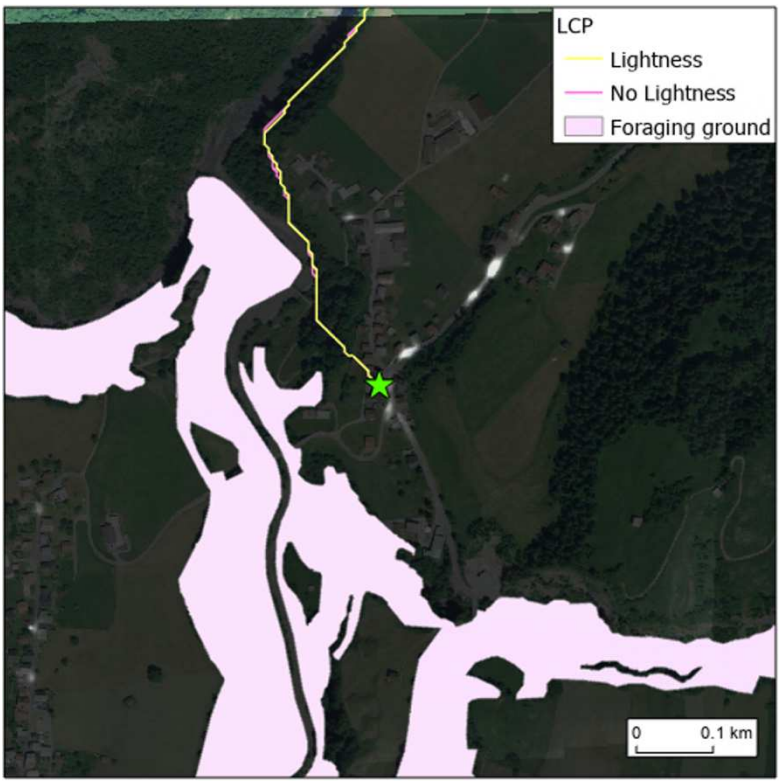

Figure_A 53: Least cost paths for RHI in Uors with the slightly transparent lightness layer underneath, and the aerial image as the bottom layer

a

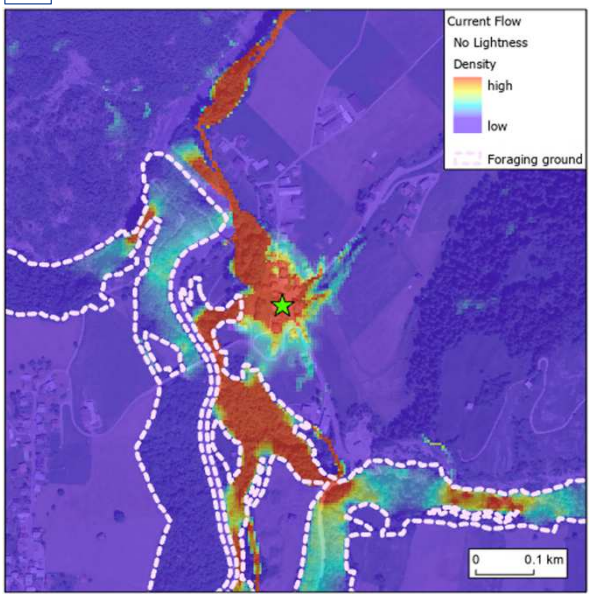

b

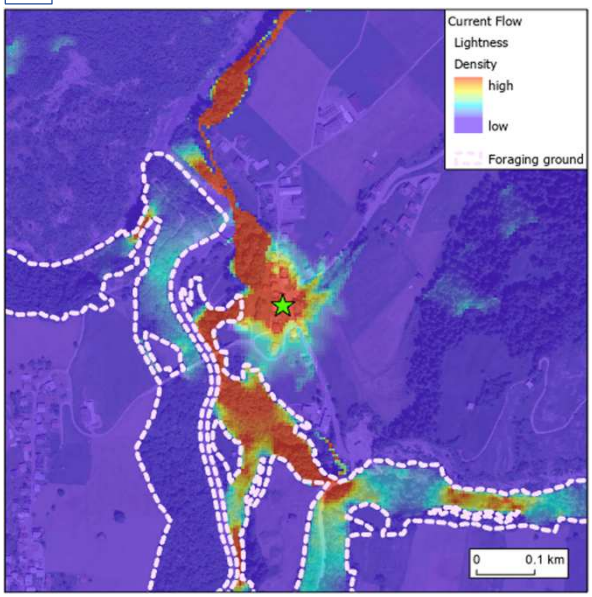

Figure_A 54: Current flow maps of RHI commuting in Uors predicted with a) no lightness and b) lightness

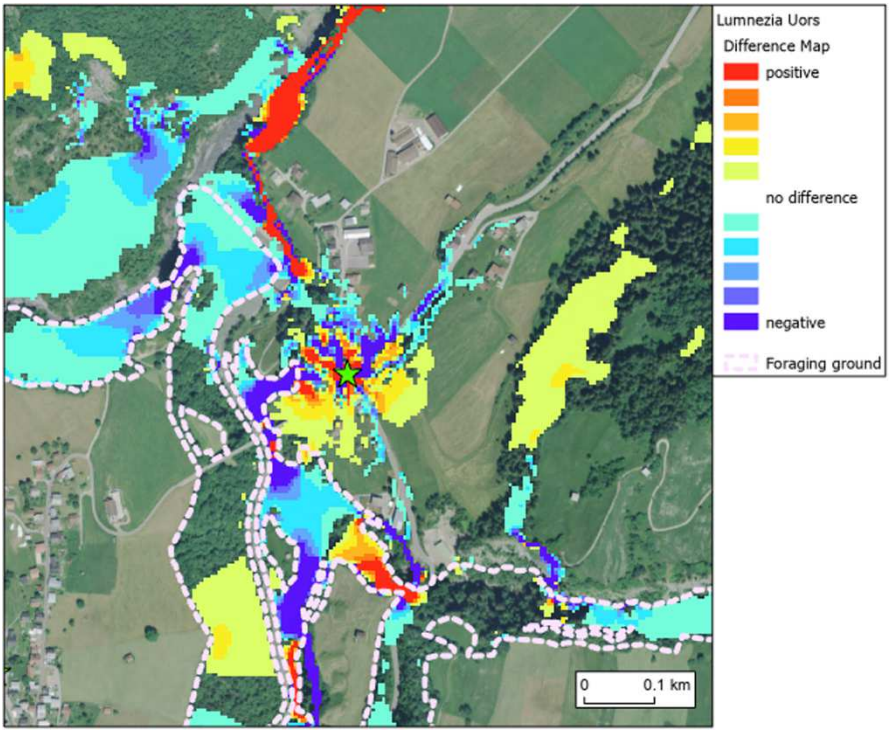

Figure_A 55: Difference map of Uors for RHI, depicting the difference in predicted current flow densities from a model with a lightness predictor to one including no light variable

WALTENSBURG – VUORZ

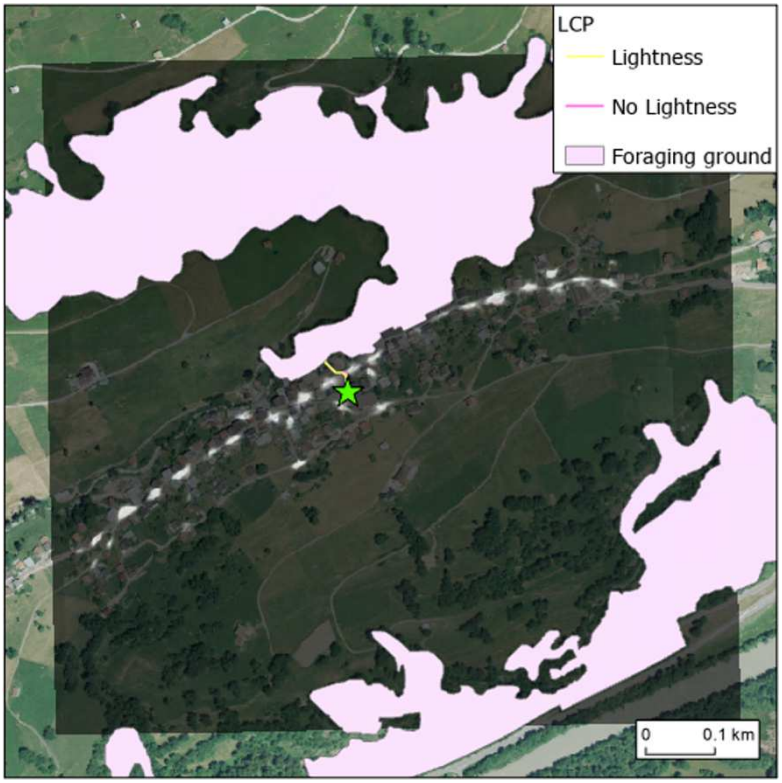

Figure_A 56: Least cost paths for RHI in Waltensburg with the slightly transparent lightness layer underneath, and the aerial image as the bottom layer

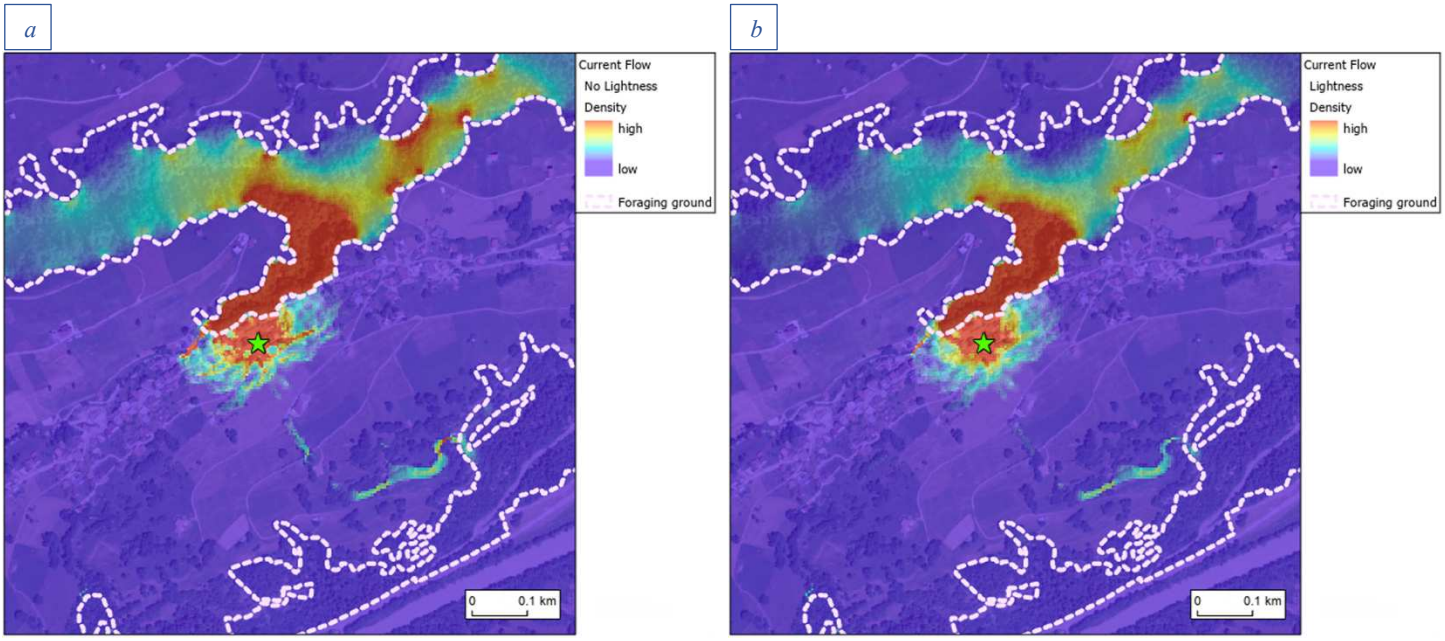

Figure_A 57: Current flow maps of RHI commuting in Waltensburg predicted with a) no lightness and b) lightness

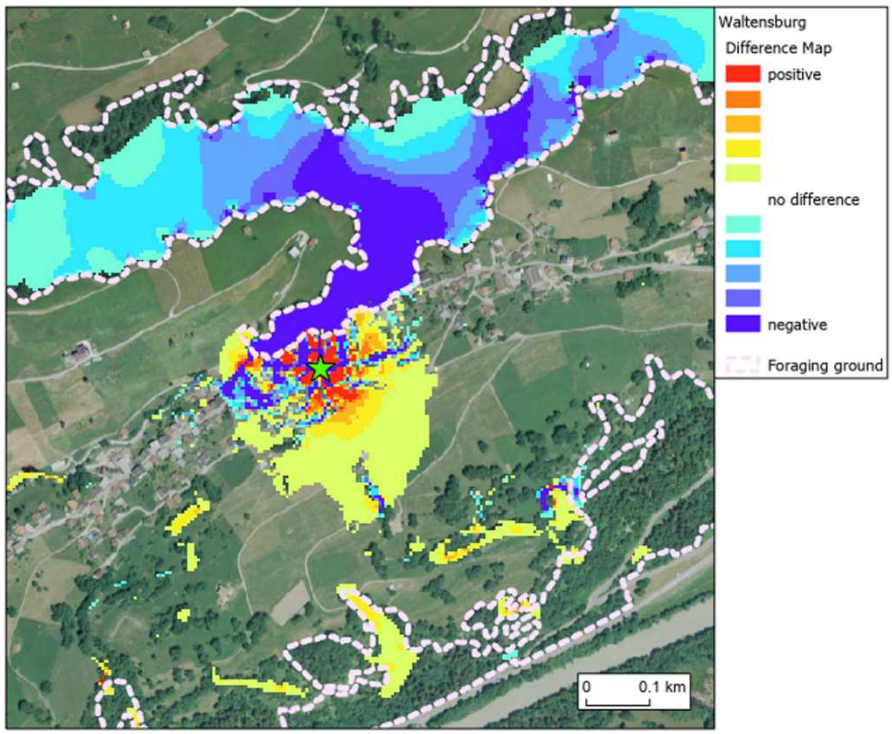

Figure_A 58: Difference map of Waltensburg for RHI, depicting the difference in predicted current flow densities from a model with a lightness predictor to one including no light variable